



***Characterization of gaseous and particulate
emissions from aircraft turbine engines:
emission, atmospheric aging and
implications***

Diss. No. 23930

Dogushan Kilic
2017

Characterization of gaseous and particulate emissions from aircraft turbine engines: emission, atmospheric aging and implications

A thesis submitted to attain the degree of

DOCTOR OF SCIENCES of ETH ZURICH

(Dr. sc. ETH Zurich)

presented by

DOGUSHAN KILIC

MSc in Climate Sciences, University of Bern

born on 09.09.1985

citizen of Turkey

accepted on the recommendation of

Prof. Dr. Urs Baltensperger (examiner)

Prof. Dr. Ulrike Lohmann (co-examiner)

Dr. André S. H. Prévôt (co-examiner)

Dr. Richard C. Miake-Lye (co-examiner)

Preface

Aviation is a growing transportation sector and accounts for a market of about \$718 billion worldwide (IATA, 2016). According to IATA, 3.3 billion passengers travelled using 500 airliners from 700 airports only in 2015. Further the number of the flights double every 15 years since 1982 (Airbus, 2013).

IATA's forecast states that air-passenger numbers will double to seven billion by 2034. This prediction implies that number of flights and flight-related activities at the airports will likewise increase dramatically. Further without alternative fuels to power this market, the airports will continue to be the source of air pollutants for the areas nearby.

Some countries are planning to build new airports or to enlarge the capacity of the existing ones. Building big facilities like airports is changing the landscape, affecting the ecosystem and resulting in important local and global atmospheric consequences. Aviation emissions due to airplanes using airports cost the society by affecting public health while the emissions at flight altitude impact climate. Policies are required to be implemented today, either to prevent or to mitigate both climate and health effects of the aviation emissions in the future. This needs to be done together with the detailed and accurate monitoring of the impacts.

Table of Contents

Summary	ix
Zusammenfassung.....	xi
1 Introduction	1
1.1 Organic gases in the troposphere	1
1.1.1 Impact of organic gases on public health.....	2
1.2 Aerosols in the atmosphere	2
1.2.1 Impact of aerosols on climate	4
1.2.2 Impact of aerosols on public health	5
2 Motivation and thesis outline.....	7
2.1 Aviation and atmosphere	7
2.1.1 Typical flight of an aircraft.....	7
2.1.2 Impact on climate and public health.....	9
2.2 The Aircraft Particulate Regulatory Instrumentation Demonstration (A-PRIDE) campaigns	11
2.3 Thesis Outline	13
3 Instrumentation and techniques.....	15
3.1 Proton-transfer-reaction time-of-flight mass spectrometer (PTR-ToF-MS)	15
3.1.1 Detection of organic gases by PTR-ToF-MS.....	15
3.2 Quantification of organic gases by PTR-ToF-MS.....	17
3.3 Fragmentation due to proton-transfer-reaction and limitations of PTR-ToF-MS	18
3.4 Detection of particulate matter by Aerosol Mass Spectrometer (AMS)	19
3.5 Oxidative processing of organic gases	20
3.5.1 Potential Aerosol Mass (PAM) chamber.....	20
3.5.2 Experimental setup of the aging experiments	21
4 Characterization of gas-phase organics using proton transfer reaction time-of-flight mass spectrometry: aircraft turbine engines.....	23
4.1 Introduction.....	24
4.2 Experimental methods.....	25
4.2.1 Sampling setup.....	25
4.2.2 PTR-ToF-MS.....	27
4.2.3 Calculation of emission indices	29
4.3 Results and discussion.....	30
4.3.1 Dependence of total NMOG on operating mode.....	30
4.3.2 Dependence of NMOG Composition on Operating Mode	31
4.3.3 Dependence of NMOG composition on engine type at idling.....	33
4.3.4 Implications for ambient air quality.....	34
4.4 Supplementary information	37
5 Identification of secondary precursors emitted by an aircraft turbofan.....	43

5.1	Introduction.....	44
5.2	Methods	45
5.2.1	Experimental setup	45
5.2.2	Instrumentation.....	46
5.2.3	Data analysis.....	48
5.3	Results and discussion.....	49
5.3.1	SOA formation as a function of OH exposure	49
5.3.2	Particle and gaseous emissions as a function of engine load	50
5.3.3	Precursor gases of SOA: Idling.....	53
5.3.4	SOA formation at cruise load	56
5.4	Conclusions and implications for ambient air quality.....	58
6	Vehicle dependent characterization of the organic gases from mobile sources: aircraft, ships and motor vehicles	61
6.1	Introduction.....	62
6.2	Instrumentation and methods.....	63
6.3	Results and discussion.....	64
6.4	Atmospheric implications	69
6.5	Supplementary information	71
6.5.1	Calculation of aircraft taxi-idle aromatic emission and equivalent distances for on-road vehicles.....	72
7	Conclusions	75
8	Outlook	77
	List of Tables.....	I
	Table of Figures.....	I
	Bibliography	V
	Acknowledgements.....	XVII
	Curriculum vitae	XIX

Summary

Organic gases (OGs) affect public health and global climate either directly or by forming secondary species in the atmosphere (e.g. ozone and aerosols). There are still open questions on the extent of their effects, partially arising from the strength and the chemical composition of different source emissions. In order to improve global model simulations and to develop mitigation strategies, a reduction of the uncertainty in the emission rates and chemical composition of OGs is necessary.

Aircraft turbine engines are one of these complex systems emitting many OGs during flight operations and at the airports. We investigated aircraft emissions using a proton-transfer-reaction mass spectrometer (PTR-ToF-MS) for the quantification of organic gases, a potential aerosol mass (PAM) chamber for the simulation of atmospheric aging and an aerosol mass spectrometer (AMS) for the quantification of non-refractory particulate matter with an aerodynamic diameter smaller than 1 micrometer (NR-PM₁). The exhaust measurements from seven in-service jet-turbine engines used in commercial aviation were performed at the test cell of SR Technics in Zurich.

As a first step, the total OG emitted by turbine engines and the variability of the exhaust chemical-composition as a function of engine load was determined. The total OG emission was highest at low load corresponding to taxi and idle operations, and decrease significantly (30-80 times) with increasing thrust. Total OG emission was also 2-3 times higher during low-load idling (2.5–5 %), a long-frequent operation at ground level, compared to idling thrust at 6-7 %. As current emission estimates are based on idling at thrust 7%, higher OG emission at low-load idling may imply that the emission from airports could be underestimated. We also observed changes in the OG relative composition with the thrust level, with higher aromatic content at low loads.

Primary aircraft emissions were aged in the PAM. The chemical composition of both particle and gas phase were monitored before and after aging for the different engine loads tested. The concentrations of the secondary aerosols formed after aging (40 hours day-time equivalent) were much higher (10 - 100 times) than those directly emitted. The secondary aerosol was dominated by the organic fraction (secondary organic aerosol, SOA) when the engine load was low (thrust 2.5 - 7 %) while sulfate particles were dominant at high load (thrust 30 - 100 %). Our results imply that much more particle mass may be formed in the atmosphere downwind of an airport than directly emitted.

Efficient abatement strategies for the improvement of air quality need quantitative assessment of the source contributions. This work provides the OG fingerprints for different transport emissions, which shall significantly aid the identification of their influence at receptor sites using top-down, statistical source apportionment methods. The studied sources include exhaust emissions from aircraft, ships and road vehicles. This compilation of emission factors (in g OG/kg fuel) with highest values for 2S-scooters, ships, light duty

vehicles and idling aircrafts can also be used for the assessment of the relative importance of each of these sources, using bottom up approaches.

Zusammenfassung

Organische Gase (OGs) beeinflussen die öffentliche Gesundheit und das globale Klima direkt oder durch in der Atmosphäre gebildete sekundäre Spezies (z.B. Ozon oder Aerosole). Es gibt aber immer noch offene Fragen zum Umfang ihrer Auswirkungen, sowie zur Stärke und chemischen Zusammensetzung der verschiedenen Emissionsquellen. Um die globalen Modellsimulationen zu verbessern und Minderungsstrategien entwickeln zu können, müssen die Unsicherheiten zu den Emissionsraten und der chemischen Zusammensetzung von OGs erforscht werden.

Flugzeugmotoren sind eines dieser komplexen Systeme, welche während des Flugbetriebs und auf den Flughäfen viele OGs emittieren. Wir charakterisierten die Emissionen von Flugzeugen mithilfe eines Protonentransferreaktions-Massenspektrometers (PTR-TOF-MS) zur Quantifizierung von organischen Gasen, einer „Potential Aerosol Mass“(PAM)-Kammer für die Simulation der atmosphärischen Oxidation und einem Aerosol-Massenspektrometer (AMS) für die Quantifizierung von nicht-refraktären Partikeln mit einem aerodynamischen Durchmesser von weniger als 1 Mikrometer (NR-PM₁). Die Abgasmessungen von sieben in Betrieb stehenden Flugzeugturbinenmotoren aus der gewerblichen Luftfahrt wurden in der Testzelle von SR Technics in Zürich durchgeführt.

Zuerst wurde der Gesamtausstoss der Turbinenmotoren an OG und die Variabilität der chemischen Zusammensetzung der Abgase als Funktion der Motorlast bestimmt. Die gesamte Abgasemission war während des Aufrollens und Wartens auf dem Rollfeld bei niedriger Drehzahl beziehungsweise niedriger Schub am höchsten. Sie nahm deutlich (30-80 mal) mit der Erhöhung des Schubs ab. Der Gesamtausstoss war 2-3 mal höher bei sehr niedriger Last im Leerlauf (2,5-5%) im Vergleich zum üblicherweise angenommen Leerlaufschub von 6-7%. Da am Boden die niedrigere Last üblich ist, erhöht dies die Belastung mit OG in der Nähe von Flughäfen deutlich. Ausserdem ergaben sich auch Veränderungen in der relativen Zusammensetzung der OG bei Veränderung des Schubs, in Form eines höheren Gehalts an Aromaten bei niedrigen Lasten.

Die primären Emissionen von Flugzeugen wurden zusätzlich in der PAM-Kammer gealtert. Die chemische Zusammensetzung sowohl der Partikel als auch der Gasphase wurde für die unterschiedlichen Motorlasten vor und nach der Alterung gemessen. Die Konzentration des sekundären Aerosols war nach simulierter Alterung (entsprechend 40 Stunden Alterung in der Atmosphäre) viel höher (10-100 mal) als die Konzentration der direkt emittierten Partikel. Darüber hinaus wurde bei niedriger Motorlast (Schub 2,5-7%) das sekundäre Aerosol von der organischen Fraktion (sekundäres organisches Aerosol, SOA) dominiert, während Sulfatpartikel bei hoher Last (Schub 30-100%) dominant waren. Unsere Ergebnisse deuten darauf hin, dass eine viel grössere Partikelmasse in der Umgebung eines Flughafens gebildet wird als direkt emittiert wird.

Effiziente Reduktionsstrategien zur Verbesserung der Luftqualität benötigen quantitative Angaben zu den Beiträgen verschiedener Quellen. Diese Arbeit liefert Fingerabdrücke von verschiedenen OG für verkehrsbezogene Quellen, welche die Anwendung statistischer Quellzuordnungsmodelle für OG-Daten verschiedener Messstandorte unterstützen sollen („Top-Down“ Ansatz). Die erforschten Emissionsquellen beinhalten Flugzeuge, Schiffe und Strassenfahrzeuge. Die Zusammenstellung von Emissionsfaktoren (in g OG / kg Kraftstoff) mit den höchsten Werten von Schiffen, benzinbetriebenen Personenwagen und Flugzeugen im Leerlauf können auch genutzt werden, um die relative Bedeutung verschiedener Quellen abzuschätzen („Bottom-Up“ Ansatz).

1 Introduction

1.1 Organic gases in the troposphere

The troposphere is the lowest layer of the atmosphere where all biotas on Earth live. Starting from the Earth surface it extends upward to an average height of 10 km (33000 feet) above sea level (*a.s.l.*) (Figure 1-1). The upper border of the troposphere, the tropopause, can be as high as 20 km (65000 feet) in the equatorial zone and as low as 7 km (23000 feet) at the poles during winter. Most of the weather events take place in the troposphere which hosts most of the clouds and dust particles. Further, the troposphere contains most of the mass in atmosphere (~75-80%) which mostly consists of nitrogen and oxygen, with 78% and 21%, respectively.

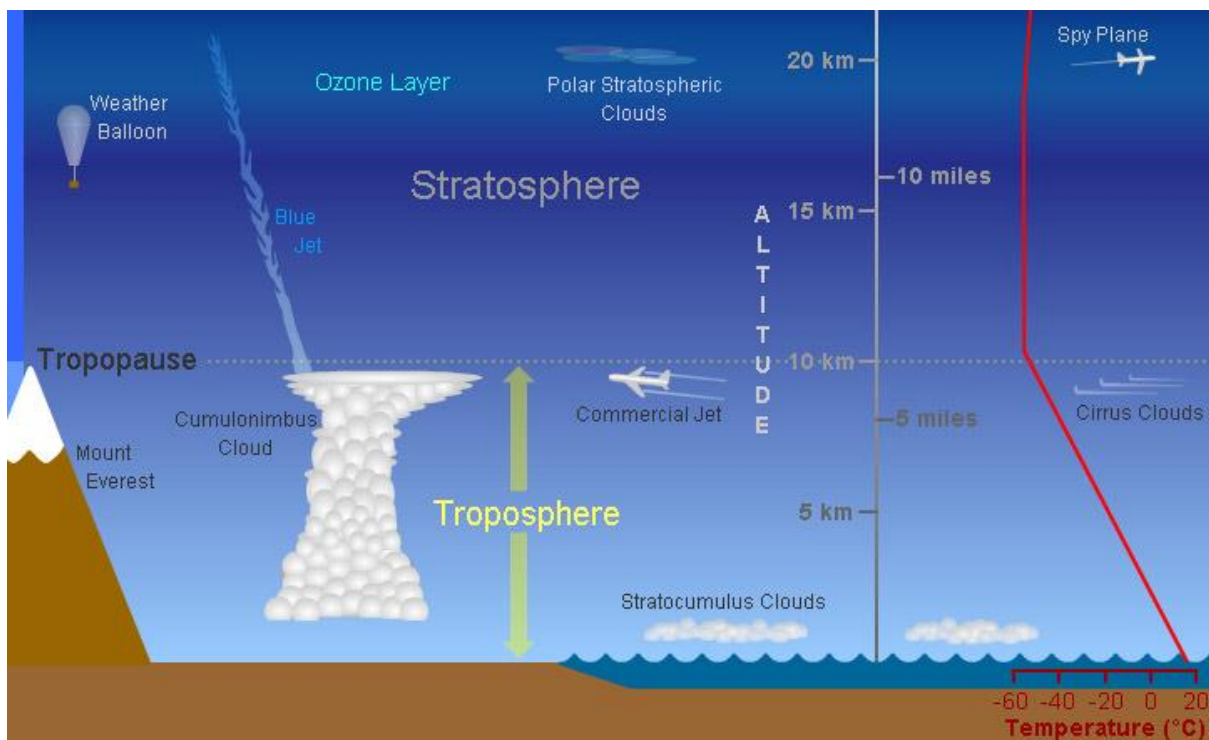


Figure 1-1: Artwork by Randy Russell showing the troposphere and stratosphere. The temperature in the troposphere decreases with the increasing altitude.

(Source: <http://www.windows2universe.org/earth/Atmosphere/troposphere.html>)

The troposphere also contains organic gases, *e.g.* methane (CH_4), hydrocarbons, in total far less than 1%. Organic gases (OGs), also known as volatile organic compounds (VOCs), are emitted both by natural and anthropogenic sources with an annual rate of 571 Tg(C)/yr (IPCC, 2002). Anthropogenic sources account for approximately 30% of the global OG emissions, assuming all fossil fuel combustion as the only anthropogenic source. This

anthropogenic fraction has a variety of sources *e.g.* vehicle traffic, industry, or residential heating and determines local air quality in cities, where the majority of the population lives.

Each of these OG sources has unique chemical characteristics. For example a light-duty gasoline vehicle emits more single-ring aromatic hydrocarbons per fuel used compared to a diesel engine (Platt et al., 2014) while an idling aircraft emits mostly carbonyls (*e.g.* aldehydes) in addition to aromatic gases (Kilic et al., 2017). Cooking can result in the emission of terpenes or sulfur containing organic gases depending on the diet and cooking habits (Klein et al., 2016). Further, wood combustion for heating purposes also results in emissions of aromatics and their oxygenated variants *e.g.* phenols varying with the burning conditions (Bruns et al., 2015). This source-dependent variability in chemical composition leads to various public and atmospheric implications (*e.g.* different health effects, different chemical characteristics for the aerosols formed by the aging of OGs in the atmosphere).

1.1.1 Impact of organic gases on public health

Inhaling organic gases may have both acute and chronic effects on health. Acute effects are sudden in onset *e.g.* an asthma attack or a heart attack while a tumor growth in years due to continuous pollutant exposure is an example of a chronic effect. The magnitude of effect and the target organ of the threat posed by OG exposure depend on the chemical structure (*e.g.* functional groups in the molecule) and the concentration in the air.

For example, exposure to high concentrations of aldehydes results in short-term effects on the respiratory system by the inflammation of the lungs. Some studies have also been associated aldehydes (*e.g.* formaldehyde) with cancer (IARC, 2006).

Polycyclic aromatic hydrocarbons (PAHs) are the other group of organic gases previously linked with cancer. The effect of individual PAHs is not identified since the studies mostly investigate the exposure to PAH mixtures. PAH exposure however increases different cancer risks according to animal experiments and epidemiological studies (Armstrong et al., 2004; Negri & La Vecchia, 2001).

1.2 Aerosols in the atmosphere

Aerosols (particulate matter, PM) are liquid or solid particles suspended in the air. They are emitted directly or formed in the atmosphere due to natural processes such as volcanic eruptions, sea spray, dust resuspension or anthropogenic activities such as fossil fuel combustion. Aerosols lead to formation of clouds by acting as condensation nuclei, by providing surfaces for water to form droplets in the clouds. Finally aerosols are either washed out within droplets (wet deposition) or settle down on the Earth's crust (dry deposition).

Aerosols are usually categorized according to their size by particle diameter. Particulate matter with an aerodynamic diameter smaller than 1 micrometer (μm) (PM_{10} and others such as $\text{PM}_{2.5}$, PM_{10} depending on their size). Particles with a diameter greater than 2.5 micron are generally referred to as “coarse” and those with a diameter smaller than 2.5 micron as “fine”.

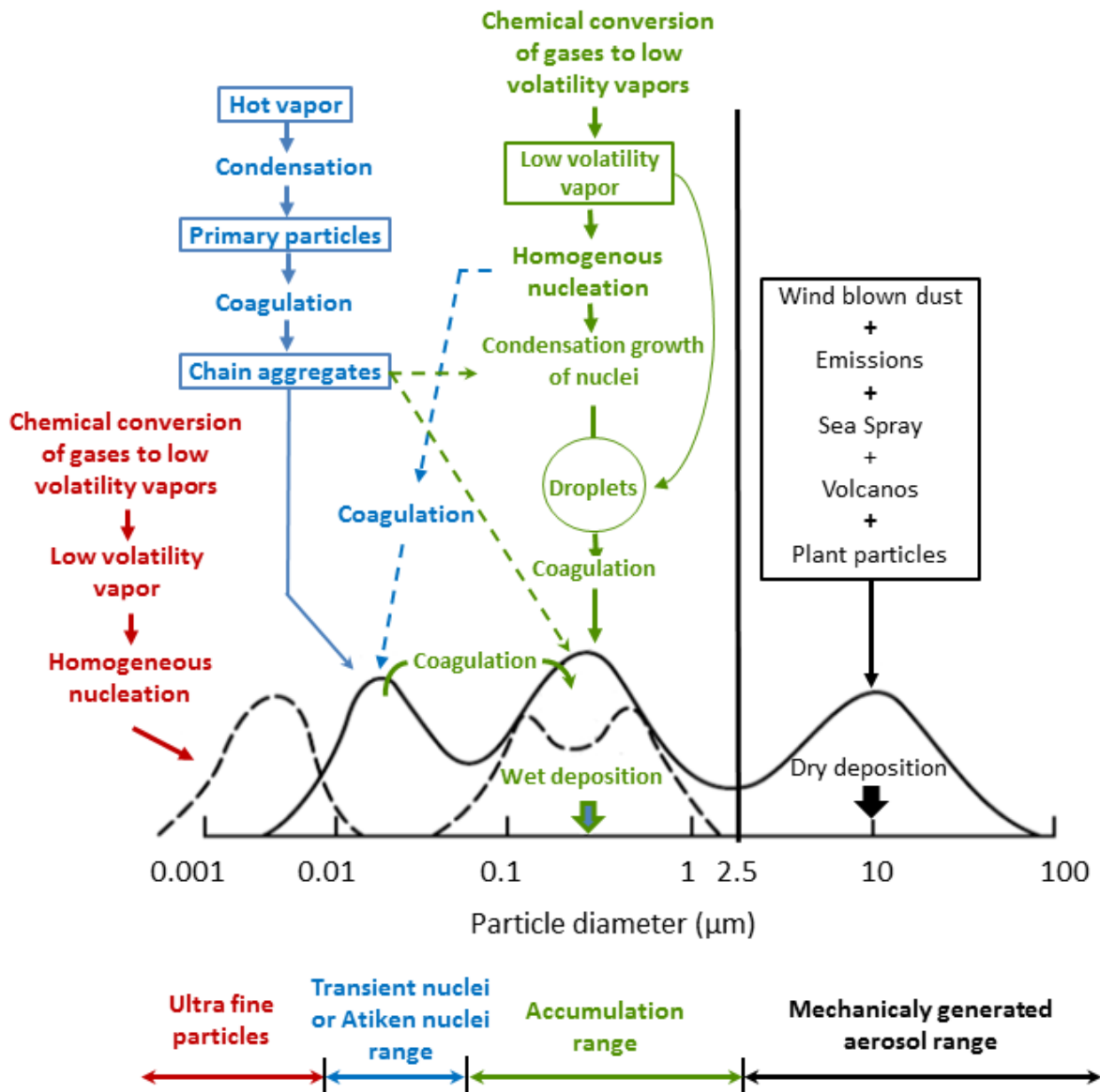


Figure 1-2: Schematic showing the atmospheric aerosol size distribution for four modes (Finlayson-Pitts & Pitts Jr., 2000).

Figure 1-2 presents the atmospheric processes leading to particle formation of different sizes. Gases chemically converted to low-volatility vapors nucleate below 10 nm. Nucleated particles grow by further vapor deposition and by coagulation into the Aitken mode (10-100 nm range). Due to their small sizes, particles with the diameter below 100 nm dominate the particle number in the atmosphere while they account for only a few percent of the total

mass of the airborne aerosols. The range from 100 nm to 2.5 μm is called the accumulation mode. Particles grow into this size range by condensation growth and coagulation. Particles larger than 100 nm act as CCN, i.e., they can form cloud droplets take place, in the presence of a super saturation of water vapor. The accumulation range (0.1-2.5 μm) accounts for the substantial amount of the total atmospheric aerosols by mass. The particles of the coarse mode ($> 2.5 \mu\text{m}$) usually are formed by processes that are different from those in the smaller range ($< 2.5 \mu\text{m}$) (e.g. nucleation, condensation, coagulation). Coarse particles are generated mechanically *e.g.* dust resuspension. Due to different sources, coarse particles also have different chemical composition.

The chemical composition of aerosols is source dependent. These sources can be natural *e.g.* sea spray, plant, wind-blown dust or anthropogenic, *e.g.* transportation, industry. The particles are either emitted directly, “primary aerosols”, or formed by the transformation of gas phase emissions (*e.g.* oxidation of organic gases in the atmosphere), “secondary aerosols”. To mention some examples, primary volcanic ash mostly consists of the most abundant components of the Earth crust such as metal oxides, carbonates (Andersson et al., 2013; Nakagawa & Ohba, 2002) while sea salt sprayed into the atmosphere mainly consists of sodium and chloride abundant in the seawater (Lewis & Schwartz, 2004). These examples of natural sources are mostly coarse particles and mostly inorganic.

The chemical composition of fine aerosols ($< 1 \mu\text{m}$) varies with location and season but is mostly comprised of carbonaceous material (organic matter, OM, and black carbon, BC), nitrate, sulfate, chloride and ammonium. Organic matter (OM) is typically the most abundant fraction of fine particles worldwide (Zhang et al., 2011) and can be emitted directly (primary organic aerosol, POA) or formed in the atmosphere (secondary organic aerosol, SOA). However, while the formation of inorganic secondary aerosol is reasonably well understood the mechanisms forming and transforming organic aerosol (OA) still awaits a thorough understanding (Hallquist et al., 2009).

1.2.1 Impact of aerosols on climate

Aerosols affect global climate directly and indirectly. The direct effect relates to aerosol radiation interaction by scattering or absorption. The indirect effect relates to aerosol cloud interaction, by modifying the cloud properties and thus the cloud albedo and lifetime. By these effects an increased aerosol concentration may lead to a colder global atmosphere as shown *e.g.* by volcanic eruptions. For example, the Mount Pinatubo eruption in the Philippines in 1991 caused the mean global temperature to decrease by 0.4-0.6 $^{\circ}\text{C}$ in 1992 (Self et al., 1993) due sulfate aerosols formed from the emitted SO_2 .

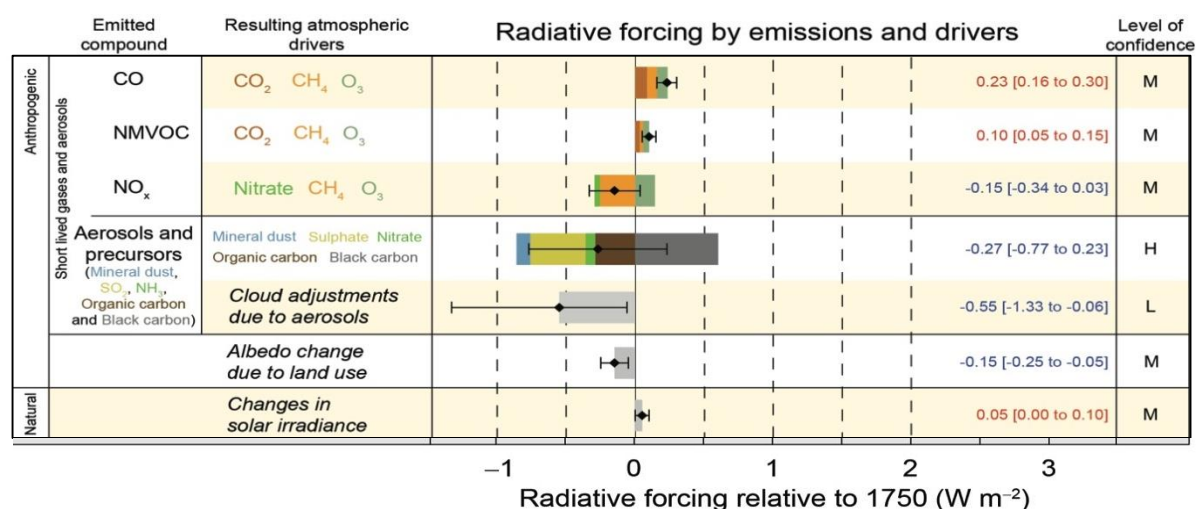


Figure 1-3: Radiative forcing estimates in 2011 relative to 1750 for the selected precursors of climate change. Global values are best estimates with the level of confidence (L: Low, M: Medium, H: High). Adapted from IPCC (2013).

The long-term climate impact of aerosols is quantified by a climate metric, the radiative forcing (RF, W m⁻²), in the recent International Panel on Climate Change (IPCC) report (IPCC, 2013). A negative RF indicates that the atmospheric driver leads to a colder climate. The impact of aerosols on incoming solar radiation due to cloud adjustments is a cooling one as shown in Figure 1-3. However the impact from aerosols on climate has the lowest confidence compared to other precursors due to the open questions regarding their formation mechanisms and atmospheric transformation.

1.2.2 Impact of aerosols on public health

According to the World Health Organization (WHO), global air pollution caused 3.7 million premature deaths in 2012 alone (WHO, 2014). Exposure to air pollution increases cardiovascular mortality and morbidity (Brook et al., 2010; Lall et al., 2004). Furthermore, air pollution exposure also increases mortality due to respiratory and cardiopulmonary diseases (Brunekreef et al., 2009). Pope et al. (2009) reported that an increased fine PM exposure of 10 µg m⁻³ caused a decreased life expectancy of ~0.6 years and increased lung cancer risk by 8%.

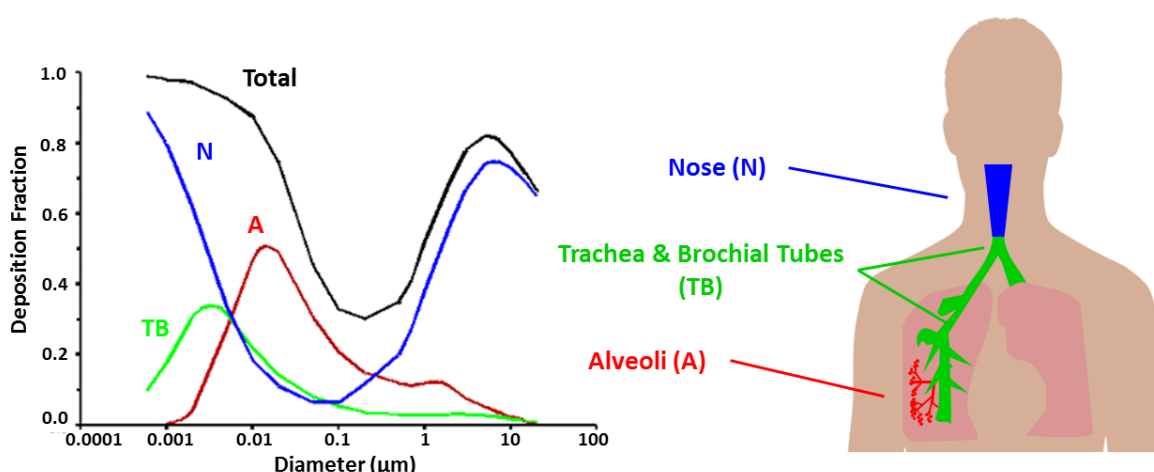


Figure 1-4: Deposition of different sized particles in different segments of the respiratory system: N=Nasal, TB= Tracheobronchial, A=Alveolar (adapted from ATSDR, 1994).

Particle size is an important determinant of the aerosols impact on health. As presented in Figure 1-4, particles of 0.1-1.0 μm range can penetrate into the lungs, passing the upper respiratory tract (blue), as well as the trachea and bronchial tubes (green), and may be accumulated in the alveoli (red). In the particle size range 0.01-1 μm , the regional deposition fraction (the ratio of deposited particles to total inhaled for the given lung segment) in alveoli increases as shown in Figure 1-4 (left). Particles in the 0.001-0.1 range can also be more hazardous to human health because they potentially include a higher fraction of carcinogenic substances, *e.g.* PAHs (Nel, 2005). Many countries and international institutions (*e.g.* WHO) have implemented daily and annual average limits (maximum allowed concentrations) for PM due to its adverse health effects as shown in *Table 1-1*.

Table 1-1: PM regulation standards from selected countries and institutions.

	PM 2.5		PM 10		Reference
	Daily	Annual	Daily	Annual	
WHO	25	10	50	20	WHO, 2006
U.S. EPA	35	12*-15**	150	-	EPA, 2012
EU	-	25	50	40	EU Commission, 2010
Switzerland	-	-	50	20	FOEN, 2010
Turkey	-	-	50	40	Cevre, 2008

*primary, **secondary

2 Motivation and thesis outline

2.1 Aviation and atmosphere

Approximately 3.5 billion passengers used commercial airliners in 2015. Aviation activity is expected to double by 2050 (IATA, 2016). Figure 2-1 shows the aircraft CO₂ emission trend for the years 1990-2050. These estimates include both present-day inventories and future projections. According to some of the projections presented in Figure 2-1, CO₂ emissions from aviation are expected to exceed 1500 Mt/yr by 2050 from a present-day level of 900 Mt/yr.

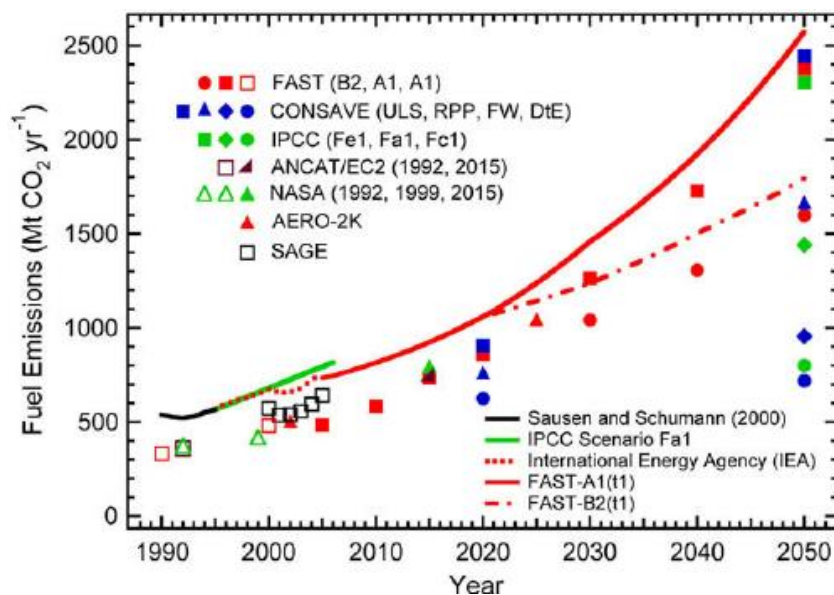


Figure 2-1: Historical inventories and future projections of civil-aviation CO₂ emissions (based on civil and military aviation fuel sale statistics (IEA, 2007)) from a variety of sources. From Lee et al., (2009).

The CO₂ emission trend is presented as an example, a surrogate for other gaseous and particulate emissions related to aviation. The increase in aviation activity, and the emissions related to it as a consequence, have both regional and global implications. Briefly the high altitude emissions are most important for climate, while near-ground level emissions impact the local air quality. Climate and health effects of aviation are discussed in the following sections.

2.1.1 Typical flight of an aircraft

There are 700 airports worldwide currently being used for commercial aviation, registered by the International Civil Aviation Organization (ICAO). Among the flight operations, the cruise mode has the longest duration for any flight taking longer than 2 hours, assuming a

typical landing and take-off (LTO) cycle of 33 minutes. Emissions from airports are mostly due to aircraft activity, specifically due to jet turbine engines (Kim, 2009). The LTO cycle summarizes near-airport activity of an aircraft below 915 meters (3000 feet) used by ICAO in the emission certification procedure. The LTO cycle consists of taxi/idle, take-off, climb, cruise and approach operations with the corresponding engine loads of $\leq 7\%$, 100%, 85%, 60-90% and 30%, (relative to full thrust), respectively.

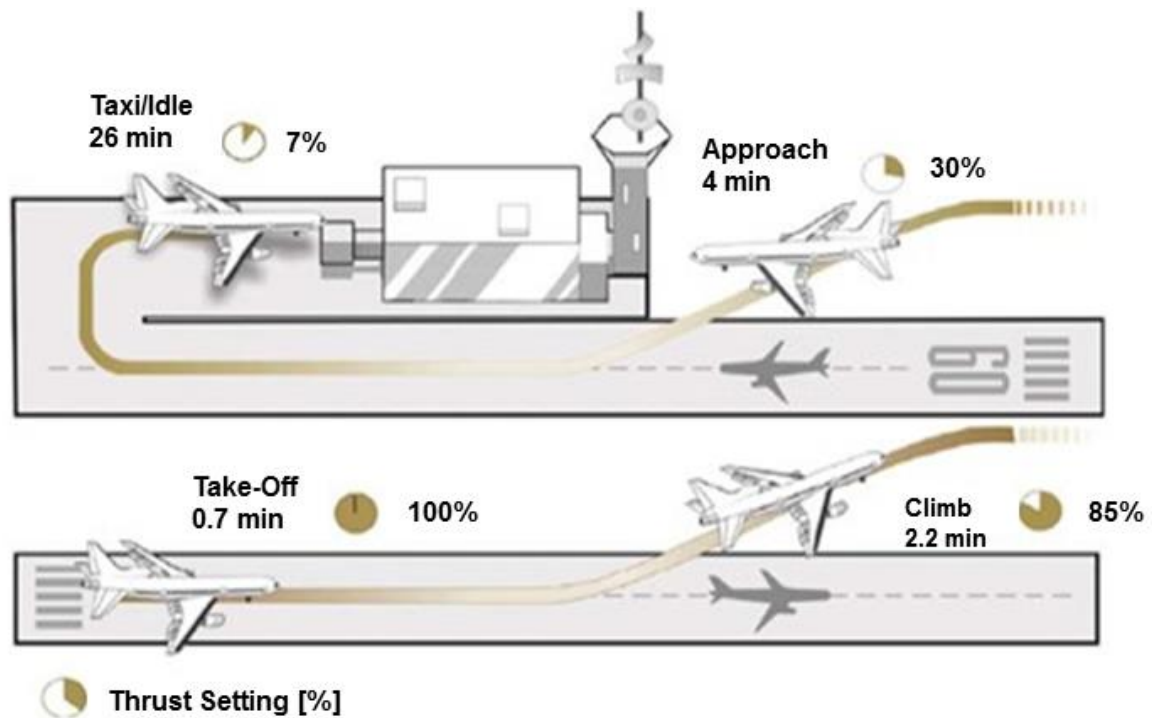


Figure 2-2: Near-ground flight operations of an aircraft: Landing take-off (LTO) cycle. Source <http://www.icao.int/environmental-protection/Pages/local-air-quality.aspx>

Figure 2-2 shows the typical LTO flight modes of a commercial aircraft with corresponding engine loads (%) and durations (min). LTO emissions are a greater concern for local air quality since the emissions are released below 915 meters. Near airport jet turbine engines mostly operate at low load (taxi/idle for 26 min) which implies idle emissions could be particularly important for local air quality near ground level while cruise emissions at high altitude (>1000 meters *a.s.l.*) are most important for global climate.

2.1.2 Impact on climate and public health

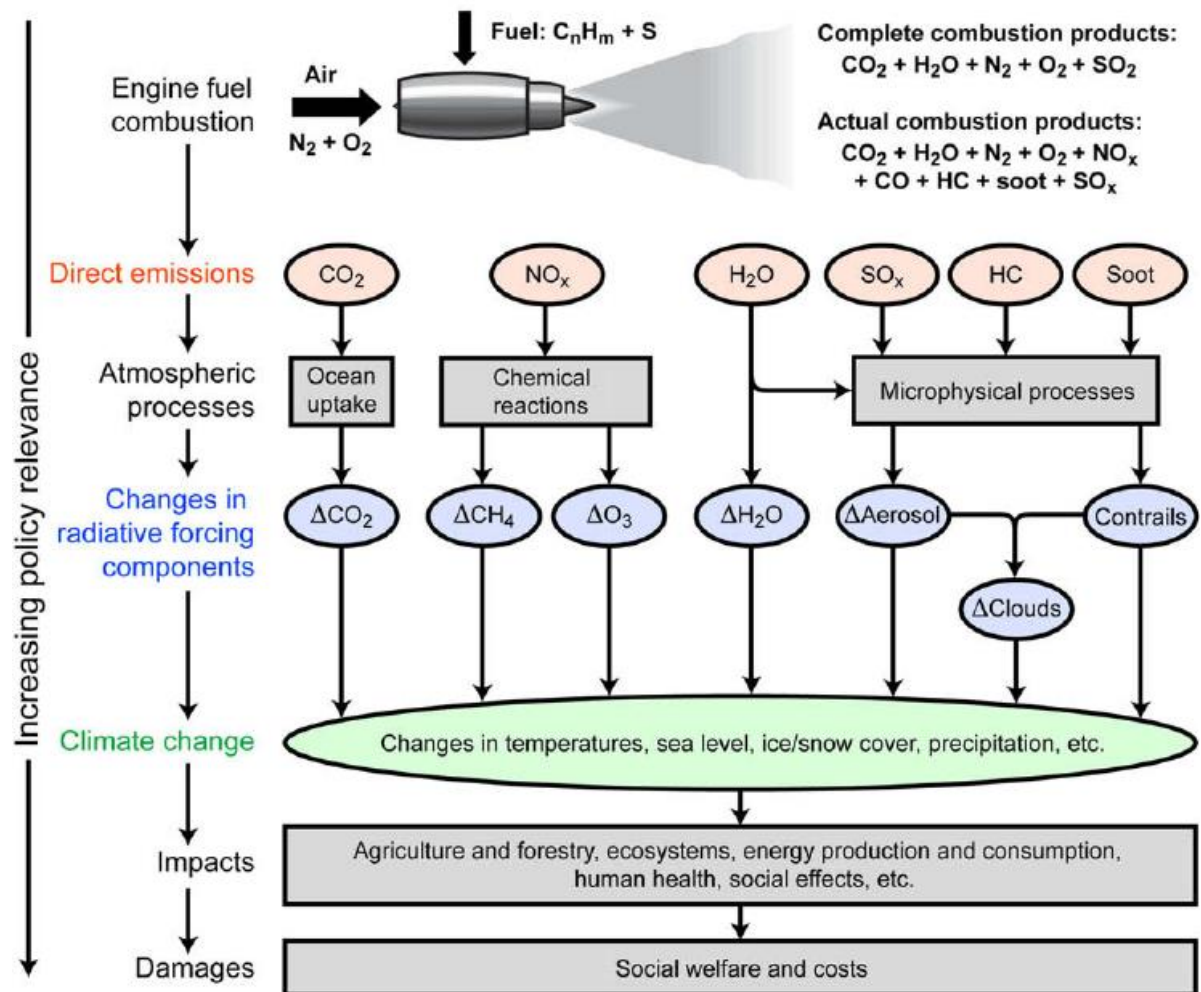


Figure 2-3: Aircraft emissions and their atmospheric implications. Figure by Lee et al. (2009) (adapted from Prather et al., 1999) and Wuebbles et al., 2007).

Figure 2-3 presents a schema showing the jet turbine engine emissions and their implications for the global atmosphere. CO_2 , NO_x , H_2O , SO_x , OGs and soot emitted by aircraft have different atmospheric consequences such as changing temperatures, sea level, ice/snow cover and precipitation.

Figure 2-4 shows the RF components for aviation and the level of scientific understanding. The top two components affecting climate with a positive RF are contrail formation and enhanced cloudiness. These also have the biggest uncertainty (Sausen et al., 2005) and their level of understanding is classified as low or very low. Except NO_x -induced methane reduction and sulfate aerosol formation, all components have a positive RF indicating that their emission results in a warmer climate.

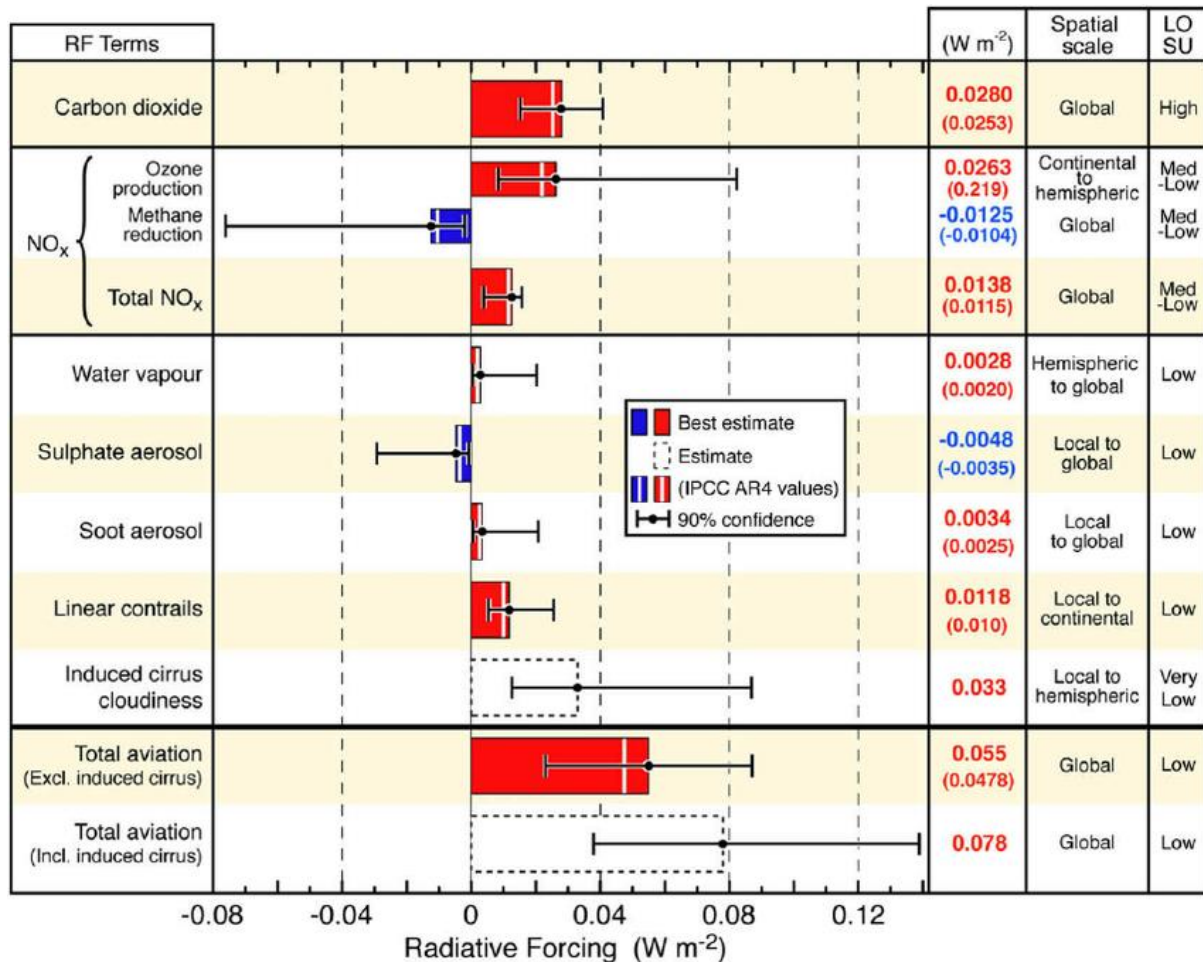


Figure 2-4: The radiative forcing due to aviation emissions with components from Lee et al. (2009).

Near ground level, emissions originating from an airport is transported downwind, affecting the ambient air quality (Unal et al., 2005). Figure 2-5 shows that downwind from Los Angeles International Airport the particle number concentrations were significantly increased up to a distance of 16 km and affecting an area of about 60 km². Further, emissions from airports affect public health. For example, hospital admissions for respiratory conditions near airport (within 5 miles) in New York State were higher compared to the areas further away (> 5 miles). However, commercial aviation remains one of the least characterized man-made sources of air pollution (Masiol & Harrison, 2014). Therefore, characterization of the particulate and gaseous emissions originating from the airports is required to evaluate their impact on the public.

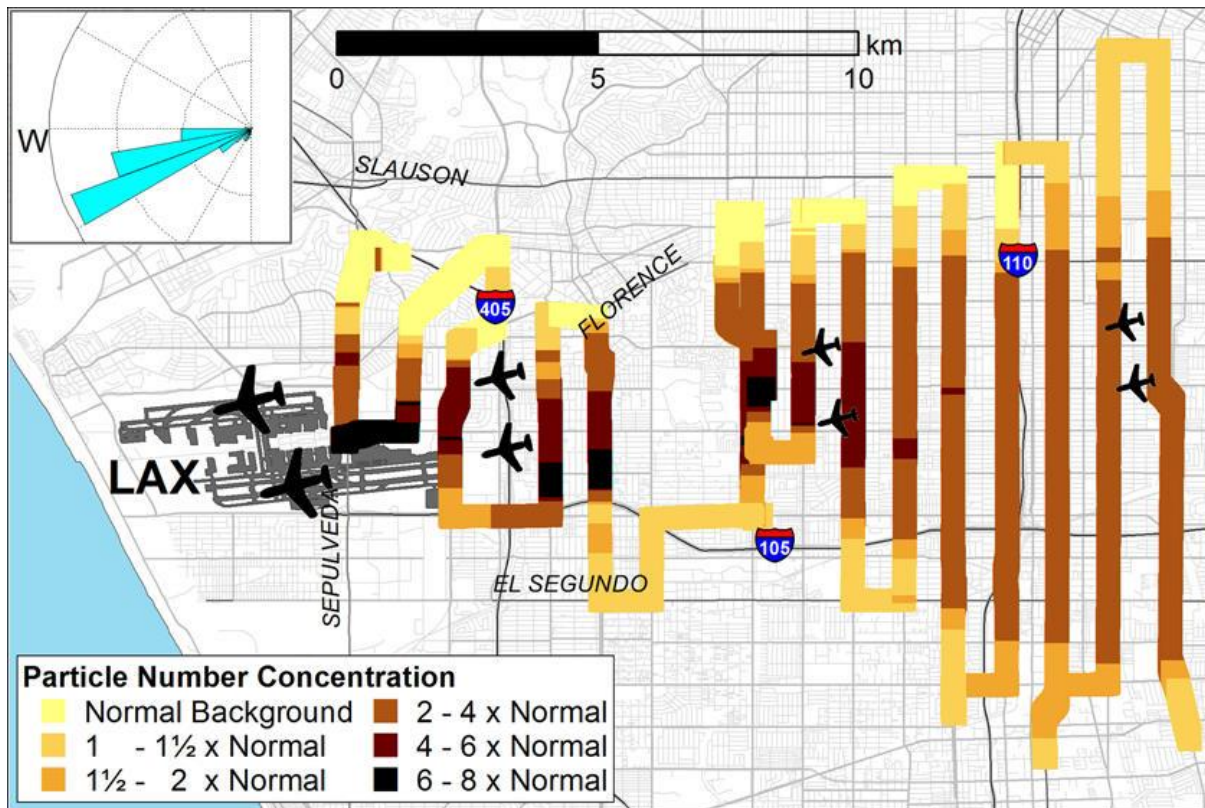


Figure 2-5: A sample spatial pattern of particle number concentrations from Los Angeles International Airport. (From Hudda et al. (2014)).

2.2 The Aircraft Particulate Regulatory Instrumentation Demonstration (A-PRIDE) campaigns

The Swiss Federal Office for Civil Aviation (FOCA) and Swiss Federal Laboratories for Materials Science and Technology (Empa) built a world-unique system in an engine test cell of SR Technics at the Zürich airport. This system enabled the measurement of the emissions from in-service commercial aircraft engines with a traversable probe. The emissions were sampled at a distance of 1.5 m to the engine exit plane from any point by moving the probe vertically and horizontally.

The scopes of the work were mainly: testing and validation of the sampling method and establishment of the repeatability and reliability of the measurements; obtaining mass- and number- based non-volatile particulate matter (nvPM) emission indices (EIs) for a variety of aircraft engines; characterization of nvPM in terms of size, morphology, effective density and chemical composition; and measurement of the ICAO-regulated gaseous pollutants. The Paul Scherrer Institute (PSI) was taking part in the A-PRIDE campaigns, and characterized aircraft gaseous and particle emissions, as well as the secondary particles formed by the aging of the emissions.

The A-PRIDE campaigns took place at SR Technics starting from 2012 with the FOCA project sponsorship. The early campaigns (A-PRIDE 3, 4, and 5) focused on the development of the

sampling methodology. The prototype sampling system was tested for the first time in a one-week campaign in August 2013 (A-PRIDE 6). In 2014, the spatial variability of emissions in the engine exit plane and the effects of different fuel aromatic content on nvPM mass and number emissions were studied (A-PRIDE 7) in a collaborative effort with General Electric and SNECMA by Empa (Brem et al., 2015).

In addition to these dedicated A-PRIDE campaigns, the sampling setup was also used to measure emissions from engines that had a service at SR Technics in so called “piggy-back runs”. These runs helped to develop and test sampling procedures intended for the A-PRIDE campaigns and provided additional experiments, improving statistical confidence.

2.3 Thesis Outline

We investigated primary and secondary aircraft emissions during A-PRIDE campaigns. Our research goals were as following:

- Quantification and characterization of the primary organic gases (OGs) and non-refractory particle matter with a diameter smaller than 1 micrometer (NR-PM₁) emissions at different engine loads
- Aging of the primary emissions and investigation of the secondary particle formation at different engine loads
 - Identification of the precursor gases of secondary aerosol
 - Characterization of the secondary aerosol
- Investigation of the OG fingerprints from aircrafts
- Comparison of the chemical composition and emission factors of OGs from different mobile sources.

Chapter three describes the gas- and particle-phase instrumentation used to measure OGs and NR-PM₁, as well as the sampling and analysis methodologies employed.

Chapter four presents total primary OG EIs quantified at different engine loads for seven engine types. Further, the exhaust chemical composition at the engine exit plane for different engine loads and its variability depending on engine maintenance history, age and capacity are presented.

Chapter five focuses on the oxidative processing of aircraft emissions and the relationship of the generated secondary organic aerosol to the primary OG composition. These experiments utilize a single, commonly used CFM56-7B/3 gas-turbine engine. Directly emitted (primary) gases and particles, and their oxidative processing (aging) were investigated for different engine loads. Further, the precursor gases of the secondary organic aerosol were identified.

Chapter six compares the chemical composition of OGs from aircraft emissions with those of other mobile sources, including ships and on-road motor vehicles. The chemical finger prints of each source were analyzed to be provided for ambient source apportionment studies.

3 Instrumentation and techniques

3.1 Proton-transfer-reaction time-of-flight mass spectrometer (PTR-ToF-MS)

3.1.1 Detection of organic gases by PTR-ToF-MS

A proton-transfer-reaction time-of-flight mass spectrometer (PTR-ToF-MS) was used for the quantification of the non-methane organic gases (NMOGs) in this study. The PTR-ToF-MS (PTR-TOF 8000, Ionicon Analytik G.m.b.H., Innsbruck, Austria) enables online detection of NMOGs with a proton affinity higher than water (Graus et al., 2010; Hansel et al., 1995).

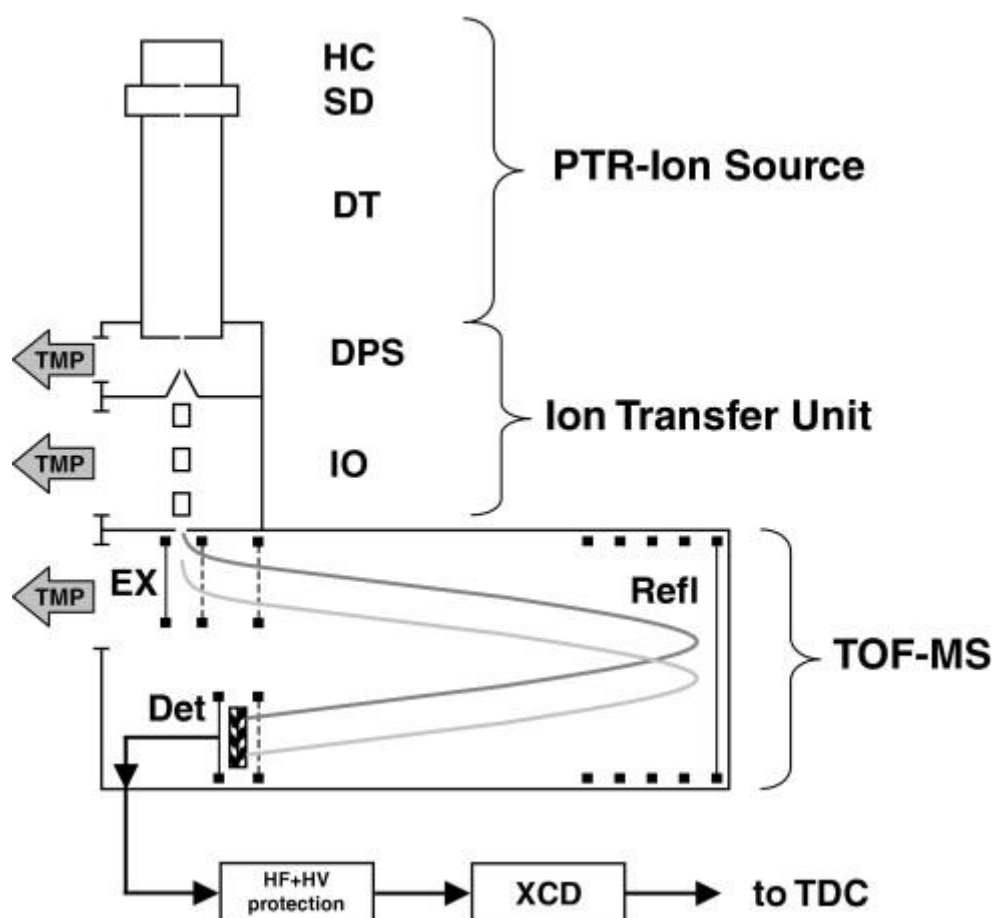


Figure 3-1: A simplified scheme of the PTR-TOF instrument (Graus et al., 2010).

Figure 3-1 presents a simplified scheme of the PTR-ToF-MS. The PTR-ToF-MS consists of three main components: (i) an ion source, (ii) an ion transfer unit and (iii) a time-of-flight mass spectrometer (ToF-MS). Hydronium ions (H_3O^+) are produced from water in a hollow cathode (HC) ion source and then transferred to the drift tube (DT) where protonation of the OGs is achieved by $\text{OG-H}_3\text{O}^+$ reaction. The gas (air) sample, containing OGs for analysis, is pulled into the drift tube. Through a differential pumping stage, ions are directed to the

time-of-flight mass spectrometer. The signals are collected by multi-channel-plates (MCP; Burle Industries Inc., Lancaster, PA, USA) then preprocessed by an amplifier-discriminator unit (Ionwerks XCD; Ionwerks Inc., Houston, TX, USA). Finally the ion counting events are processed by a time to digital-converter (TDC).

The use of this instrument requires an operational choice for the ratio of the electric field strength (E) – the voltage gradient down the drift tube – to the buffer gas number density (N) (i.e., the drift tube pressure). The choice of reduced electric field strength, E/N , affects the reaction dynamics in the drift tube because it influences the primary reagent ion signal, i.e., particularly the ratio of intensities of the hydronium ions to protonated water cluster signals, the drift time, the reagent ion-neutral collisional energy and the collisional induced dissociation of the product ions leading to their fragmentation. Maintaining an E/N ratio of 120 Townsends (Td), sum of the protonated water ion clusters are reduced to below 20% of the total reagent ion intensity in the drift tube both for dry and humidified air samples (Brown et al., 2010). Thus the protonated water cluster ions reaction with an OG in the drift tube is minimized. The PTR-ToF MS was operated with one second time resolution, a drift voltage (U_{drift}) of 550 V, a drift chamber temperature (T_{drift}) of 60°C, and a drift pressure (p_{drift}) of 2.2 mbar maintaining a reduced electric field (E/N) of ~ 120 Td during the experiments of this work (Kilic et al. 2017).

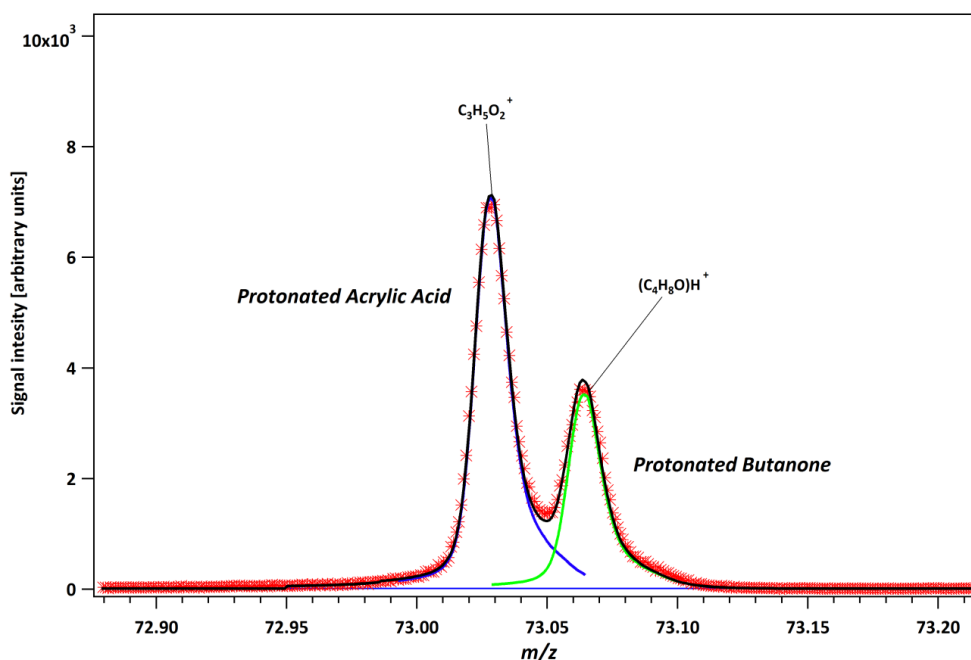


Figure 3-2: Separation of two OGs at the same integer m/z : Measured-ion signal of a gas sample containing acrylic acid (blue line) and butanone (green line) and modified-Gaussian fitted peaks (black line).

The PTR-ToF-MS also enables distinguishing of the individual ions at the same integer mass-to-charge (m/z) ratio. A small range in the mass spectrum obtained during aircraft emissions

experiment is presented in Figure 3-2. Two OGs occurring at the same integer m/z , acrylic acid and butanone, are accurately separated as shown in Figure 3-2. However, the PTR-ToF-MS cannot distinguish isomeric compounds, and spectral interpretations are complicated by ion fragmentation as discussed in Section 3.3.

3.2 Quantification of organic gases by PTR-ToF-MS

Tofware post-processing software (version 2.4.5, TOFWERK AG, Thun, Switzerland; PTR module as distributed by Ionicon Analytik GmbH, Innsbruck, Austria), running in the Igor Pro 6.3 environment (Wavemetrics Inc., Lake Oswego, OR, USA), was used for data analysis. Volume mixing ratios (ppbv) of the protonated OGs were calculated according to De Gouw and Warneke (2007) as shown in Eqn 3-1:

$$OG_{\text{ppbv}} = 1.657 \times 10^{-11} \times \frac{OG^+}{H_3O^+} \times \frac{U_{\text{drift}}[V]T_{\text{drift}}^2[K]}{k\left[\frac{\text{cm}^3}{\text{s}}\right]p_{\text{drift}}^2[\text{mbar}]} \times \frac{TR_{H_3O^+}}{TR_{OG^+}} \quad \text{Eqn 3-1}$$

Here OG^+ is the protonated OG molecule counts, H_3O^+ is the hydronium ion count (cps, counts per second), and $TR_{H_3O^+}$ and TR_{OG^+} are the hydronium and OG transmission coefficients (relative transmission efficiency), respectively. When available, reaction rate coefficients, k , measured by Cappelin et al. (2012) and Zhao and Zhang (2004), were used for the H_3O^+ -OG reaction. For species with no reported reaction rate coefficients, a rate coefficient of $2 \times 10^{-9} \text{ cm}^3/\text{s}$ was assumed (Table S4-2).

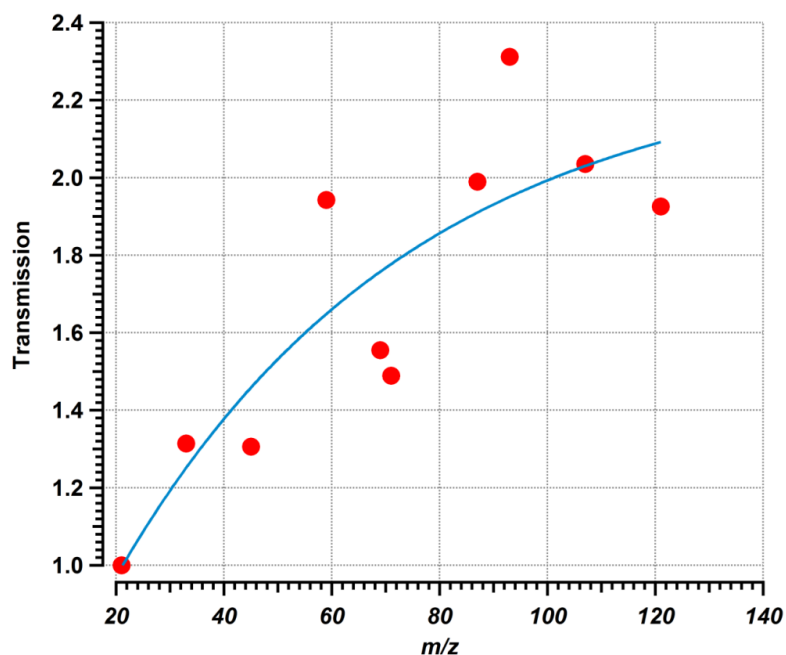


Figure 3-3: Transmission coefficient (TR_{OG^+}) of the reference compounds (red) and the fitted transmission function (blue line).

The transmission function is needed to calculate the m/z -dependent transmission coefficient (TR_{OG+}). The transmission function of the mass spectrometer was quantified using gas standards of 12 compounds (~100 ppbv each, see Table 3-1 for further details) with m/z 33 to 181 (Carbagas AG., Zurich, Switzerland). Figure 3-3 shows the individual transmission for these compounds and the curve fitted to estimate the m/z -dependent transmission function. Because the concentration of the reference compounds is equal and by assuming a transmission of 1 for reagent ion H_3O^+ , the transmission coefficient (TR_{OG+}) of each compound can also be calculated by using Eqn 3-1.

Table 3-1: Calibration gases and their abundance in the gas bottle.

Gas	Formula	m/z (protonated)	Mixing ratio (ppbv)
Methanol	CH ₄ O	33.034	100.3
Acetaldehyde	C ₂ H ₄ O	45.034	100.3
Acetone	C ₃ H ₆ O	59.049	100.0
Isoprene	C ₅ H ₈	69.070	99.3
Methacrolein	C ₄ H ₆ O	71.049	100.3
3-Pentanone	C ₅ H ₁₀ O	87.080	100.0
Toluene	C ₇ H ₈	93.070	100.3
p-Xylene	C ₈ H ₁₀	107.086	100.2
α-Pinene	C ₁₀ H ₁₆	137.132	99.9
1,3,5-Trimethylbenzene	C ₉ H ₁₂	121.101	99.9
1,2,4-Trichlorobenzene	C ₆ H ₃ Cl ₃	180.937	100.0

3.3 Fragmentation due to proton-transfer-reaction and limitations of PTR-ToF-MS

The proton-transfer-reaction takes place in the drift tube where the OG sample is introduced. The choice on operational setting leads to an E/N that influences the fragmentation of product ions due to the collision induced dissociation.

Due to the exothermic proton-transfer reaction, some intra-molecular bonds are broken in the drift chamber. This causes fragmentation of some compounds, influenced by E/N , and depending on the geometry of the molecules. Assignment of these fragment ions to the corresponding parent ions is required for an accurate quantification. A detailed fragmentation table for aldehydes using the current drift chamber conditions can be found in Klein et al. (2016). Additionally fragmentation patterns for alcohols (Brown et al., 2010),

aliphatic and aromatic HCs (Erickson et al., 2014; Gueneron et al., 2015), ketones, esters and other species (Buhr et al., 2002), sesquiterpenes (Kim et al., 2009) under the same chamber conditions have been reported previously.

Besides the fragmentation in the drift tube during proton-transfer-reactions, the PTR-ToF-MS does not detect OGs with a proton affinity lower than that of water, including alkanes with carbon numbers less than 8 and two alkenes (ethylene and acetylene). Therefore, the sum of all OG mixing ratios measured by PTR-ToF-MS is expected to be lower than the actual sum of OGs. Compounds not detected by the PTR-ToF-MS can be measured using alternative methods. Specifically, methane can be quantified by a flame ionization hydrocarbon detector, while undetected alkanes and alkenes can be quantified by gas chromatography mass spectrometry.

3.4 Detection of particulate matter by aerosol mass spectrometer (AMS)

A high-resolution time-of-flight aerosol mass spectrometer (HR-ToF-AMS) was used for the characterization of the aerosols. The HR-ToF-AMS uses flash thermal vaporization under high vacuum to volatilize aerosols, followed by electron ionization to ionize the resulting gas molecules and finally a mass spectrometer to analyze mass (DeCarlo et al., 2006).

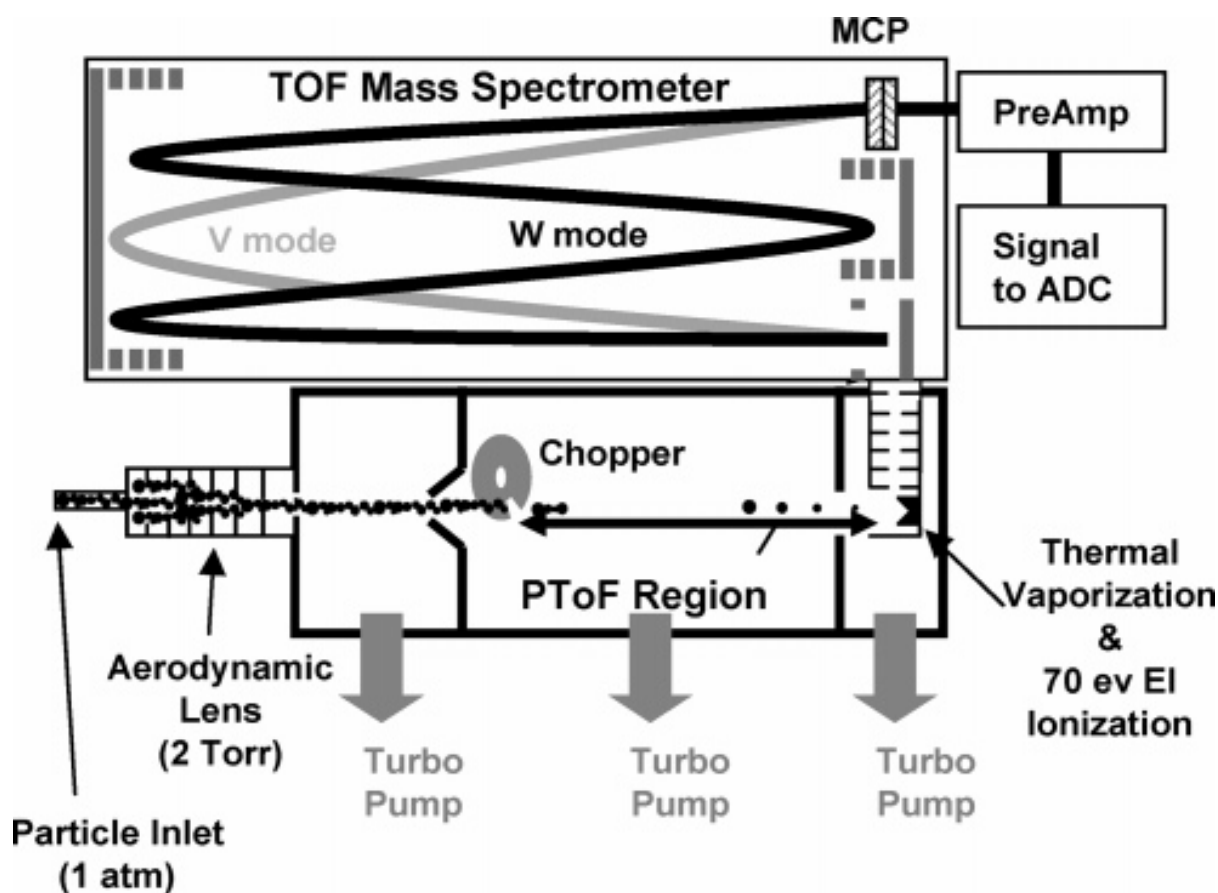


Figure 3-4: Schematic showing the main component of the AMS (DeCarlo et al., 2006).

Figure 3-4 shows the sample introduction system (particle inlet & aerodynamic lens), sizing region (PToF, particle time-of-flight region), vaporization and ionization, and mass quantification systems of the ToF mass spectrometer. A gas sample containing particles is pulled through a critical orifice into an aerodynamic lens, which generates a beam of particles (with a diameter smaller than 1 μm). After the lens the particles are accelerated into the sizing region (10^{-5} Torr) by a supersonic expansion, where particle size is determined by the particle flight time through the PToF-Region. Particle flight starts with passing a rotating mechanical chopper, and the end of the particle flight is defined as the time of mass spectrometric detection. Particles are vaporized by impaction at 600 $^{\circ}\text{C}$ and the resulting gas is ionized by electron ionization (70 eV). Only non-refractory particulate matter, which includes organic species and most atmospherically-relevant nitrate and sulfate salts, are vaporized and detected whereas coarse particles such as crustal material, sea salt, and refractory carbon, i.e. black carbon are not. The mass-to-charge ratios (m/z) of the fragments are determined by a high resolution, orthogonal ToF mass spectrometer (H-TOF Platform, Thun, Switzerland). The AMS was operated in the V-mode during the experiments, with a time resolution of 30 sec. The AMS data were analyzed using the SQUIRREL (version 1.52L) and PIKA (1.11L) analysis software in Igor Pro 6.3 (WaveMetrics Inc., Lake Oswego, OR, USA). Further details on mass quantification can be found elsewhere (DeCarlo et al., 2006).

3.5 Oxidative processing of organic gases

3.5.1 Potential Aerosol Mass (PAM) chamber

The Potential Aerosol Mass (PAM) chamber is a highly oxidizing flow tube used for the rapid oxidation of precursor gases to monitor aerosol formation mechanisms. The PAM uses much higher-than-ambient concentrations of oxidants (100 – 10000 times) to simulate days of atmospheric aging on experimental timescales of minutes.

The PAM operates under continuous flow conditions using a flow-through chamber with a volume of 13.3 liters. Two mercury lamps (emission lines at wavelength $\lambda=182\text{ nm} - 254\text{ nm}$, BHK Inc.), mounted inside the PAM, were used to irradiate HONO and O_2 for hydroxyl radical (OH) formation. The amount of the oxidants ozone (O_3), hydroxyl (OH), and hydroperoxyl (HO_2) can be controlled by varying the UV light and the relative humidity. HONO to boost OH concentrations, and D9-butanol (butanol-D9, 98%, Cambridge Isotope Laboratories) to trace OH exposure (Barmet et al., 2012), were injected with flows of 1.8 and 0.4 l min^{-1} , respectively. The PAM is also humidified ($\sim 20\%$) by injecting synthetic air with water vapor (with a flow of 1.6 l min^{-1}) in order to maintain the required H_2O concentration for OH formation. The ratios OH/ O_3 and HO_2 /OH in the PAM are similar to tropospheric values although the oxidant amounts are 100 to 1000 times larger than the daytime troposphere (Kang et al., 2007).

This PAM method was developed to measure the potential aerosol mass in the atmosphere, but is also used for examining SOA formation mechanisms in the laboratory and in environmental chambers. The aerosol production mechanism and the aerosol mass yield were studied for single precursors (Lambe et al., 2015) (e.g. α -pinene) and complex emissions e.g. from wood combustion (Bruns et al., 2015) in the PAM chamber and are similar to batch-style environmental chambers.

3.5.2 Experimental setup of the aging experiments

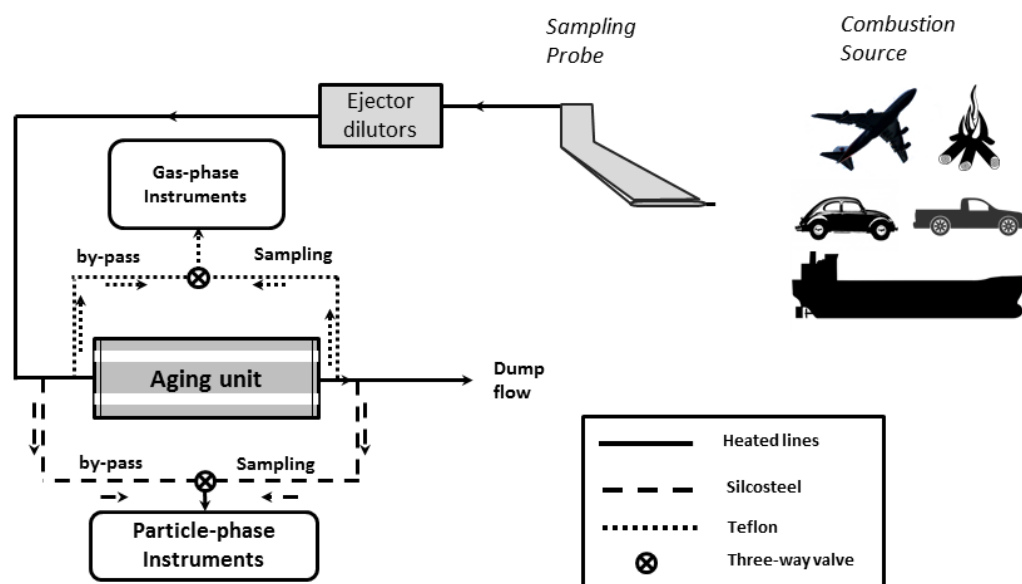


Figure 3-5: Simplified scheme of the experimental setup used for aging experiments.

Figure 3-5 shows a simplified version of the setup used during aging experiments and sampling of the combustion exhaust. The exhaust sample is pulled to the ejector dilutors (DEKATI DI-1000) with electrically heated lines (up to 120°C). The lines are heated to prevent condensation in the transfer lines. The sample is also usually diluted by 10-100 times with synthetic air (99.999% purity) to prevent extensive condensation inside the transfer lines or aging units and to bring pollutant concentrations down to instrument detectable levels (e.g. PTR-ToF-MS, HR-ToF-AMS). After dilution, the exhaust is first directed to a bypass line which is heated to the same temperature. Primary emissions are measured by bypassing the aging unit while secondary formation is measured after the aging unit (Figure 3-5). This aging unit can be portable e.g. a PAM or a portable smog chamber (SC) to conduct measurements especially when space is limited. Using SCs, however, the primary/secondary emissions are more easily separated by reaction coordinate (pre/post-lights on) rather than by a bypass lines.

For the measurement of the gaseous emissions Teflon transfer lines (6 mm \varnothing) are used as shown in Figure 3-5 due to their high chemical stability. However, Teflon is not the optimum

material for the sampling of the particles. Some particles losses may occur due to absorption i.e. ammonia (Kosmulski, 2001) in Teflon lines. To minimize particle losses in the transfer line, silcosteel lines are used with a minimum number of bends possible (Wang et al., 2002).

4 Characterization of gas-phase organics using proton transfer reaction time-of-flight mass spectrometry: aircraft turbine engines

Dogushan Kilic¹, Benjamin T. Brem^{2,3}, Felix Klein¹, Imad El-Haddad¹, Lukas Durdina^{2,3}, Theo Rindlisbacher⁴, Ari Setyan^{2,3}, Ru-Jin Huang¹, Jing Wang^{2,3}, Jay G. Slowik¹, Urs Baltensperger¹ and Andre S. H. Prevot¹

¹Laboratory of Atmospheric Chemistry, Paul Scherrer Institute, 5232 Villigen, Switzerland

²Laboratory for Advanced Analytical Technologies, Empa, 8600 Dübendorf, Switzerland

³Institute of Environmental Engineering, ETH Zurich, 8093, Zurich, Switzerland

⁴Federal Office of Civil Aviation, 3003 Bern, Switzerland

Published in Environmental Science & Technology, 2017, 51 (7), pp 3621–3629

Abstract

Non-methane organic gas emissions (NMOGs) from in-service aircraft turbine engines were investigated using a proton transfer reaction time-of-flight mass spectrometer (PTR-ToF-MS) at an engine test facility at Zurich Airport, Switzerland. Experiments consisted of 60 exhaust samples for seven engine types (used in commercial aviation) from two manufacturers at thrust levels ranging from idle to take-off. Emission indices (EIs) for more than 200 NMOGs were quantified, and the functional group fractions (including acids, carbonyls, aromatics, and aliphatics) were calculated to characterize the exhaust chemical composition at different engine operation modes. Total NMOG emissions were highest at idling with an average EI of 7.8 g/kg fuel and were a factor of ~40 lower at take-off thrust. The relative contribution of pure hydrocarbons (particularly aromatics and aliphatics) of the engine exhaust decreased with increasing thrust while the fraction of oxidized compounds, e.g. acids and carbonyls increased. Exhaust chemical composition at idle was also affected by engine technology. Older engines emitted a higher fraction of non-oxidized NMOGs compared to newer ones. Idling conditions dominated ground level organic gas emissions. Based on the EI determined here, we estimate that reducing idle emissions could substantially improve air quality near airports.

4.1 Introduction

Most emissions of non-methane organic gases (NMOGs) at airports come from aircraft turbine engines during flight-related operations (Kim, 2009). These emissions, including oxygenated species and both saturated and unsaturated hydrocarbons, potentially impact human health by inhibiting respiratory function or serving as precursors for ozone and secondary organic aerosol production, which has a variety of harmful effects (Ferry et al., 2011; Hallquist et al., 2009; Lai et al., 2012; Tunnicliffe et al., 1999; Westerdahl et al., 2008; Whelan et al., 2003). For example, NMOGs observed at airports include polycyclic aromatic hydrocarbons (PAHs) (Iavicoli et al., 2007), which have been identified as carcinogens in animal experiments and epidemiological studies (Armstrong et al., 2004; Negri & Vecchia, 2007), and may increase childhood obesity risk upon maternal exposure (Rundle et al., 2012). Air pollution from aircraft emissions is a concern not only within the airport itself but also in surrounding regions (Hudda et al., 2014; Unal et al., 2005). For example, hospital admissions for respiratory conditions were found to be significantly higher for residents living within five miles of three airports in New York State compared to those living farther than five miles away (Lin et al., 2008).

NMOG emission inventories are based on engine emissions certification data for an idealized landing and take-off cycle (LTO). The LTO defined by the International Civil Aviation Organization (ICAO) consists of four operating modes defined by thrust setting and time in each mode. These operating modes represent idling (7%), approach (30%), climb-out (85%), and take-off (100%), respectively. Engine emissions calculated with the LTO cycle are then used to verify that engines comply with regulatory emission limits. Although not originally intended for quantitative assessment of airport air quality, the ICAO LTO cycle and standard atmosphere emission factors are often used to generate airport emission inventories below 3000 ft (~915 m) (ICAO, 2011). Emissions of organic gases by aircraft engines are highest on the ground at low power settings (thrust <30%) (ICAO, 2008). Aircraft NMOG emissions decrease with increasing engine thrust by about two orders of magnitude (Anderson et al., 2006; Herndon et al., 2006; Knighton et al., 2007; Slemr et al., 2001; Spicer et al., 1994; Timko et al., 2010). Although ICAO suggests 7% thrust as a reference for idle and taxi operations, in practice aircraft operate between 2.5 and 7% thrust, depending on ambient conditions (Gerencher, 2005; Morris, 2005).

At low thrust, total hydrocarbon (HC) emissions are extremely sensitive to whether the engines are operated at the low or high end of the idling range. For example, compared to 7% thrust, HC emissions at 5% thrust could be 130% higher (Kim & Rachami, 2008). This variability in the idling conditions, as differences between measurement methods, has led to uncertainties of an order of magnitude in total HC EI (~1-10 g/kg fuel) reported in previous studies (Anderson et al., 2006; Herndon et al., 2006; Knighton et al., 2007; Slemr et al., 2001; Spicer et al., 1994; Timko et al., 2010; Yelvington et al., 2007). These previous studies have

indicated that additional measurements for engine thrust levels below 7% are required in order to better quantify and characterize the NMOG emissions from turbine engines.

Previous studies relied mostly on either offline measurements or sampling of only a few compounds from a single engine operated over a limited thrust range. Spicer et al. (1994) reported the mixing ratios of non-oxidized HCs (alkanes, alkenes, alkynes, aromatics) and some oxidized NMOGs (aldehydes and ketones) for varying thrust levels. Anderson et al. (2006) measured the non-methane HC relative contribution (%) by mass and number of carbons in each compound as a function of thrust. Beyersdorf et al. (2012) determined aldehydes and other selected oxygenated HCs as well as pure HCs at varying thrust levels corresponding to the LTO cycle. However, more comprehensive speciation and quantification of NMOGs emitted by aircraft are required in order to better understand, predict, and mitigate the impact of aircraft operations on local air quality.

In this study, more than 200 compounds measured online by using a high-resolution proton transfer reaction time-of-flight mass spectrometer (PTR-ToF-MS) for seven in-service aircraft turbine engine types at varying thrust settings. This study focuses particularly on the potential differences between the taxi mode emission factors obtained from ICAO emission certification and emission factors measured in the engine test cell at various low thrust conditions.

4.2 Experimental methods

4.2.1 Sampling setup

All measurements were conducted at the SR Technics engine test cell during July-October 2014. The emission measurements were performed on ten engines during engine maintenance inspection runs, utilizing seven engine types from two manufacturers (Table S4-1). Inspection runs typically consisted of a standardized thrust matrix including ten minutes of engine idle, a five-minute stepwise increase to take-off thrust and an additional 15-minute idling phase at the end, although the precise protocol depended on the maintenance service performed.

The engines were measured in a standard test configuration, meaning that they did not mechanically drive accessory loads and there was no compressor bleed air extraction during these tests. The thrust levels reported here correspond to measured static force produced by the engine corrected for ambient (temperature and pressure) and test cell (airflow) effects. The correction reference is the international standard atmosphere (ISA) at sea level (15°C, 1013.25 hPa). Due to variable ambient conditions on the different test days, the actual combustor conditions required to reach the same thrust in each experiment are slightly different, and this difference affects the emissions. Ambient conditions can be found in Table S4-1. In addition, we note that in-service engines were used for these tests, while

ICAO engine emission certification applies to the emission performance of a certain number of brand new engine specimens.

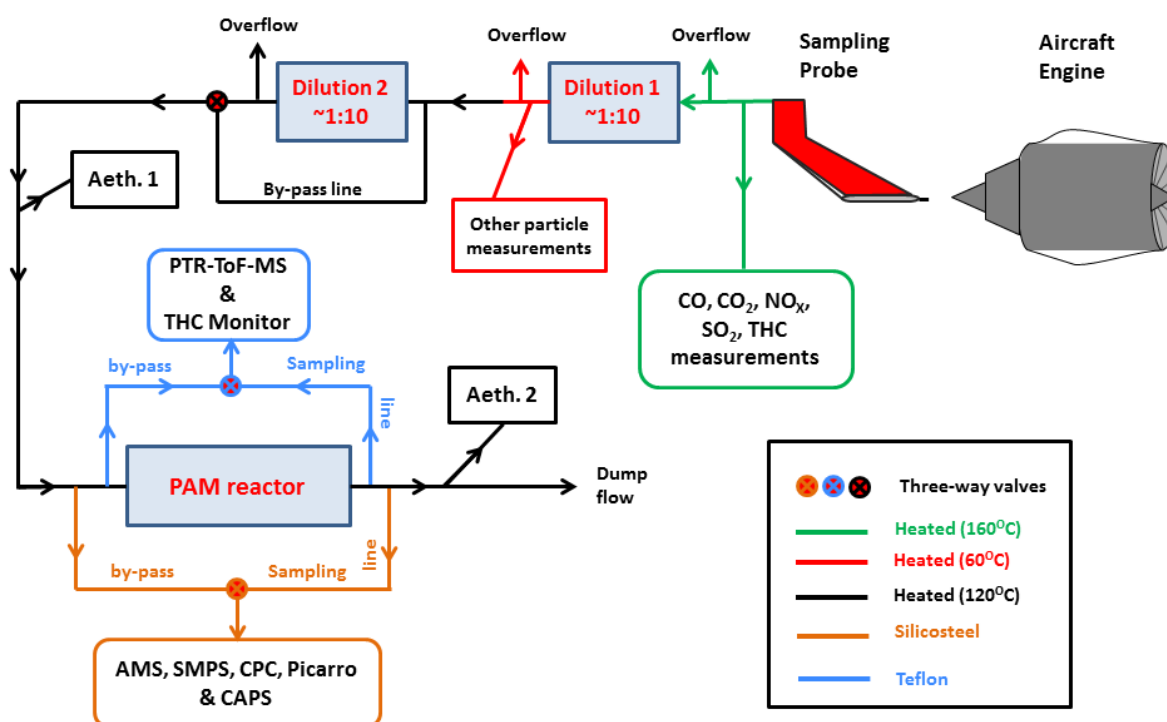


Figure 4-1: Simplified sketch of the experimental setup.

The measurement setup is shown in Figure 4-1. The aircraft engine exhaust was sampled by a single point 8 mm inner diameter probe located ~ 1.5 m downstream of the engine exit plane. The single point measurement has limitations in terms of representativeness of the entire exhaust in comparison with the ICAO certification measurement, where at least 12 sampling locations have to be used and carbon balance checks have to be performed. The location of the single point probe has been optimized to match expected CO_2 emissions at specific thrust settings for engine 1 (Table S4-1). The sampling flow was directed through a line heated to 160°C and diluted with synthetic air (99.999% purity) using two ejector dilutors (DEKATI DI-1000) to 1/10 for most of the tests and $\sim 1/100$ for idling tests (thrusts $\leq 7\%$). Sampling was then performed from 3 points: raw gas line (undiluted), diluted line, and aged-diluted line. CO , CO_2 , NO_x , and SO_2 were measured on the raw gas line with a multi-gas analyzer (PG250, Horiba Inc.).

Diluted emissions were sampled through lines heated to 120°C and used for the primary gas and particle measurements. A flame ionization hydrocarbon detector (APHA 370 THC Monitor) and a PTR-ToF-MS (discussed below) were used to quantify and characterize NMOG emissions. CO_2 , CO , CH_4 and H_2O mixing ratios were measured by a Picarro G2401 Cavity Ring-Down Spectroscopy (CRDS) analyzer. An Aerodyne high-resolution time-of-flight aerosol mass spectrometer (AMS) was used to measure the chemical composition of the

non-refractory submicron particles (NR-PM₁) (DeCarlo et al., 2006). Particle size and number distribution in the size range 20 to 640 nm were measured with a time resolution of 130 s by a scanning mobility particle sizer (SMPS), consisting of a neutralizer (Kr-85 source), a TSI-type PSI-built short differential mobility analyzer (DMA), and a TSI model 3772 condensation particle counter (CPC). Particle optical extinction (both absorption and scattering) was monitored by Cavity Attenuated Phase Shift Spectroscopy (CAPS, Particle Extinction Monitor, Aerodyne Research Inc.) (Kebabian et al., 2007). The concentration of optically absorbing particles for varying wavelengths was also measured before and after aging by two aethalometers (Magee Scientific Model AE33), denoted Aeth.1 and 2 in Figure 4-1 (Drinovec et al., 2015).

In addition, a potential aerosol mass (PAM) reactor was used to simulate emission aging, with a volume of 13.3 liters and a continuous flow of 7.6 l min⁻¹. Two mercury lamps (λ =182 nm) were used to irradiate O₂ for the formation of OH radical as a consequence (Bruns et al., 2015; Kang et al., 2007). Measurements of the aged exhaust including the secondary aerosol were conducted after passing the emissions through the PAM, while the primary emissions were measured by bypassing the PAM. Here only the gas phase emissions are presented while the primary and secondary aerosols will be discussed in a future publication.

4.2.2 PTR-ToF-MS

The PTR-ToF-MS (PTR-TOF 8000, Ionicon Analytik G.m.b.H.) quantifies organic gases (OG) having a higher proton affinity than water (Graus et al., 2010; Jordan et al., 2009). It consists of (i) a hollow cathode ion source where the hydronium ions (H₃O⁺) are produced from water, (ii) an ion transfer unit ("drift tube") where protonation of the OGs is achieved by OG-H₃O⁺ reaction and (iii) a time-of-flight mass spectrometer. H₃O⁺ from the ion source and sample containing OGs are pulled into the drift tube where proton transfer reactions occur between hydronium ions and OGs. Protonated OGs are directed to the time-of-flight mass spectrometer where the H₃O⁺ and positively charged OG molecules are extracted. The PTR-ToF MS was operated with one second time resolution, a drift voltage (U_{drift}) of 550 V, a drift chamber temperature (T_{drift}) of 60 °C, and a drift pressure (p_{drift}) of 2.2 mbar maintaining a reduced electric field (E/N) of ~120 Townsends (Td). Tofware post-processing software (version 2.4.5, TOFWERK AG, Thun, Switzerland; PTR module as distributed by Ionicon Analytik GmbH, Innsbruck, Austria), running in the Igor Pro 6.3 environment (Wavemetrics Inc., Lake Oswego, OR, USA), was used for data analysis. Volume mixing ratios (ppbv) of the protonated VOCs were calculated according to De Gouw and Warneke (2007) as shown in Eqn 4-1:

$$OG_{ppbv} = 1.657E-11 \times \frac{OG^+}{H_3O^+} \times \frac{U_{drift}[V]T_{drift}^2[K]}{k\left[\frac{cm^3}{s}\right]p_{drift}^2[mbar]} \times \frac{TR_{H_3O^+}}{TR_{OG^+}} \quad \text{Eqn 4-1}$$

Here OG^+ is the protonated OG molecule counts, H_3O^+ is the hydronium ion count, and $TR_{H_3O^+}$ and TR_{OG^+} are the hydronium and OG transmission coefficients, respectively. We used rate coefficients for the H_3O^+/OG reaction, k , measured by Cappelin et al. (2012). For species with no reported reaction rate coefficients, a rate coefficient of $2 \times 10^{-9} \text{ cm}^3/\text{s}$ was assumed (Table S4-2). The transmission function of the mass spectrometer was quantified using gas standards of 12 compounds (100 ppbv each) with varying mass-to-charge ratio (m/z) from m/z 33 to 181 (Carbagas AG., Zurich, Switzerland).

Due to the exothermic proton-transfer reaction, some intra-molecular bonds are broken during the chemical ionization in the drift chamber. This causes fragmentation of some compounds, depending on the chamber conditions and the functional groups in the molecules (Gueneron et al., 2015). Assignment of these fragment ions to the corresponding parent ions is important to for quantification. The EIs were corrected by accounting for this fragmentation. A detailed fragmentation table for aldehydes using the current drift chamber conditions can be found in Klein et al. (2016), and fragmentation patterns for other functional groups under similar chamber conditions are reported ($E/N \sim 120 \text{ Td}$) in other studies (Brown et al., 2010; Buhr et al., 2002; Erickson et al., 2014).

Identified peaks and their associated molecular formulas were determined based on high-resolution analysis and are given in Table S4-2 with their functional group-based classification (acids, alcohols, aliphatics, aromatics, carbonyls, unclassified hydrocarbon fragments, nitrogen and sulfur containing compounds, other oxygen containing compounds and unidentified peaks). Unclassified hydrocarbon fragments denote hydrocarbon fragments that cannot be unambiguously assigned to a parent ion. These include not only fragments of larger hydrocarbons (mostly molecules with a carbon number greater than five), but also from carbonyls or alcohols. The oxygen-containing molecules class consists of oxygen-containing ions whose molecular structure and/or parent ion is uncertain.

The PTR-ToF-MS does not detect OGs with a proton affinity lower than that of water, including most alkanes with carbon numbers less than 14 and two alkenes (ethylene and acetylene). Therefore, the total OG mixing ratios measured by PTR-ToF-MS were expected to be lower than the total NMOG concentration. Compounds not detected by the PTR-ToF-MS were measured using alternative methods. Specifically, methane was quantified by a flame ionization hydrocarbon detector (APHA 370 THC Monitor), while undetected alkanes and alkenes were quantified by gas chromatography/mass spectrometry.

4.2.3 Calculation of emission indices

NMOG mixing ratios were averaged for at least three minutes at stable engine conditions (Figure S4-1). The averaging periods began with the stabilization of the NMOG signal and lasted until the change of the thrust (Figure S4-1). NMOG emission indices were quantified on a fuel-consumption basis using carbon balance:

$$NMOG EI \left[\frac{g}{kg_{fuel}} \right] = \frac{NMOG}{C_{consumed}} \times \frac{M_{NMOG}}{M_C} \times Cf \quad \text{Eqn 4-2}$$

where $NMOG$ is the background-subtracted NMOG mixing ratio (ppbv), M_{NMOG} and M_C are the molecular weights of NMOG and carbon, respectively. Cf is the carbon fraction of fuel, calculated as 0.857, by analyzing the JET-A1 fuel hydrogen, carbon and nitrogen content (H:C molecular ratio of 1.99) based on ASTM D 5291 (ASTM, 1996) (Eqn 4-2).

$$Cf = \frac{M_C}{M_C + [1.99 \times M_H]} \quad \text{Eqn 4-3}$$

Here M_H is the molecular weight of hydrogen. The total carbon mixing ratio ($C_{consumed}$, ppbv C), was calculated as:

$$C_{consumed} = [CO_2 + CO + C_{NMOG}] \quad \text{Eqn 4-4}$$

The carbon contributions from CO and NMOGs were typically ~0.6% and <0.1%, respectively, except at thrust $\leq 5\%$ when both increased to the range of 10-15% and 3-5%, respectively.

Average NMOG (kg/LTO) emitted by aircraft during LTO cycle, were quantified based on ICAO suggested flight mode durations and fleet average fuel consumptions (Table S 4-3):

$$NMOG \left[\frac{kg}{LTO} \right] = \sum_{n=1}^4 \left(FC_n \left[\frac{kg_{fuel}}{sec} \right] \times NMOG EI_n \left[\frac{g}{kg_{fuel}} \right] \times FD_n [sec] \times \left[\frac{kg}{10^3 g} \right] \times N \right) \quad \text{Eqn 4-5}$$

where FC_n denotes the fuel consumption during one of four LTO flight modes, N is the number of engines operating and the FD_n is its duration.

4.3 Results and discussion

4.3.1 Dependence of total NMOG on operating mode

Figure 4-2 shows the NMOG EIs measured as a function of thrust for all experiments, separated by engine model. Figure 4-2 also shows this data reclassified into six thrust bins, corresponding approximately to the LTO operating modes. The thrust range below 8% was split into two bins to highlight the dependence of NMOG emissions on the specific idling conditions. Each NMOG EI in Figure 4-2 is the sum of all compounds quantified via PTR-ToF-MS per fuel consumed (an example mass spectrum is shown in Figure S4-2 for an idling test).

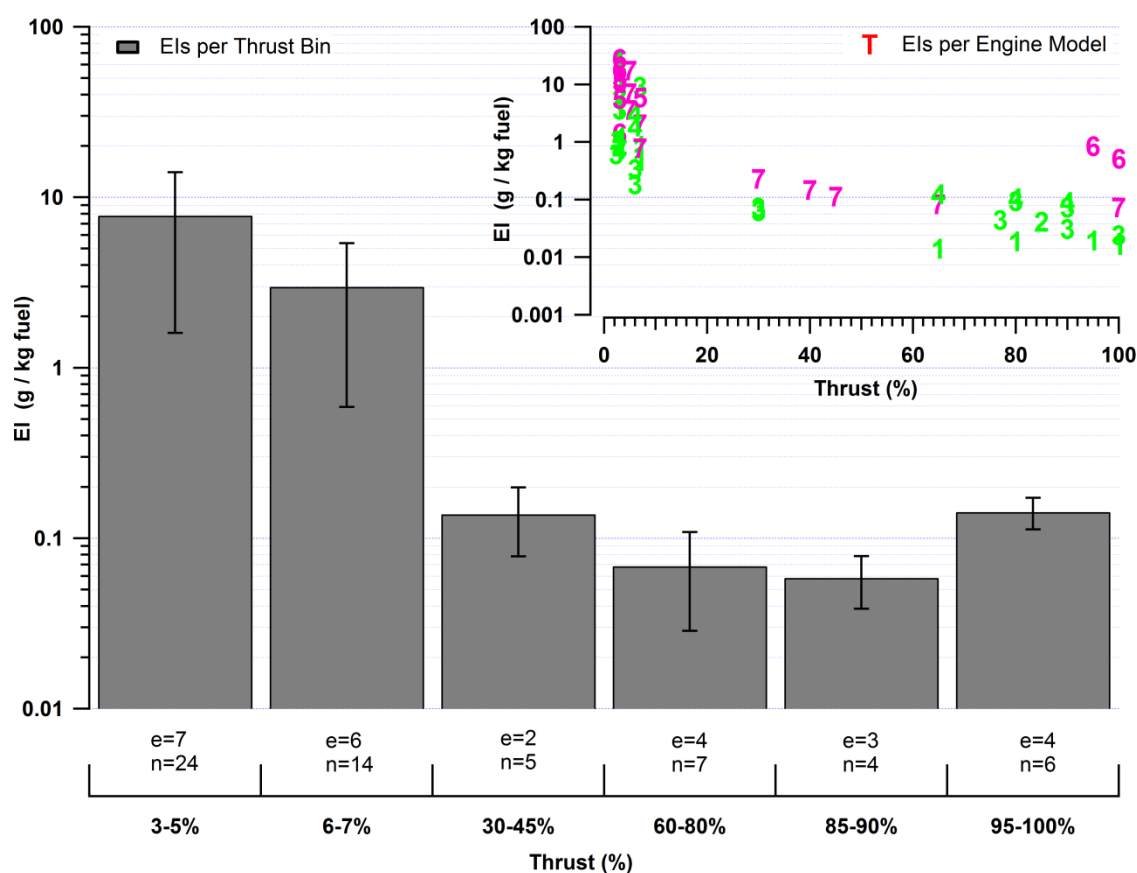


Figure 4-2: Mean total NMOG emission index (g/kg fuel) and standard deviation (CI: 95%) as a function of thrust for engines operated in the SR Technics test cell. “e” is the number of engines tested and “n” is the total number of tests at the designated thrust. Inset: NMOG EIs for individual measurements as a function of thrust, separated by engine model (numbers) and thrust rating (pink=engines of the higher thrust rating with a range of 244.6 – 311.4 kN, green= engines of the lower thrust rating with a range of 111.2 – 155.7 kN).

NMOG EIs at idling (thrust $\leq 7\%$) were much higher than in all other LTO flight modes (Figure 4-2). Further, average NMOG EIs observed at 2.5-5% (average ~ 7.8 g/kg fuel) were higher

than at 6-7%. It was previously proposed that reducing the ICAO standard idling thrust of 7% by 1% leads to a rise of the idling THC EI by ~60% (Kim & Rachami, 2008). Here, NMOG EI at thrust levels below 7% could be about three times higher than the ICAO standard idling thrust of 7%. The mean NMOG EI at a thrust of 7% and below 7% was about 2.9 and 7.8 g/kg fuel, respectively. Assuming a 7% thrust level for idling, as used in ICAO emission certification leads to an underestimated EI when actual (in-operation) thrust levels are lower than 7%.

Total NMOG emission was highest at idle with an average EI of 7.8 g/kg fuel and decreased with increasing thrust by a factor of ten at thrust of 30-45%, reaching 0.15 g/kg fuel at take-off thrust. The 60-100% thrust range had relatively constant EIs of ~0.1 g/kg fuel, with a slight increase at 95-100% thrust. This trend is consistent with expectations, as jet engines are optimized for the higher loads required for higher thrusts, and the combustion at these conditions is thus more efficient.

Compared to test cell conditions, installation of an engine in an operating aircraft can increase the load required up to 2.6% of the thrust to achieve a given thrust while using air bleed extraction. The increased power demand during real-world operation includes driving accessory loads like generators (for in-cabin demands) and compressor bleed air off-take for air conditioning or de-icing. Thus, while test cell measurements enable improved control over both engine thrust settings (engine stability at a given thrust) and sampling conditions (robustness, repeatability, removal of ambient factors such as wind speed), real-world engine emissions will correspond to a higher-than-expected test cell thrust. In the case of idle operation, where NMOG emissions decrease sharply with increasing load, Figure 4-2 represents a worst case for real-world operation at a given idle thrust setting (3-7%). Conversely, Figure 4-2 underestimates the emissions at higher-than-optimal thrust (e.g. take-off), but as the total NMOG emission factors at the highest thrusts are 1-2 orders of magnitude lower than idle and only a short time is spent at such conditions the effect of such an underestimation on near-airport air quality is expected to be small. Additionally, the average idle thrust during an aircraft taxi also depends on the number of stops and accelerations required to reach the runway or gate. This significantly increases uncertainty in aircraft emission indices and environmental impacts.

4.3.2 Dependence of NMOG Composition on Operating Mode

Figure 4-3 plots EIs and mass fractions of different compound classes for the investigated thrust bins. Carbonyls were the most abundant compound class in exhaust, comprising 39% of the total NMOG during idle (thrust $\leq 7\%$) with an EI of ~3 g/kg fuel. Hydrocarbons with a fraction of 38% were the second most abundant compound class in the exhaust for these idling thrust settings consisting of aliphatics, aromatics, and unclassified hydrocarbon fragments, which contributed 6.7%, 17.3%, and ~14%, respectively. Acids accounted for 9.2% of the total NMOG. The remaining 20% consisted of nitrogen containing compounds

(~5%), other oxygen containing compounds (~11%), alcohols (~3%) at idling. Moreover, there was a 1% fraction of sulfur containing compounds together with “unidentified” compounds quantified at all thrust settings.

Functional group EIs and mass fractions (derived from attribution of NMOGs shown in Table S4-2) indicate that the hydrocarbon fraction decreased with thrust while the oxygenated fraction increased, as shown in Figure 3. At low thrust levels (<8%) aromatics, as part of the HC fraction, accounted for ~17% of the total NMOG mass. This aromatic fraction decreased to ~8% of the total NMOG mass with an average EI of ~15 mg/kg fuel at take-off thrust. Similar to aromatics, the aliphatic fraction was also reduced to 3.8% at take-off from a fraction of ~7% at idle.

About 60% of the aromatic fraction by mass consisted of benzene derivatives. At thrust setting $\leq 7\%$, the most abundant benzene derivatives were from highest to lowest contribution C4-benzenes ($C_{10}H_{14}$), C3-benzenes (C_9H_{12}) benzene (C_6H_6), C2-benzenes (C_8H_{10}) toluene (C_7H_8) and C5-benzenes ($C_{11}H_{16}$), with mass fractions of 14%, 11%, 11%, 10%, 7% and 5% of the total aromatics, respectively. The remaining individual aromatic compounds contributing to the total aromatic fraction were styrenes (13%), polycyclic aromatics (6%), unspciated compounds with the formula $C_{11}H_{14}$ (3%) and other single-ring aromatic compounds with a carbon number higher than 11 (18%).

To evaluate whether gas-phase aromatics in the exhaust originate from the fuel aromatic content, the evaporation of JET-A1 fuel at room temperature (24°C) and pressure (970 hPa) was measured. The aromatic composition of the vapors was similar to idle emissions (see Figure S4-3), but contained less benzene and toluene. C4-benzenes, C3-benzenes, C2-benzenes and C5-benzenes were the top four most abundant aromatics measured in the fuel vapor, while benzene and toluene comprised only 1.5%. However, as benzene and toluene mixing ratios (ppbv) were ten times more abundant in the exhaust at idle relative to fuel vapor, they are likely formed as a result of the pyrolysis of other hydrocarbons in the engine combustion chamber (Erickson et al., 2014).

The mass fraction of the oxygenated species increased with engine thrust. Carbonyls dominated at each thrust level, ranging from 33% to 43% (by mass). Among the carbonyls, formaldehyde (CH_2O) and acetaldehyde (C_2H_4O) alone accounted for 5% and 8% of the total NMOG emission by mass, respectively. Although carbonyls were the most abundant species at each thrust level, the rise in the oxygenated fraction at thrust levels above 40% thrust was mostly due to the acids. The carboxylic acid fraction increased to 27% at take-off thrust from a fraction of ~10% at thrusts < 8% (Figure 4-3). Acetic ($C_2H_4O_2$) and formic (CH_2O_2) acid constituted ~61% and 31% of the acidic fraction at during idle, respectively. The fraction of $C_2H_4O_2$ and CH_2O_2 accounted for ~49% each when the thrust was increased to take-off thrust.

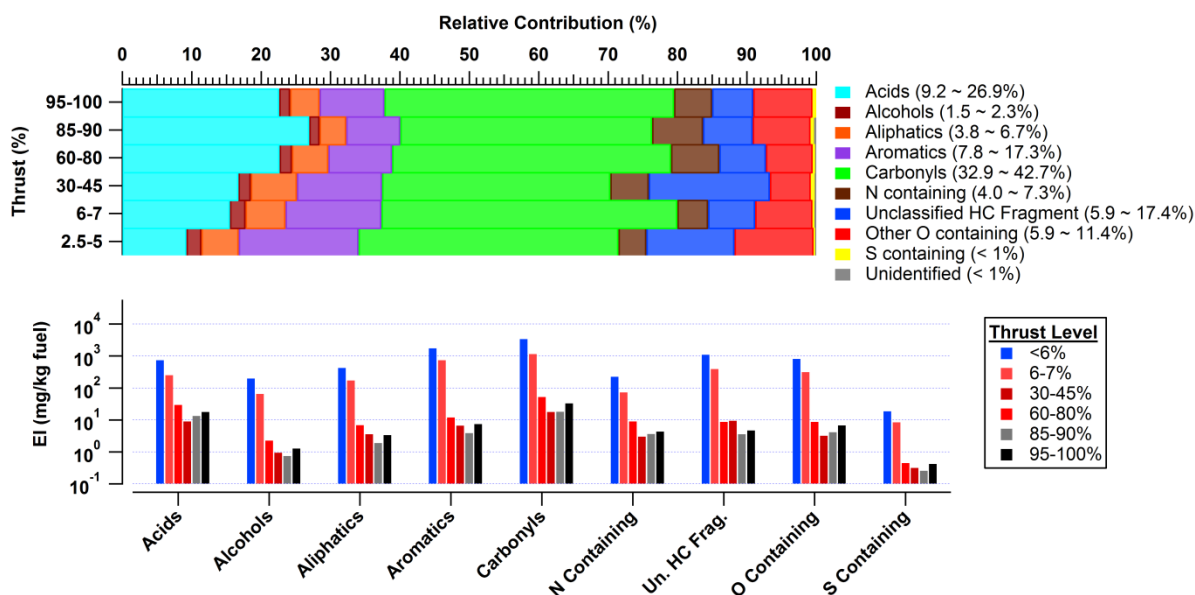


Figure 4-3: Mass fractions (%) of different compound classes presented as horizontal bars for the thrust bins (top panel). The emission indices of functional groups (in log scale) are shown in the bottom panel.

4.3.3 Dependence of NMOG composition on engine type at idling

The impact of thrust rating (engine size), last maintenance date and technology on NMOG emission was studied by estimating total NMOG EI and composition for idling as shown in Figure 4-2 and Figure 4-4, respectively. Figure 4-4 indicates the compound class fractions and EIs of the seven engines for the thrust settings $\leq 7\%$. The engines 1, 2, 3 and 4 were built by one manufacturer, and engines 5, 6, and 7, by another. Engines 5, 6 and 7 use at least a 10 years older technology compared to the others. This second set of engines also had higher maximum thrust rating, enabling them to generate greater thrust (Table S4-1). In addition, maintenance procedures varied from engine to engine. For example, engines 1, 5, 6 and 7 were tested without being refurbished. This engine refurbishment includes cleaning and/or renewal of the engine parts.

Engines 1, 5, 6 and 7 (non-refurbished engines) had higher total NMOG EIs on average during idling (See Figure 4-2, thrust $\leq 7\%$) compared to engines 2, 3 and 4 (refurbished). This may imply that the used engines emit higher NMOG at idle or the time in service – duration of use after last maintenance– may affect the total NMOG emission at idle. Engine 2 had the lowest idling-NMOG-EIs at idle as shown in Figure 4-4. However engine 2 also had fewer samples compared to other engines.

Corresponding differences were also observed in the NMOG composition. The HC fraction (sum of aliphatics, aromatics, unclassified HC fragments) of engines 6 and 7, with fractions of 39% and 40% respectively, were at least 3.5% higher compared to the engine 4 which had the third highest HC fraction among the engines tested with 35.5% (Figure 4-4 top panel).

Most of the variability in the HC fraction was due to the varying aromatic and aliphatic contribution. In addition to not being in the freshly maintained engine group (non-refurbished), engines 6 and 7 generate biggest take-off thrust and have bigger dimensions compared to other engines. This implies that engine thrust rating (maximum take-off thrust capacity) also affects exhaust chemical composition at idle.

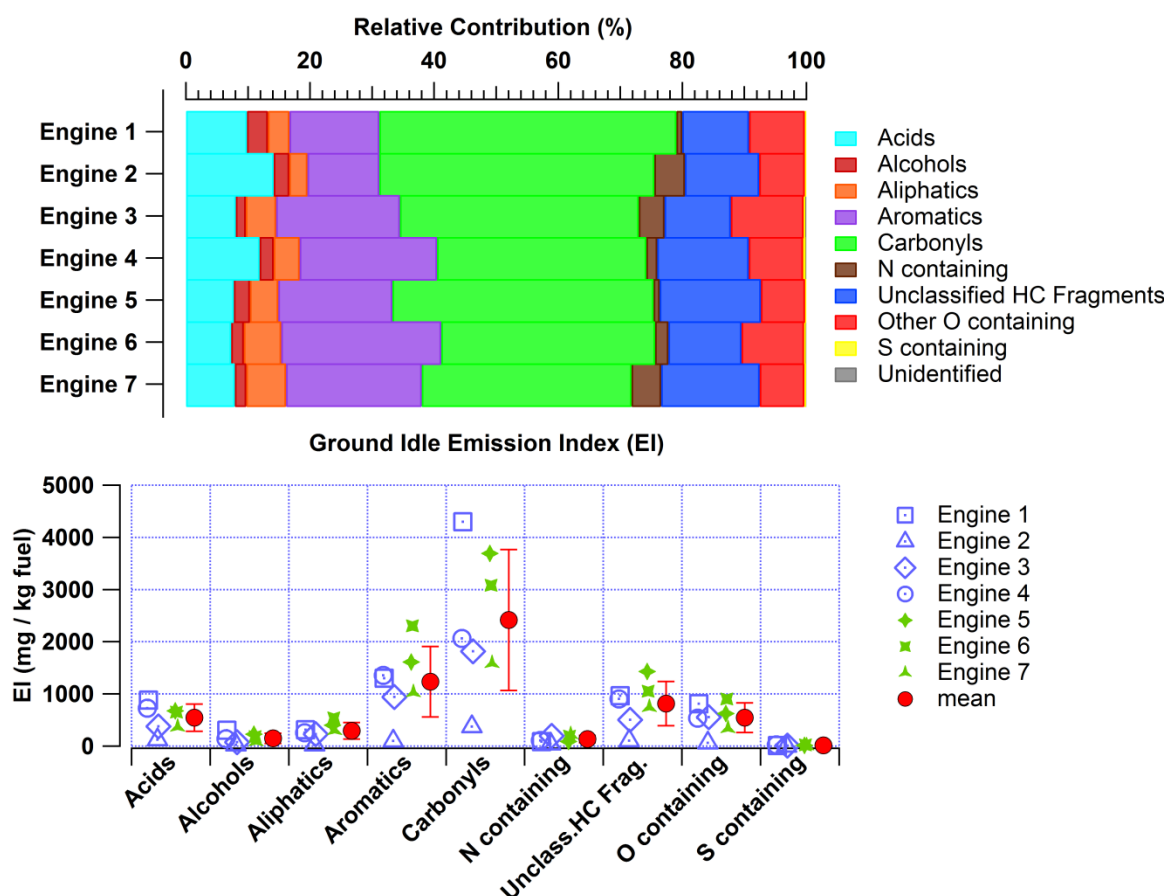


Figure 4-4: NMOG composition at idle for the different engines tested (top). The engines are sorted according to their thrust rating from lowest (top) to highest (bottom). Average idling (thrust $\leq 7\%$) EI of the different compound classes with the confidence interval (CI: 95%) are shown in the bottom panel. Blue markers denote engines within the thrust rating range of 111.2-155.7 kN, green markers those within the range of 244.6-311.4 kN.

4.3.4 Implications for ambient air quality

More than 90% by mass of aircraft NMOG emissions during an LTO cycle can be attributed to taxi-idle operation. Emissions from these conditions dominate because of both the high idling EIs observed during idling (Figure 4-2) and the large fraction of time spent by an aircraft in idling during near-airport operation; i.e., idling accounts for 26 minutes of the 33 minute standard LTO cycle (ICAO emissions certification procedure LTO cycle as shown in Table S 4-3).

LTO emissions for idling aircraft utilizing several engine operation protocols were calculated using Eqn 4-5. The amount of NMOGs emitted by each turbine engine installed was 0.56 kg/LTO when idling at 6-7% while this amount was elevated to 1.26 kg/LTO at idling <6% (Table S 4-3). Although all engine operation at $\leq 7\%$ thrust is nominally classified as taxi/idle, it was shown above that the precise thrust used has a major effect on the total NMOG emissions.

Currently, ICAO recommends 7% thrust to estimate aircraft NMOG emissions at the airport. Our LTO-based estimates, using test-cell EIs, indicate that this value may underestimate real emissions by up to $\sim 50\%$. Note that the magnitude of the difference in LTO emissions between 2.5-5% and 6-7% thrust levels is smaller than the EIs measured at these conditions (Figure 4-2) would indicate, since a lower fuel consumption rate is obtained at 2.5-5% (see Table S 4-3), partially offsetting the less efficient engine operation.

The NMOG emissions indices and NMOG composition reported in Figure 4-2 and Figure 4-3 can be used in conjunction with emission inventories to assess the impact of airports on local air quality. As a frame of reference, we compare aircraft emission factors at idle (which as discussed above govern near-airport emissions) to those measured from on-road vehicles during regulatory driving cycles. Here we use the emissions of benzene and other light aromatics measured, such as toluene and C2-C4 alkylated benzenes, as an example. Benzene and light aromatics account for 0.12 and 0.6 g/kg fuel of the total NMOG emission from an aircraft at idle (thrust 2.5-5%), respectively. Platt et al. (2014; 2017) compiled emissions from several types of on-road vehicles using the New European Driving Cycle (NEDC). The study reports 0.01 and 0.03 g/kg fuel for benzene and light aromatics, respectively from a new heavy-duty diesel vehicle (HDV), and 0.03 and 0.1 g/kg fuel for benzene and light aromatics, respectively for a light-duty Euro 5 gasoline vehicle (LDV). Compared to an HDV vehicle (during NEDC), an idling twinjet (aircraft powered by two engines) can emit up to 24 times more benzene and 40 times more light aromatics per kg fuel. Further, the same airliner at idle can emit 12 times more benzene and light aromatics compared to an LDV vehicle during NEDC. Given that aromatic compounds are linked with SOA formation (Ng et al., 2007), an international airport could be a major source of SOA for the regions nearby.

Due to the dominant contribution of idling emissions to total ground-level aircraft NMOG emissions, shut-down of half the aircraft engines at idle represents a potentially beneficial emission reduction strategy. This shut-down not only eliminates emissions from the deactivated engine, but increases the power load of the engines remaining in operation, which as shown in Figure 4-2 leads to more efficient operation and lower emissions per fuel consumed. For a twin-engine aircraft, operation of a single engine at idle increases the load by about 1.5 – 3% (Morris, 2005). For a four-engine aircraft, operation of only two engines at idle increases the load by about 1%. The effects of this shut-down on aircraft emissions from a single engine can be roughly estimated as a change from the 2.5-5% to 6-7% thrust

bins in Figure 4-2. As shown in Eqn 4-5, the total LTO emissions for an aircraft depend not only on EI, but also on the number of engines (N) in operation and the fuel consumption rate of each engine. Although operation of only a single engine increases the per engine fuel consumption (FC_n) at idle to 0.114 kg/sec from 0.09 kg/sec, NMOG emission ($NMOG\ EI$) decreases to 2.9 g/kg fuel from 7.8 g/kg fuel. We therefore estimate that average NMOG emission from a twinjet would decrease from 2.23 kg/LTO to 0.56 kg/LTO (approximately a factor of 4) when only a single engine is used during taxi/idle operations (Table S 4-3). This reduction in NMOG emission results from increased engine efficiency due to increasing engine power demand, as well as a decrease in the total fuel consumed. Therefore, engine shut-down at idling could improve air quality in the airport micro-environment because it may reduce NMOG emission from aircraft. However, this emission reduction only applies in practice if the aircraft does not use its auxiliary power unit when a reduced number of engines are operating. Other alternatives to reduce gaseous pollutant concentrations from aircraft could be the use of electric tow tractors, which reduce the idling duration.

Acknowledgements

Funding was provided by the Swiss Federal Office of Civil Aviation (FOCA). This project would not have been possible without the support of SR Technics personnel and Rene Richter (PSI). We thank Simone Pieber (PSI) for assistance with the sampling line configuration and Michel J. Rossi for his support during the identification of the compounds. Many individuals from SR Technics contributed to the project but we owe special thanks to those from the Maintenance and Test Cell Group. Key contributors included Frithjof Siegerist, Michael Weiner, and Burak Arpacioğlu. JGS acknowledges support from the Swiss National Science Foundation starting grant BSSGI0_155846.

4.4 Supplementary information

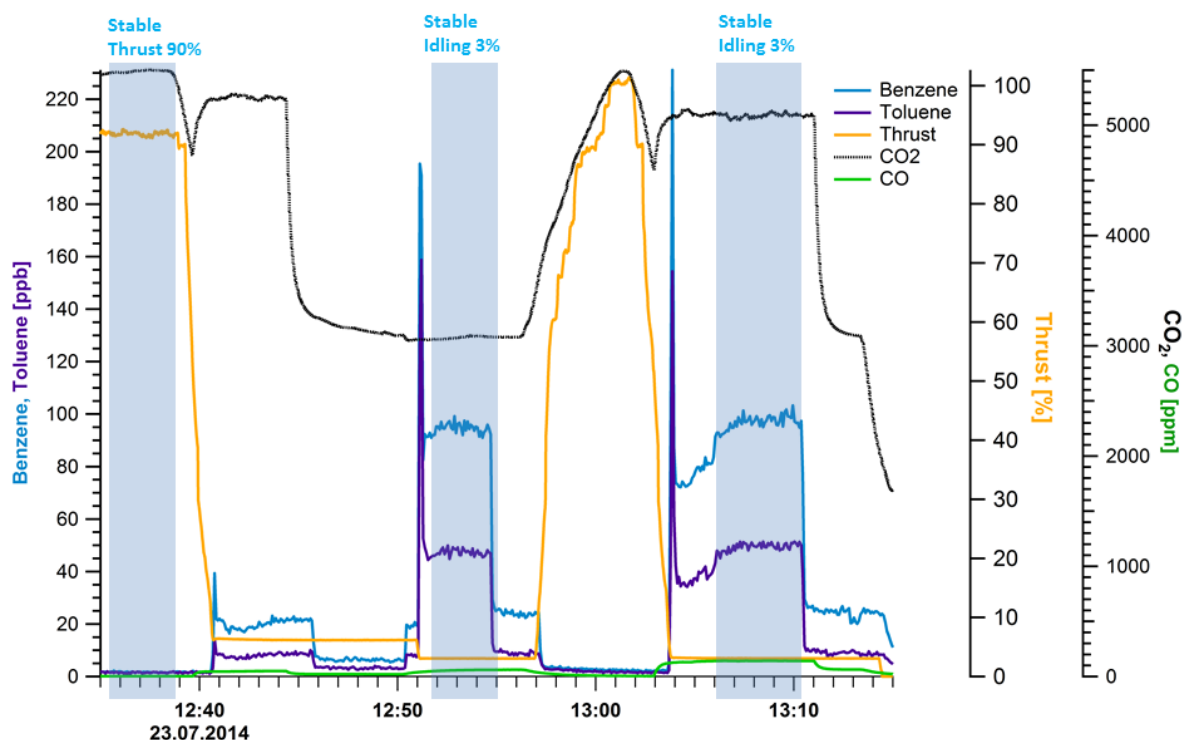


Figure S4-1: Time series data from the engine test performed on 23.07.2014 is given as an example. CO₂, CO (ppmC) measured from the raw gas line. Benzene and toluene mixing ratios (ppbv) were measured by the PTR-ToF-MS. The blue shaded regions highlight stable engine conditions (90% and 3% thrust). Only data from the stable periods (shaded areas) were used to estimate average EI. Such engine tests performed after maintenance services had shorter durations e.g. at most 10 minutes at a given thrust setting. Because of the short test durations, the NMOG signal was not stable in the unshaded regions. The durations of “dedicated engine tests”, performed in September-October 2014, were longer (at least 10 minutes at given thrust setting) compared to these technical checks.

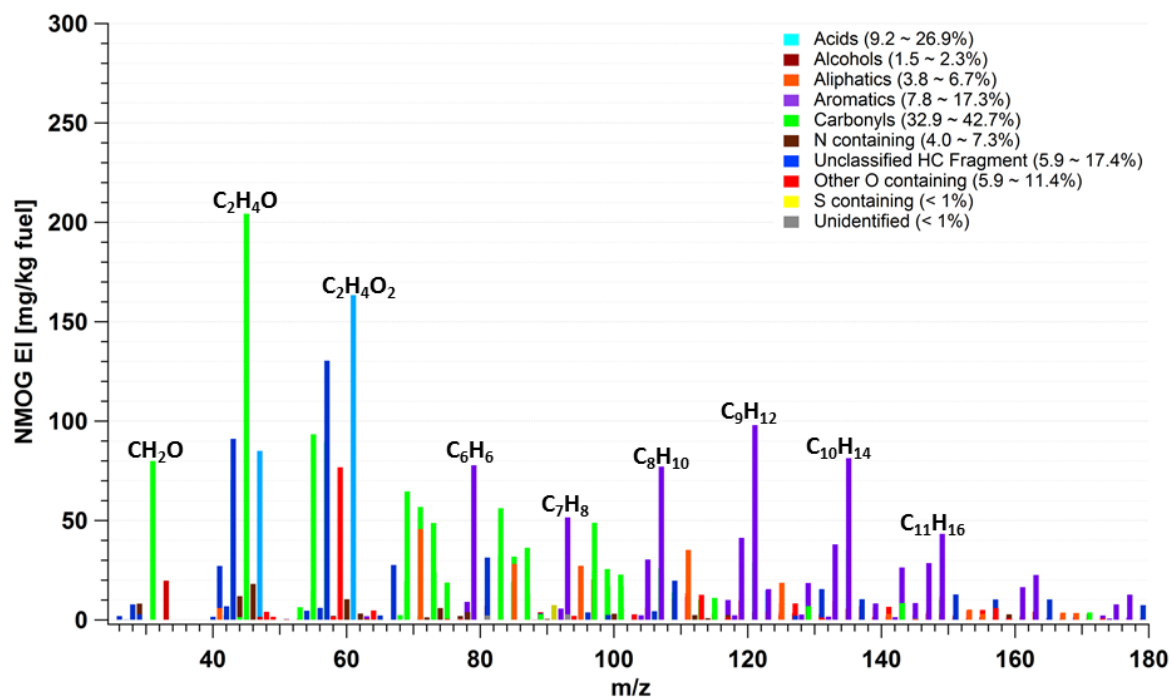


Figure S4-2: A sample PTR-ToF-MS mass spectrum at idling 5% for a turbine engine from July 2014.

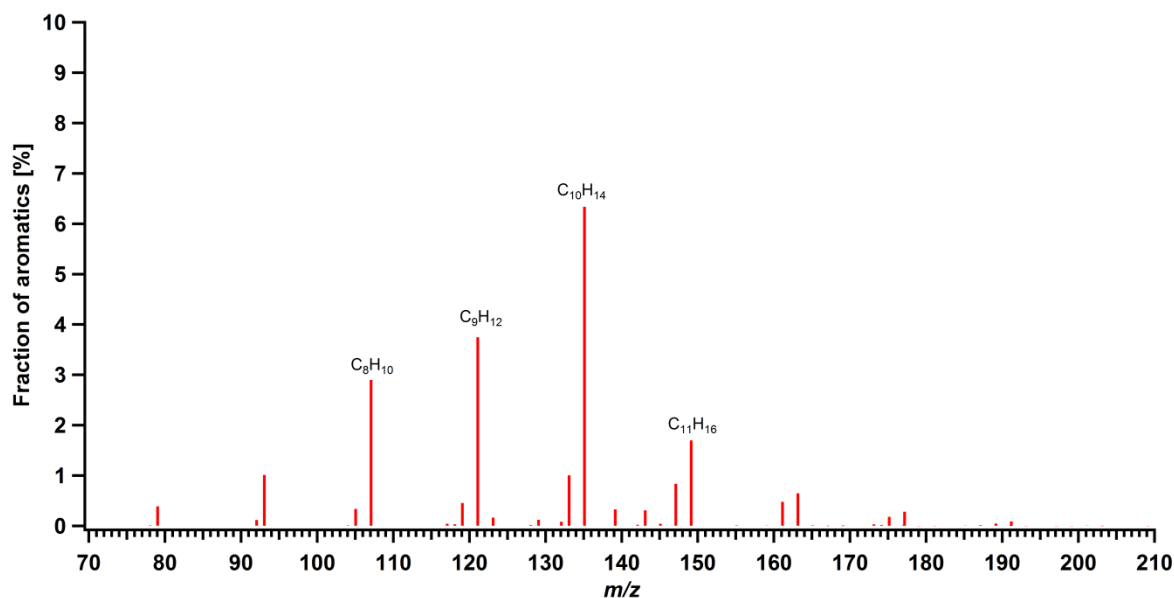


Figure S4-3: Molar fractions of aromatics during the fuel evaporation test at laboratory temperature (24°C). The four most abundant peaks were $C_{10}H_{14}$, C_9H_{12} , C_8H_{10} and $C_{11}H_{16}$ in JET-A1 fuel as shown by text on the mass spectrum.

Table S4-1: Engine test parameters.

Engine model	Thrust rating (kN)	Ambient temperature (°C)	Ambient pressure (hPa)
Engine 1	111.2-155.7	~13.0	958
		16.0-18.0	972
		17.0-20.0	979
Engine 2	111.2-155.7	~15.0	965
		19.0-23	972
Engine 3	111.2-155.7	24.3-27.0	972
Engine 4	111.2-155.7	22.3-24.6	965
Engine 5	244.6-311.4	~20.0	965
Engine 6	244.6-311.4	~19.0	965
Engine 7	244.6-311.4	17.0-21.0	972

Table S4-2: PTR-ToF-MS peak list (accounts for 95% of the total NMOG mass) including compound formula, molecular mass, corresponding functional group, the reaction rate constant for “NMOG+ H3O+” reaction from (Cappellin et al., 2012), and the average emission indices with the standard deviation (+/-) for varying thrust settings.

Compound Formula	m/z detected	Category	k rates [10 ⁻⁹ cm ³ /s]	Thrust Setting							
				3-5%		6-7%		30-45%		95-100%	
				Average EI [mg / kg fuel]	+/-	Average EI [mg / kg fuel]	+/-	Average EI [mg / kg fuel]	+/-	Average EI [mg / kg fuel]	+/-
C ₂ H ₅ O ⁺	45.034	Carbonyl	2	446	571.5	236.4	149.4	6.7	2.2	8.4	7.6
C ₂ H ₅ O ₂ ⁺	61.028	Acid	2.25	356.2	591.2	206.8	181.5	10.7	3	15.1	10.3
C ₄ H ₉ ⁺	57.070	Non-arom HC	1.8	282.9	456.3	101.7	92.4	20.4	15.5	4.2	1.6
C ₉ H ₁₃ ⁺	121.101	Aromatic	2.4	212.5	431.6	36.4	26.7	1.9	1.5	1.2	0.8
C ₄ H ₇ ⁺	55.054	Non-arom HC	1.76	202.5	348.7	55.7	36.9	1.9	1.2	2.8	1.5
C ₃ H ₇ ⁺	43.054	Non-arom HC	1.62	197.4	292.4	60.9	48.7	1.8	1.1	1.5	1.5
C ₃ H ₅ O ⁺	57.034	Carbonyl	3.55	193.6	335.3	80.3	70.6	0.7	0.1	0.9	0.6
CH ₃ O ₂ ⁺	47.013	Acid	1.99	184.3	255.5	147.3	134.3	11.2	1.1	15.9	13.1
C ₁₀ H ₁₅ ⁺	135.117	Aromatic	2	176.4	344.3	29.3	22.2	1.7	1.3	1.4	0.6
C ₃ H ₇ O ⁺	59.049	Carbonyl	3.32	173.5	240.2	90.7	70.3	9.7	6.4	7.6	7.7
CH ₃ O ⁺	31.018	Carbonyl	2.73	173.3	162.35	127.5	107.8	2.6	0.7	1.8	2.9
C ₆ H ₇ ⁺	79.054	Aromatic	1.93	188.3	349.1	46.6	33	0.5	0.3	0.5	0.4
C ₈ H ₁₁ ⁺	107.086	Aromatic	2.26	167.4	339.7	31.2	23.8	1.7	1.4	0.9	0.7
C ₂ H ₃ O ⁺	43.018	O-containing	3.12	152.7	194.1	83.3	54.2	4.1	1	6.6	6.4
C ₅ H ₉ ⁺	69.070	Non-arom HC	2.06	140.1	255.8	31.2	21.1	1.4	0.9	1.7	1
C ₄ H ₇ O ⁺	71.049	Carbonyl	3.3	123.2	220.2	44.2	36.6	0.7	0.2	1	0.6
C ₆ H ₁₁ ⁺	83.086	Non-arom HC	2.08	121.8	227.2	25.6	17.3	2.5	1.8	2.5	1.1
C ₇ H ₁₃ ⁺	97.101	Non-arom HC	2.09	114.2	216.8	26.2	24.4	2.3	1.9	1.4	0.8

(Table S4-2 continued)

Compound Formula	m/z detected	Category	k rates [10 ⁻⁹ cm ³ /s]	Thrust Setting							
				3-5%		6-7%		30-45%		95-100%	
				Average EI [mg / kg fuel]	+/-	Average EI [mg / kg fuel]	+/-	Average EI [mg / kg fuel]	+/-	Average EI [mg / kg fuel]	+/-
C ₇ H ₉ ⁺	93.070	Aromatic	2.08	111.9	217.5	27.6	20.6	2.1	1.7	1.5	2
C ₃ H ₅ O ₂ ⁺	73.029	Carbonyl	2	105.8	159.8	56	60.6	2.2	0.5	3.3	1.8
C ₅ H ₁₁ ⁺	71.086	Alkene	1.9	99.1	179.6	17.9	11.3	1.4	1	1	0.6
C ₁₁ H ₁₇ ⁺	149.133	Aromatic	2	93.8	180.7	15.9	11.5	1.1	0.8	0.8	0.4
C ₉ H ₁₁ ⁺	119.086	Aromatic	2	89.4	187.6	15.9	9.5	0.4	0.3	0.5	0.2
C ₁₀ H ₁₃ ⁺	133.101	Aromatic	2	82.4	171.3	12.8	8	0.5	0.4	0.5	0.3
C ₄ H ₇ O ₂ ⁺	87.044	Carbonyl	1.7	78.7	117.8	37.5	40.7	1.9	0.7	2.8	1.4
C ₈ H ₁₅ ⁺	111.117	Alkyne	2	76.4	148.4	12.4	9	1.5	1.2	0.9	0.5
C ₉ H ₁₁ O ⁺	135.080	Carbonyl	2	76.1	174.1	19.3	14.6	0.6	0.4	0.6	0.6
C ₃ H ₅ ⁺	41.039	Alkene	2	71.6	47.5	59.2	44.3	1.9	1.1	2.1	2.7
C ₅ H ₇ O ⁺	83.049	Carbonyl	2	69.9	140.2	20.8	15.7	0.3	0.2	0.5	0.3
C ₅ H ₉ O ⁺	85.065	Carbonyl	2.2	69	125.6	19.9	16.1	0.6	0.3	1.4	0.9
C ₆ H ₉ ⁺	81.070	Non-arom HC	2	67.9	127.2	12.4	7.7	0.8	0.6	0.8	0.6
C ₈ H ₉ ⁺	105.070	Aromatic	2.27	65.9	136.5	13.4	8.4	0.3	0.2	0.4	0.3
C ₆ H ₇ O ⁺	95.049	Alcohol	2	62.9	142.9	20.3	13.6	0.9	0.6	1	0.9
C ₈ H ₉ O ⁺	121.065	Carbonyl	3.48	62.3	138.6	19.6	14.7	0.4	0.2	0.4	0.4
C ₁₁ H ₁₅ ⁺	147.117	Aromatic	2	61.9	124.5	9.6	6.4	0.7	0.5	0.5	0.3
C ₆ H ₁₃ ⁺	85.101	Alkene	2.04	61.1	114	10	6.4	0.8	0.6	0.6	0.3
C ₅ H ₇ ⁺	67.054	Non-arom HC	1.83	59.8	112.9	11.4	7.6	0.2	0.2	0.3	0.3
C ₇ H ₁₁ ⁺	95.086	Alkane (fragment)	2	59	107.7	10.7	6.5	0.9	0.7	0.6	0.4
C ₁₁ H ₁₁ ⁺	143.086	Aromatic	2	57.2	114.5	16	16.7	0.8	0.5	0.8	0.6
C ₇ H ₇ O ⁺	107.049	Carbonyl	3.82	56.3	111.9	22.2	17.9	0.8	0.3	0.7	0.4
C ₄ H ₃ O ₃ ⁺	99.008	Carbonyl	2	55.5	71.6	47.7	78.7	2	0.6	4.1	3.8
C ₆ H ₉ O ⁺	97.065	Carbonyl	2	53.1	110.1	13.2	10.2	0.3	0.2	0.5	0.3
C ₄ H ₉ O ⁺	73.065	Carbonyl	3.2	51.8	77.2	27.5	25.8	2	1.2	5.4	7.5
C ₄ H ₅ O ₃ ⁺	101.023	Carbonyl	2	49.5	70.9	31.6	48	2	0.3	3.6	1.6
C ₁₂ H ₁₉ ⁺	163.148	Aromatic	2	49	93.7	8.6	6.6	0.7	0.5	0.5	0.4
C ₄ H ₅ O ⁺	69.034	Carbonyl	1.7	47.1	84.5	17.3	12.3	0.3	0.1	0.5	0.3
C ₅ H ₅ O ₂ ⁺	97.028	O-containing	2	44	85.4	22.3	22.6	0.5	0.2	1.2	0.9
C ₈ H ₁₃ ⁺	109.101	Non-arom HC	2	42.8	79.1	7.3	4.7	0.5	0.4	0.4	0.3
CH ₅ O ⁺	33.034	Alcohol	2.22	42.7	40	32	26.4	1.2	0.3	0.8	1.2
C ₄ H ₅ O ₂ ⁺	85.028	O-containing	2	41.6	79.5	19.3	18.4	0.5	0.2	1	0.6
C ₃ H ₇ O ₂ ⁺	75.044	Carbonyl	2.41	40.7	70.1	17.9	14	1.1	0.2	2	1.1
C ₉ H ₁₇ ⁺	125.133	Alkyne	2	40.5	79.6	6.1	4.5	0.7	0.5	0.4	0.2
C ₁₀ H ₉ ⁺	129.070	Aromatic	2.45	40.2	76.4	12.8	11.6	0.3	0.1	0.3	0.1
CH ₄ NO ⁺	46.029	N-containing	2	39.3	58.5	19.6	28.7	1.2	0.3	1.2	0.5

(Table S4-2 continued)

Compound Formula	m/z detected	Category	k rates [10 ⁻⁹ cm ³ /s]	Thrust Setting							
				3-5%		6-7%		30-45%		95-100%	
				Average EI [mg / kg fuel]	+/-	Average EI [mg / kg fuel]	+/-	Average EI [mg / kg fuel]	+/-	Average EI [mg / kg fuel]	+/-
C ₅ H ₉ O ₂ ⁺	101.060	Carbonyl	2.2	36.3	60.5	16.1	16.1	1.1	0.5	1.9	1.2
C ₆ H ₁₁ O ⁺	99.080	Carbonyl	3.8	35.8	68.1	15.7	12	1.6	0.9	3.9	2.3
C ₁₂ H ₁₇ ⁺	161.133	Aromatic	2	35.7	70.7	6.1	4.6	0.5	0.4	0.4	0.3
C ₉ H ₁₅ ⁺	123.117	Non-arom HC	2	33.7	62.6	5.4	3.7	0.3	0.2	0.3	0.2
C ₁₀ H ₁₁ ⁺	131.086	Non-arom HC	2	33.6	74.5	4.4	2.6	0.1	0.1	0.1	0.1
C ₇ H ₇ O ₂ ⁺	123.044	Acid	2	32	74	10.1	7	0.3	0	0.4	0.2
C ₃ H ₃ O ⁺	55.018	Carbonyl	2	32	47.7	12	8.1	0.1	0	0.3	0.3
C ₆ H ₅ O ₂ ⁺	109.028	Carbonyl	2	29.5	53.4	11	11	0.2	0.1	0.4	0.2
C ₇ H ₁₁ O ⁺	111.080	O-containing	2	29	61.4	6.6	5.5	0.1	0.1	0.2	0.1
C ₅ H ₁₁ O ⁺	87.080	Carbonyl	2.3	28.3	45.5	10.4	9.5	0.8	0.6	1.1	0.5
C ₁₁ H ₁₉ ⁺	151.148	Non-arom HC	2	27.7	51.6	4.8	3.4	1	0.9	0.4	0.3
C ₁₃ H ₂₁ ⁺	177.164	Aromatic	2	27.6	53	5.7	5.1	0.5	0.4	0.4	0.3
C ₇ H ₁₃ O ⁺	113.096	Carbonyl	2	27.2	52.4	6.2	5	0.3	0.2	0.4	0.2
CH ₂ NO ⁺	44.014	N-containing	2	25.8	38.6	14.6	19.4	0.7	0.1	1.1	1
C ₁₀ H ₁₃ O ⁺	149.096	Carbonyl	2	25.6	57.1	7.3	6.2	0.3	0.2	0.4	0.3
C ₆ H ₇ O ₂ ⁺	111.044	O-containing	2	24.9	53.3	9.1	8.7	0.2	0.1	0.3	0.2
C ₆ H ₁₁ O ₂ ⁺	115.075	Carbonyl	2	24.1	42.2	8.7	8.7	0.5	0.2	0.8	0.4
C ₂ H ₆ NO ⁺	60.044	N-containing	2	22.6	39.3	9.1	16.3	0.3	0.1	0.5	0.4
C ₁₀ H ₁₇ ⁺	137.133	Non-arom HC	2.44	22.4	41.2	4	2.6	0.5	0.4	0.2	0.2
C ₁₂ H ₂₁ ⁺	165.164	Non-arom HC	2	22.4	41.2	3.9	2.8	0.7	0.6	0.4	0.2
C ₁₂ H ₁₃ ⁺	157.101	Aromatic	2	22.3	44.7	6.1	6.2	0.4	0.2	0.5	0.4
C ₇ H ₉ O ⁺	109.065	Alcohol	2.3	22	50.7	5.9	4	0.3	0.2	0.4	0.4
C ₅ H ₅ O ₃ ⁺	113.023	Carbonyl	2	22	31.8	13.3	19	0.4	0.1	0.8	0.4
C ₈ H ₅ O ₃ ⁺	149.023	O-containing	2	21.9	41.7	16.8	22.8	0.9	0.9	2.1	2
C ₉ H ₉ ⁺	117.070	Aromatic	2.43	21.6	47.4	3.5	2.1	0.1	0	0.1	0
C ₈ H ₇ O ⁺	119.049	O-containing	2	21.1	40.8	6.1	4.2	0.1	0.1	0.1	0.1
C ₉ H ₉ O ⁺	133.065	O-containing	2	20.6	46.1	5.4	3.9	0.2	0.1	0.2	0.1
C ₈ H ₁₃ O ⁺	125.096	O-containing	2	18.4	38.9	4.2	3.5	0.1	0.1	0.2	0.1
C ₉ H ₁₉ O ⁺	143.143	Carbonyl	2	18.4	37.4	5.4	5.2	0.3	0.2	0.5	0.3
C ₁₁ H ₁₃ ⁺	145.101	Aromatic	2	18.4	37	2.9	2.2	0.2	0.1	0.1	0.1
C ₈ H ₁₅ O ⁺	127.112	O-containing	2	18	36.2	4	3.3	0.2	0.1	0.3	0.1
C ₁₀ H ₁₉ ⁺	139.148	Non-arom HC	2	18	34.6	2.9	2.2	0.5	0.5	0.2	0.1
CH ₃ N ⁺	29.026	N-containing	2	17.8	20.3	17.1	21.2	1.3	0.1	1.6	1.5
C ₇ H ₁₅ O ⁺	115.112	Carbonyl	2	17.7	31.8	5.9	4.9	0.6	0.4	0.8	0.4
C ₂ H ₄ ⁺	28.031	Non-arom HC	2	16.9	14	11.8	9.6	0.1	0	0.1	0.1
C ₁₃ H ₁₉ ⁺	175.148	Aromatic	2	16.9	33.1	3.5	3	0.4	0.3	0.3	0.3

(Table S4-2 continued)

Compound Formula	m/z detected	Category	k rates [10 ⁻⁹ cm ³ /s]	Thrust Setting							
				3-5%		6-7%		30-45%		95-100%	
				Average EI [mg / kg fuel]	+/-	Average EI [mg / kg fuel]	+/-	Average EI [mg / kg fuel]	+/-	Average EI [mg / kg fuel]	+/-
C ₈ H ₁₁ N ⁺	121.089	N-containing	2	16.6	21.6	4.9	6.4	0.2	0.1	0.3	0.2
C ₆ H ₉ O ₂ ⁺	113.060	Carbonyl	2	16.6	31.6	5.8	5.6	0.2	0.1	0.4	0.2
C ₄ H ₁₁ S ⁺	91.058	S-containing	2	16	33.2	6.3	4.5	0.8	0.5	0.7	0.6
C ₁₃ H ₂₃ ⁺	179.179	Non-arom HC	2	16	29.1	3	2.5	0.4	0.3	0.2	0.1
C ₅ H ₅ O ⁺	81.034	O-containing	2	15.1	30.1	4.2	3	0.1	0	0.2	0.1
C ₈ H ₉ O ₂ ⁺	137.060	O-containing	2	15.1	36.5	4	2.8	0.1	0	0.2	0.1
C ₈ H ₁₇ O ⁺	129.127	Carbonyl	2	15	28.7	4.7	3.9	0.4	0.2	0.5	0.2
C ₃ H ₆ ⁺	42.046	Non-arom HC	1.62	14.9	17.7	4.4	2.8	0.1	0	0.1	0.1
C ₉ H ₁₇ O ⁺	141.127	Carbonyl	2	14.2	29.5	3	2.6	0.1	0.1	0.1	0.1
C ₃ H ₅ N ⁺ /C ₂ H ₃ N ₂ ⁺	55.039	N-containing	2	13.9	42.2	4.7	3.9	1.6	0.8	1.5	1
C ₄ H ₅ ⁺	53.039	Carbonyl	2	13.7	23.7	3.9	2.8	0	0	0	0
C ₉ H ₁₅ O ⁺	139.112	Carbonyl	2	13.5	28.2	2.9	2.4	0.1	0.1	0.2	0.1
C ₇ H ₅ O ⁺	105.034	O-containing	2	13.4	22.1	4.8	4.4	0.1	0.1	0.2	0.2
C ₆ H ₁₃ O ⁺	101.096	Carbonyl	3.35	13.2	22.5	5.2	4.1	0.6	0.4	0.7	0.3
C ₄ H ₈ ⁺	56.062	Non-arom HC	1.8	13.1	14.3	4.4	2.3	1	0.8	0.6	0.8
C ₇ H ₇ ⁺	91.050	Aromatic	2	12.9	22	4.4	3.8	0.6	0.4	0.6	0.5
C ₁₀ H ₂₁ O ⁺	157.159	O-containing	2	12.9	28.1	2.8	2.8	0.1	0.1	0.2	0.1
C ₂ H ₄ NO ₂ ⁺	74.024	N-containing	2	12.9	20.1	6.5	9.3	0.5	0.1	0.8	0.4
C ₇ H ₁₃ O ₂ ⁺	129.091	Acid	2	12.7	23.1	4.3	4.4	0.2	0.1	0.4	0.3

Table S 4-3: ICAO reference thrust levels and average fuel consumption per engine at different operating modes (ICAO, 2011).

Operating Mode	Thrust Setting (%)*	Fuel Consumed (kg/sec)	Average Duration (minutes)	EI (g/kg fuel)	EI (kg/LTO)
Take-off	100	0.946	0.7	0.13	0.005
Climb	85	0.792	2.2	0.05	0.005
Approach	30	0.29	4	0.13	0.01
Taxi-Idle	6-7 / 3-5	0.114 / 0.09**	26	2.9 / 7.8	0.52 / 1.22
Total NMOG per LTO for Twinjet (idling 3-5%):					2.23
Total NMOG per LTO by single-engine use at idle 3-5%:					1.26
Total NMOG per LTO by single-engine use at idle 6-7%:					0.56

* % of the take-off thrust, **fuel consumption is ~18-50% less at idling power setting 2.5-5% depending on the thrust setting compared to 7% (Kim & Rachami, 2008).

5 Identification of secondary precursors emitted by an aircraft turbofan

Dogushan Kilic¹, Imad El Haddad¹, Benjamin T. Brem^{2,5}, Emily Bruns¹, Carlo Bozetti¹, Joel Corbin¹, Lukas Durdina^{2,5}, Ru-Jin Huang¹, Jianhui Jiang¹, Felix Klein¹, Avi Lavi⁴, Simone M. Pieber¹, Theo Rindlisbacher³, Yinon Rudich⁴, Jay G. Slowik¹, Jing Wang^{2,5}, Urs Baltensperger¹, and Andre S. H. Prévôt¹

¹Laboratory of Atmospheric Chemistry, Paul Scherrer Institute, 5232 Villigen PSI, Switzerland

²Laboratory for Advanced Analytical Technologies, Empa, 8600 Dübendorf, Switzerland

³Federal Office of Civil Aviation, 3003 Bern, Switzerland

⁴Department of Earth and Planetary Sciences, Weizmann Institute of Science, Rehovot, Israel

⁵Institute of Environmental Engineering, ETH Zurich, 8093 Zurich, Switzerland

Submitted for publication: Atmospheric Chemistry and Physics

Abstract

Oxidative processing of aircraft turbine-engine exhaust was studied using a potential aerosol mass (PAM) chamber at different engine loads corresponding to typical flight operations. Measurements were conducted at an engine test cell. Organic gases (OGs) and particle emissions pre/post PAM were measured. A suite of instruments, including a proton-transfer-reaction mass spectrometer (PTR-MS) for OGs, a multi-gas analyzer for CO, CO₂, NO_x, and an aerosol mass spectrometer (AMS) for non-refractory particulate matter (NR-PM₁) were used. Total aerosol mass was dominated by secondary aerosol formation, which was approximately two orders of magnitude higher than the primary aerosol. The chemical composition of both gaseous and particle emissions were also monitored at different engine loads and were thrust dependent. At idling load (thrust 2.5-7%), more than 90% of the secondary particle mass was organic and could be explained by the oxidation of gaseous aromatic species/ OGs; *e.g.* benzene, toluene, xylenes, tri-, tetra-, and pentamethyl-benzene and naphthalene. The oxygenated-aromatics, *e.g.* phenol, furans, were also included in this aromatic fraction and their oxidation could alone explain up to 25% of the secondary organic particle mass at idling loads. The organic fraction decreased with thrust level, while the inorganic fraction increased. At an approximated cruise load sulfates comprised 85% of the total secondary particle mass.

5.1 Introduction

Airport activities emit both particulate and gaseous emissions (Unal et al., 2005; Hudda et al., 2014), and are a significant source of local gas- and particle-phase pollutants (Westerdahl et al., 2008). These emissions affect public health (Lin et al., 2008) and local air quality by increasing pollutant concentrations, e.g. ultrafine particulate matter (PM) number concentrations, at the surrounding residential areas (Hudda and Fruin, 2016; Hudda et al., 2016).

The dominant source of airport aerosol is aircraft engine exhaust (Kim, 2009), and is classified as either directly emitted primary aerosol (PA) or secondary aerosol (SA). Due to the high combustion efficiency, PA from aircraft engines contains mainly black carbon (BC) whereas SA is formed by the oxidation of emitted precursor gases. PA and SA precursor emissions such as non-methane organic gases (NMOGs) strongly depend on aircraft engine operating conditions (Kinsey et al., 2010) e.g. the BC emission index (EI, g/kg fuel) of a gas-turbine engine is usually higher at cruise climb-out and take-off loads (above 60% of the maximum thrust) than at lower loads used at idle, taxi (7%) and approach (30%) (Liatì et al., 2014; Brem et al., 2015). In contrast to BC, NMOG emissions, including e.g. aromatic hydrocarbons, aliphatic hydrocarbons and carbonyls, are clearly highest at low loads (Spicer et al., 1994; Slemr et al., 2001; Anderson et al., 2006; Herndon et al., 2006; Kilic et al., 2017).

Aging of fossil fuel combustion exhaust leads to SA:PA ratios higher than 1. Single-ring aromatics are traditionally thought to be the most important secondary organic aerosol (SOA) precursors from combustion emissions. While this has been shown to be the case for some emissions, e.g. from 2-stroke engines (Platt et al., 2014), in other cases non-traditional precursors were assessed to be responsible for the bulk of the SOA mass formed, e.g. for biomass smoke (Bruns et al., 2016) or on-road vehicles (Platt et al., 2013; 2017; Pieber et al., 2017). Similar to these emissions, aging of aircraft emissions studied by Miracolo et al. (2011; 2012) in a smog chamber produced substantial amounts of secondary PM exceeding primary PM emissions several-fold. The authors showed the dominance of secondary organic aerosol (SOA) at low loads, while at high loads sulfate was the main SA produced. While single-ring aromatic compounds determined using gas-chromatography/mass spectrometry seemed to be important precursors of the SOA formed, a greater part of SOA was believed to originate from non-traditional precursors, whose nature remains to be identified (Miracolo et al., 2011; 2012).

In this study, we measured the SA production potential of aircraft jet engine exhaust as a function of engine load and examined the bulk gas-phase organic emissions and their SOA formation potential. SOA was produced by OH-initiated oxidation of aircraft NMOG emissions in a potential aerosol mass (PAM) flow reactor (Kang et al., 2007). Primary and secondary PM mass was characterized for different engine loads, using an aerosol mass spectrometer (AMS). SOA precursors were analyzed in real-time by a proton-transfer-

reaction mass spectrometer (PTR-MS) and SOA closure was examined under different conditions. The impact of these emissions and their SOA potential in typical urban atmospheres, at the proximity of airports was assessed and compared to other mobile sources.

5.2 Methods

5.2.1 Experimental setup

Exhaust measurements were conducted to characterize NMOG and non-refractory submicron particulate mass (NR-PM₁) emissions from an in-production CFM56 variant turbofan in the test cell of SR Technics at Zurich Airport. The test engine was fueled with standard JET A-1 fuel, and was operated at several engine loads, selected to represent aircraft activities during a typical landing/take-off (LTO) cycle. Engine loads were set by specifying the combustion chamber inlet temperature values which correlate with a specific thrust in pound-force (lbf) at standard atmospheric conditions. The selected loads included idle-taxi (3-7% of the maximum thrust), approach (30% of the maximum thrust), and an approximated cruise load (50-65% of the maximum static thrust). After starting the engine, a warm-up sequence of 25 minutes ran before each test, consisting of five minute-long steps at thrusts of 5%, 15%, 7%, 65% and 85% in sequence.

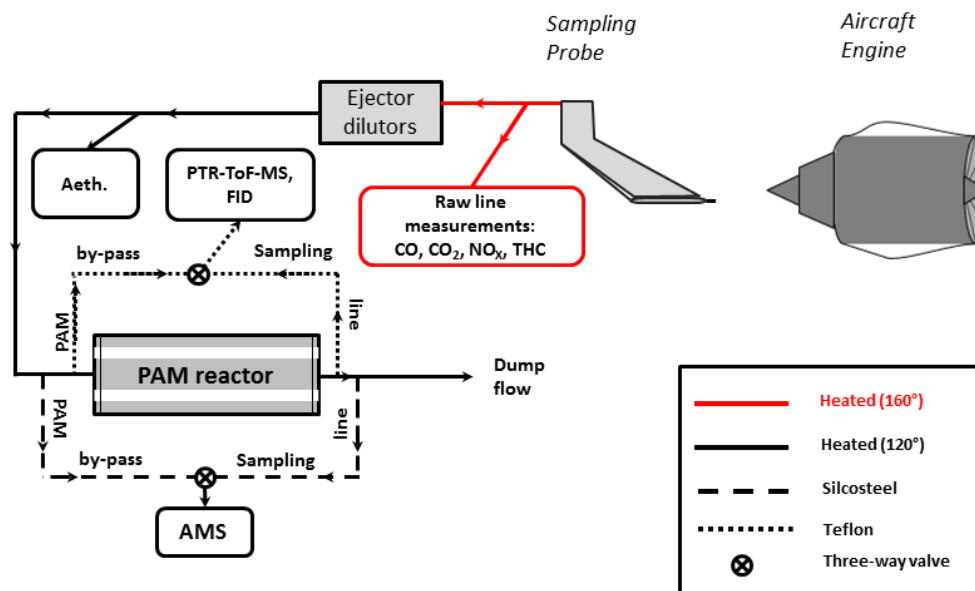


Figure 5-1: Simplified scheme of the experimental setup.

A simplified scheme of the experimental setup is shown in Figure 5-1 and is discussed in detail elsewhere (Kilic et al, 2017). Details about the sampling system for non-volatile particle emissions can be found in Durdina et al. (2017) and Brem et al. (2015). The turbine engine exhaust was sampled by a single-point probe with an inner diameter of 8 mm,

located 0.7 m downstream of the engine exit plane. The exhaust drawn by the probe was directed through a heated (160°C) transfer line to three different lines: (i) the raw gas line, (ii) diluted emissions line and (iii) diluted aged emissions line. CO, CO₂, and NO_x were measured by a multi-gas analyzer (PG250, Horiba Inc.) installed on the raw line. On the diluted line, primary gas and particle measurements were performed. Two ejector dilutors (DEKATI DI-1000) were installed in sequence on this transfer line; after the first dilution, sampling lines were heated to 120°C. The sample was diluted with synthetic air (99.999% purity) either by a factor of 10 or 100, depending on the NMOG concentration. The NMOGs were quantified and characterized by a proton-transfer-reaction time-of-flight mass spectrometer (PTR-ToF-MS) together with a flame ionization hydrocarbon detector (FID) (APHA 370 THC Monitor). The concentration of equivalent black carbon (eBC) was determined by a 7-wavelength aethalometer (Drinovec et al., 2015) based on optical absorption.

Aging of the engine exhaust emissions was achieved by using a potential aerosol mass (PAM) chamber with a continuous flow of 7.6 l/min and a volume of 13.3 liters. Two mercury lamps (emission lines at wavelengths $\lambda=182$ nm – 254 nm, BHK Inc.), mounted inside the PAM, were used to irradiate HONO and O₂ required for hydroxyl radical (OH) formation. Different time-integrated OH exposures (molecules cm⁻³ h) were achieved by modulating the UV lamp intensity *e.g.* at 80%, 90%, or 100%. HONO to boost OH concentrations, and D9-butanol to trace OH exposure (Barmet et al., 2012), were injected with flows of 1.8 and 0.4 l/min, respectively. Further, the PAM was also humidified (~20% relative humidity) by injecting synthetic air with water vapor (with a flow of 1.6 l/min). All measurements were conducted at 295-298°K. Secondary aerosol formation was measured after the PAM, while the primary emissions were measured from the bypass line.

Aging in a PAM is not completely analogous to that in a smog chamber, due to higher oxidant concentrations. However, intercomparison studies suggest that the amount of SOA production and its bulk elemental composition are comparable for both single precursors (*e.g.* α -pinene) Lambe et al., 2015) and complex emissions (*e.g.* wood combustion) (Bruns et al, 2015). In addition, in both the PAM and chambers, the dominant oxidation pathways are similar to those in ambient air (Peng et al, 2015; 2016).

5.2.2 Instrumentation

5.2.2.1 PTR-ToF-MS

NMOGs having a higher proton affinity than water were quantified by a PTR-ToF-MS (PTR-TOF 8000, Ionicon Analytik G.m.b.H., Innsbruck, Austria) (Jordan et al., 2009). NMOG molecules were positively charged in the ionization unit (drift tube) of the instrument via hydronium ions (H₃O⁺), and the generated ions/fragments were measured by a time-of-flight mass spectrometer. The PTR-ToF-MS utilized a drift voltage (U_{drift}) of 550 V, a drift chamber temperature (T_{drift}) of 60°C and a drift pressure (p_{drift}) of 2.2 mbar, maintaining a

reduced electric field (E/N) of ~ 120 Townsends (Td). Data were collected with one second time resolution.

ToFware post-processing software (version 2.4.5, TOFWERK AG, Thun, Switzerland; PTR module as distributed by Ionicon Analytik GmbH, Innsbruck, Austria), running in the Igor Pro 6.3 environment (Wavemetrics Inc., Lake Oswego, OR, USA), was used for data analysis. The ion transmission function, required to convert counts (cps) to volume mixing ratios (ppbv), was quantified using a gas standard containing a mixture of 12 compounds (100 ppbv each) spanning mass-to-charge ratios (m/z) from m/z 33 to 181 (Carbagas AG., Zurich, Switzerland). Volume mixing ratios (ppbv) were calculated according to De Gouw and Warneke, 2007, using $H_3O^+/NMOG$ reaction rate constants (k) from Cappellin et al., 2012, when available, and assuming $2 \times 10^{-9} \text{ cm}^3 \text{ s}^{-1}$ otherwise (Table S4-2).

During the exothermic proton-transfer reaction, some molecular fragments are formed in the drift chamber, with the extent of fragmentation depending on the chamber conditions and functional groups in the molecules (Gueneron et al., 2015). In particular, hydrocarbon fragments are obtained from aldehydes and dehydration of some oxygenated ions. Assignment of these fragment ions to the corresponding parent ions is important for quantification. The NMOG mixing ratios were corrected by accounting for this fragmentation. The compounds were measured based on their parent ions, then their fragments were subtracted based on reference fragmentation patterns. These subtractions combine a detailed fragmentation table for aldehydes using the current drift chamber conditions from Klein et al. (2016) and fragmentation patterns for aromatic compounds measured under similar chamber conditions reported ($E/N \sim 120$ Td) in other studies (Buhr et al., 2002; Brown et al., 2010; Gueneron et al., 2015). The fragmentation of detected compounds containing other functional groups (e.g. hydrocarbons and non-aldehyde oxygenated compounds) cannot be fully excluded but are not expected to cause significant error since the observed parent molecules were primarily low molecular weight alcohols and acids (e.g. methanol, formic and acetic acid) that are less susceptible to fragmentation (de Gouw and Warneke, 2007). The NMOGs were then classified (acids, alcohols, aromatics, non-aromatics hydrocarbons and unclassified hydrocarbon fragments, nitrogen and sulfur containing compounds, other oxygen containing compounds, unidentified peaks) according to Kilic et al. (2017).

5.2.2.2 AMS

The condensed phase was continuously monitored before and after the PAM using a high resolution time-of-flight aerosol mass spectrometer (AMS) and a scanning mobility particle sizer (SMPS). The reader is referred to DeCarlo et al. (2006) for a more detailed description of the AMS operating principles, calibrations protocols, and analysis procedures. Briefly, a particle beam sampled through an aerodynamic lens is alternately blocked and unblocked, yielding the bulk particle mass spectra (MS mode) of the non-refractory (NR) species, including organic aerosols (OA), NO_3^- , SO_4^{2-} , NH_4^+ , and Cl^- . The NR particles are flash

vaporized by impaction on a heated tungsten surface (heated to $\sim 600^{\circ}\text{C}$) at $\sim 10^{-7}$ Torr. The resulting gases are ionized by electron ionization (EI, 70 eV) and the mass-to-charge ratios (m/z) of the fragments are determined by the ToF mass spectrometer. The AMS was operated in the V-mode, with a time resolution of 30 sec. The AMS data were analyzed using the SQUIRREL (version 1.52L) and PIKA (1.11L) analysis software in Igor Pro 6.3 (WaveMetrics). Standard relative ionization efficiencies (RIE) were assumed for the organic aerosol and chloride (RIE = 1.4, and 1.3, respectively) and experimentally determined for sulfate and ammonium (RIE = ~ 1.1 and ~ 4 , respectively). The collection efficiency due to the particle bounce was determined to be ~ 1 under our conditions for organic rich aerosols by comparing the AMS mass to the SMPS volume (assuming an OA density of 1.4).

5.2.3 Data analysis

Emissions from the aircraft turbofan were measured at different thrust levels referred to as “test points” hereinafter. Test point durations were 18 minutes, except for one 60 minute-long run. Test points were systematically interspersed with five minute-long periods to clean the PAM and the transfer lines by flushing the setup with synthetic air. The averaging of the primary emissions started from the third minute of a test point when the engine operation was stable. After sampling primary emissions for five to eight minutes while bypassing the PAM, secondary formation was measured after the PAM during the last five to eight minutes of the test point. This allowed SOA to reach steady state in the PAM. During each test, the PA concentration was measured by bypassing the PAM, while the SA concentration was calculated by subtracting PA from the OA measured after aging (after the PAM). Both PA and SA concentrations were determined by AMS. .

The expected SOA concentration from the sum of all NMOGs detected by the PTR-ToF-MS was also calculated by multiplying the NMOGs oxidized in the PAM by its corresponding SOA yields, according to Eqn 5-1:

$$\sum_{i=1}^n SOA_{modelled} = \sum_{i=1}^n \Delta NMOG_i \times Yield_i \quad \text{Eqn 5-1}$$

where n is the number of NMOGs quantified and $\Delta NMOG$ is the difference between the primary NMOG concentration and the NMOG concentration after aging. The same approach was applied by Bruns et al. (2016) and yields used can be found in Table 5-1. SOA yields available in the literature were used when possible. Otherwise, SOA yields of 0.2 were assumed as a lower limit estimate for aromatic and oxy-aromatics for which no SOA-yield values were reported (Presto et al., 2010; Tkacik et al., 2012), similar to Bruns et al. (2016). A yield of 0.15 was assumed for other NMOGs, including non-aromatic hydrocarbons and carbonyls. As NO is completely consumed in the PAM, we have chosen yields from low NO_x conditions for aromatic hydrocarbons (Ng et al., 2007; Chan et al., 2009; Hildebrandt et al., 2009; Nakao et al., 2011). The SOA contribution from organic gases lighter than benzene

(C₆H₆) was neglected. Predicted NMOG contributions to SOA are provided in the Results section).

Emission Indices (*EI*, g/kg fuel) were calculated using a mass balance on fuel carbon:

$$EI = [X] \times \left[\frac{MW_{CO_2}}{MW_C \times \Delta CO_2} + \frac{MW_{CO}}{MW_C \times \Delta CO} \right] \times C_f \quad \text{Eqn 5-2}$$

where *X* denotes the pollutant concentration (µg/m³) and *MW* (g/mole) is the molecular weight of the species denoted by the subscript. Background-subtracted CO and CO₂ concentrations (µg/m³) are denoted as ΔCO and ΔCO_2 , respectively. *C_f* is the carbon fraction of the JET-A1 fuel used during the campaign and was measured as 0.857 based on ASTM D 5291 method (ASTM, 1996).

5.3 Results and discussion

5.3.1 SOA formation as a function of OH exposure

The evolution of the chemical composition of the primary organic gases and NR-PM₁ components with increasing OH exposure is shown in Figure 5-2 for engine idling operation (thrust 3%). Measurements were conducted for primary emissions, as well as for OH exposures of 59x10⁶, 88x10⁶, and 113x10⁶ molecules cm⁻³ h, which correspond to approximately 39, 58, and 75 hours of atmospheric aging under an average tropospheric OH concentration of 1.5 x 10⁶ molecules cm⁻³ (Mao et al., 2009). The OH exposure, calculated using d9-butanol as a tracer, was varied by varying the light intensity.

Figure 5-2a shows the OG composition under these conditions with compounds classified as a function of their molecular composition, as described in Kilic et al. (2017). A stepwise increase of the OH exposure reduced the NMOG mass detected in the chamber by 35%, 40% and 50%. Except for carboxylic acids, the concentrations of all NMOGs decreased during aging, indicating that their loss rate exceed their production from other NMOGs. For example, aromatic compounds and carbonyls were oxidized in the PAM by up to 90% and 50%, respectively, while the acids doubled after 75 hours of daytime-equivalent aging.

Figure 5-2b shows a time series of secondary NR-PM₁ composition, as well as the concentrations of two of the most abundant aromatic gases, C₁₀H₁₄ and C₁₁H₁₆, for the same experiment. Here stable oxidation conditions were alternated with sampling of primary emissions, with OH exposures indicated in the figure. Secondary aerosol, especially SOA, dominated the total NRPM₁. By increasing the OH exposure from 59x10⁶ to 88x10⁶, the generated SOA increased by approximately 14%. However, increasing the OH exposure further to 113x10⁶ molecules cm⁻³ h yielded only an additional 3% increase in SOA mass. This suggests that at these OH exposures, the bulk of SOA precursors have reacted and the

additional SOA production did not significantly exceed its loss. Under these conditions, the formed SOA may be considered as a reasonable estimate for the total SOA potential. The observed production rate of SOA against OH exposure is consistent with precursor reaction rates of $8 \times 10^{-12} \text{ molecule}^{-1} \text{ cm}^3 \text{ s}^{-1}$. This estimate is based on the assumption of a constant SOA mass yield with aging and instantaneous equilibrium partitioning of the condensable gases, and is therefore lower than the reaction rates of the main identified precursors (see below). SOA production rates are thus expected to be faster in the ambient atmosphere.

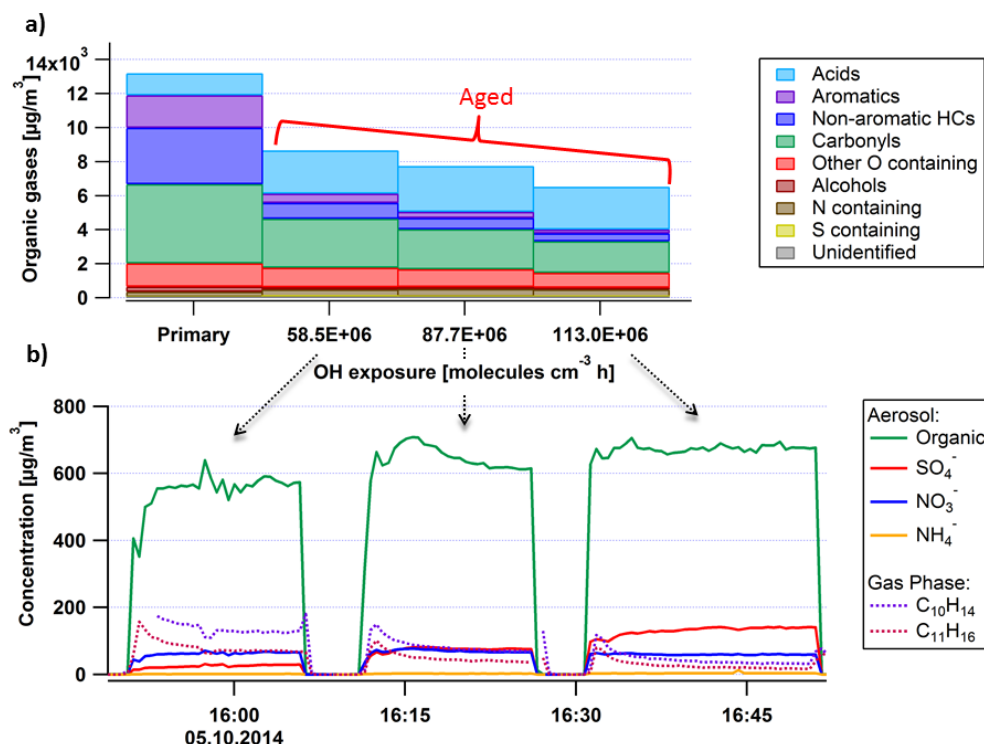


Figure 5-2: Sample experiment showing mean NMOG emissions (top) and representative time series for particle and NMOG components (bottom) for varying OH exposures. Hydrocarbon concentrations (non-aromatic HCs (dark blue), aromatic HCs (purple) and carbonyls (green)) decrease in the PAM while the concentrations of acids (mostly formic and acetic ~90% of the total acids) increase. The bottom panel shows the aerosol (Organic, SO₄⁻, NO₃⁻, NH₄⁻) formed and gaseous aromatics (C₁₀H₁₄, C₁₁H₁₆) for the different OH exposures in the PAM given in the top panel.

5.3.2 Particle and gaseous emissions as a function of engine load

Figure 5-3 shows both average primary and secondary emission indices for varying engine loads (left) and EIs from individual test points (right). The NMOG EI decreased from 30 to 0.8 g/kg fuel when the thrust level increased from 3-5% to 90%. At thrust 3-5%, the emissions of gaseous aromatic-hydrocarbons were highest (with an EI of ~5g/kg fuel) and decreased with increasing thrust (with an EI of ~0.15 g/kg fuel at thrust 90%). Similar to aromatic gases, SOA formed mostly at 3-5% thrust and had a declining trend with thrust. In contrast, BC, POA and secondary SO₄ EIs were highest during the approximated cruise load (thrust

60%). At these conditions, secondary NR-PM₁ was mostly inorganic and SOA mass was comparable to that of primary carbonaceous emissions (BC + POA). SOA was approximately 100 times higher than POA at idle and only 10 times higher at cruise (Figure 5-3). This dependence of the aged aerosol composition on the thrust level, obtained using the PAM reactor, confirm quite readily the previous results obtained in a smog chamber (Miracolo et al., 2011; 2012).

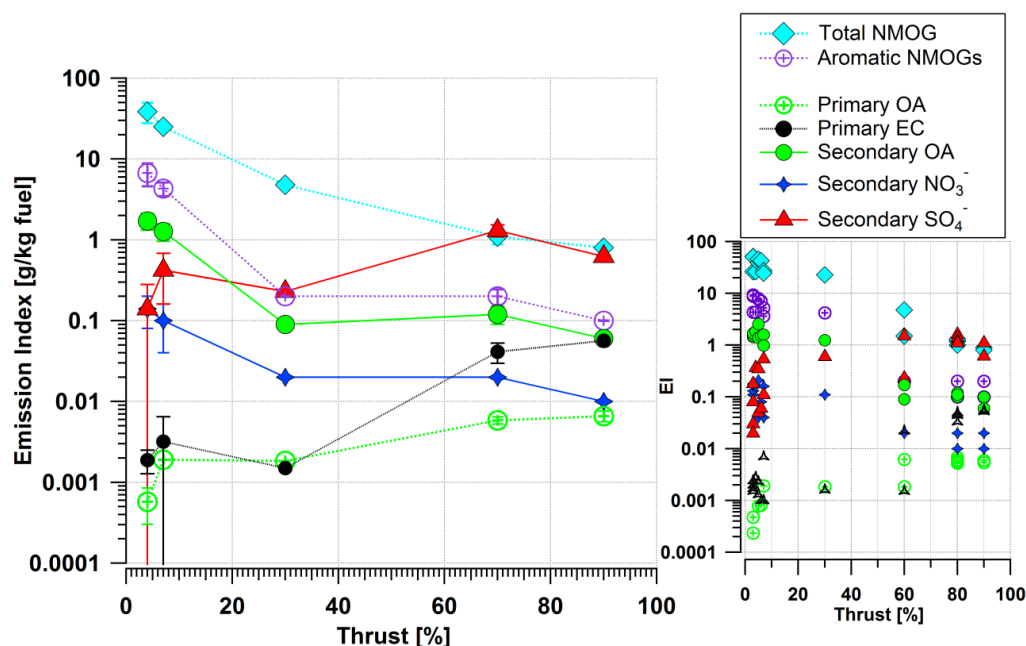


Figure 5-3: Average emission indices (left) and EIs from individual test points (right) for primary non-methane organic gases (NMOGs), aromatic gases, primary organic aerosol (POA), equivalent black carbon (BC), secondary organic aerosol (SOA), nitrate (NO₃) and sulfate (SO₄). Error bars (+/-) are the standard deviations of the means with a confidence interval of 95%. The OH exposure was in the range of 91-113 x 10⁶ molecules cm⁻¹ h for the secondary aerosol cases.

Table 5-1: Volume mixing ratios of gaseous emissions, engine parameters and emission indices (EIs) for primary (directly emitted) and secondary (after aging) for all experiments.

Thrust (%)	Primary									Aged			
	CO ₂ (ppmv)	CO (ppmv)	THC (ppmvC)	NO _x (ppmv)	Fuel (kg/sec)	NMOG (g/kg fuel)	Aromatic Gases (g/kg fuel)	BC (g/kg fuel)	POA (g/kg fuel)	NO ₃ (g/kg fuel)	SO ₄ (g/kg fuel)	OH exposure (molec. cm ⁻³ h)	SOA (g/kg fuel)
3	1863	764	239	14	0.09	51.38	9.35	1.70E-06	2.34E-04	0.11	0.03	8.8E+07	1.43
3	1831	766	244	14	0.09	50.78	8.82	2.00E-06	4.74E-04	0.13	0.02	8.8E+07	n/a
3	1560	709	222	14	0.09	26.32	4.31	1.50E-06	<2.0E+03	0.17	0.08	6.0E+07	1.53
3	1560	709	222	14	0.09	26.32	4.31	2.40E-06	<2.0E+03	0.18	0.18	9.0E+07	1.69
3	1560	709	222	14	0.09	26.32	4.31	2.80E-06	<2.0E+03	0.16	0.37	11.3E+07	1.85
4	1884	543	173	n/a	n/a	39.16	7.65	2.30E-06	<2.0E+03	0.21	0.35	10.0E+07	2.55
5	1829	442	114	17	0.11	45.55	7.90	1.30E-06	7.81E-04	0.04	0.05	8.8E+07	1.39
5	1758	422	98	17	0.11	42.46	7.07	1.00E-06	8.13E-04	0.08	0.06	8.8E+07	1.51
6	1934	410	113	21	0.12	27.65	5.21	1.00E-06	<2.0E+03	0.16	0.54	10.0E+07	1.58
7	1909	168	45	23	0.14	24.53	3.58	7.00E-06	1.91E-03	0.04	0.11	8.8E+07	0.98
7	1978	385	94	23	0.14	22.75	4.17	1.60E-06	<2.0E+03	0.11	0.60	10.0E+07	1.24
30	2953	40	8	62	0.31	4.83	0.19	1.50E-06	1.84E-03	0.02	0.23	8.8E+07	0.09
60	3709	12	7	131	0.65	1.50	0.21	2.20E-05	6.21E-03	0.02	1.51	8.50E+07	0.17
60	3709	12	7	131	0.65	1.15	0.16	3.30E-05	6.80E-03	0.01	1.61	8.5E+07	0.12
80	4344	16	6	195	0.9	1.00	0.08	4.60E-05	5.55E-03	0.01	1.39	10.0E+07	0.10
80	4291	14	7	195	0.9	1.29	0.17	4.40E-05	6.01E-03	0.02	1.16	8.5E+07	0.12
80	4291	14	7	195	0.9	1.01	0.16	5.00E-05	5.24E-03	0.02	1.10	8.5E+07	0.11
80	4291	14	7	195	0.9	0.91	0.16	5.20E-05	5.37E-03	0.02	1.10	8.5E+07	0.10
90	4657	16	6	202	1.1	0.78	0.12	5.50E-05	5.89E-03	0.01	0.61	8.5E+07	0.06
90	4657	16	6	202	1.1	0.78	0.12	5.80E-05	7.30E-03	0.01	0.63	8.5E+07	0.06

5.3.3 Precursor gases of SOA: Idling

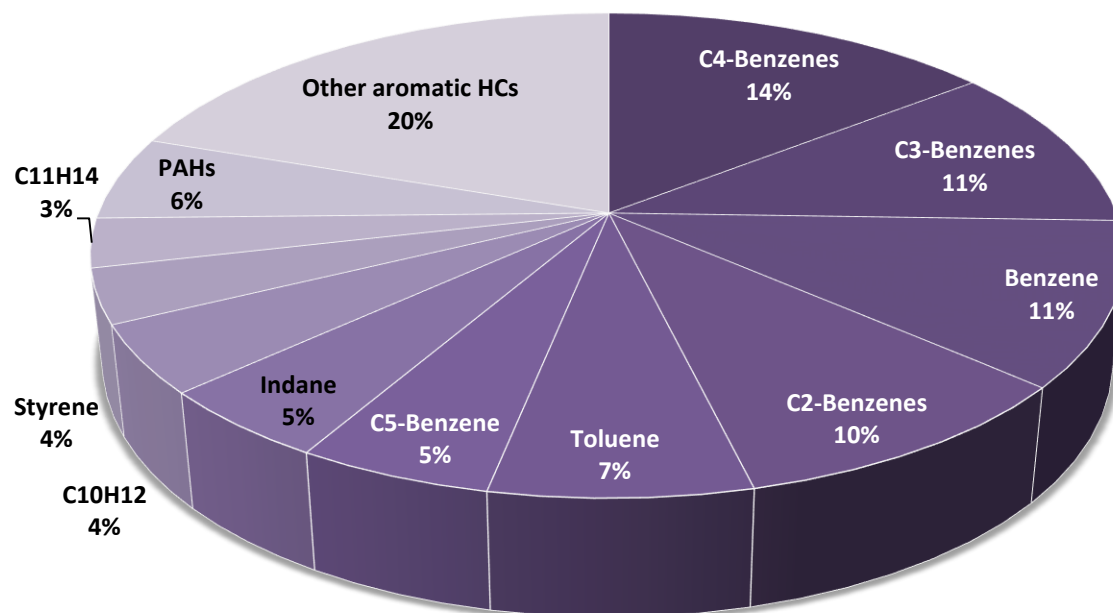


Figure 5-4: Fractions of aromatic compounds for primary emissions (directly emitted) at idle (thrust 3-7%). Benzene derivatives, xylenes, tri-, tetra-, pentamethylbenzene, benzene and toluene account for ~60% of all aromatics.

Single-ring aromatics, such as xylenes, methylbenzenes, toluene and benzene, were previously linked with SOA formation (Ng et al., 2007; Odum et al., 1997). Further, many of the aromatics gases are important SOA precursors for combustion sources such as 2S-scooters (Platt et al., 2014), or wood burning (Bruns et al., 2016). Figure 5-4 presents the mass fractions of aromatic hydrocarbons in primary exhaust for an idling turbine engine. More than half of the aromatic hydrocarbons emitted were single-ring aromatics. Idling exhaust contained 20% (mass weighted) aromatic HCs. 75 - 95% of these aromatics were oxidized with an OH exposure of $\sim 90 \times 10^6$ molecules cm^{-3} h in the PAM.

By using previously reported SOA yields (Table 5-2) for NMOGs, SOA production was predicted from individual precursors according to Eqn 5-1. Figure 5-5 shows a comparison of the predicted SOA with the SOA determined by AMS measurements (top) and the predicted SOA contribution by the oxidation of NMOGs in the PAM (bottom), for two idling thrusts, 2-5% (left) and 6-7% (right). The predicted SOA from the NMOGs reacted are shown at the bottom panel of the figure and compound class-specific SOA fractions are separated for aromatic HCs, oxygenated-aromatics, other HCs, N-containing OGs and other OGs.

Table 5-2: Precursor OGs, their corresponding functional group and protonated m/z, SOA yields from literature, and average SOA EI estimated for different thrusts.*

VOC formula	m/z	Group	SOA yield*	SOA Emission Index (g/kg fuel)			
				Thrust 3-5%		Thrust 6-7%	
				Average	±	Average	±
(C ₉ H ₁₂)H ⁺	121.101	Aromatic	0.32	0.19	0.11	0.07	0.04
(C ₆ H ₆)H ⁺	79.054	Aromatic	0.33	0.16	0.06	0.07	0.03
(C ₁₀ H ₁₄)H ⁺	135.117	Aromatic	0.2	0.11	0.07	0.03	0.02
(C ₉ H ₁₀)H ⁺	119.086	Aromatic	0.32	0.10	0.06	0.03	0.02
(C ₈ H ₁₀)H ⁺	107.086	Aromatic	0.2	0.10	0.05	0.04	0.02
(C ₁₀ H ₁₂)H ⁺	133.101	Aromatic	0.32	0.10	0.06	0.03	0.02
(C ₇ H ₈)H ⁺	93.070	Aromatic	0.24	0.08	0.04	0.03	0.02
C ₁₁ H ₁₁ ⁺	143.086	Aromatic	0.52	0.08	0.05	0.03	0.02
(C ₈ H ₈)H ⁺	105.070	Aromatic	0.32	0.07	0.04	0.03	0.02
(C ₁₀ H ₈)H ⁺	129.070	Aromatic	0.52	0.07	0.03	0.03	0.02
C ₁₁ H ₁₇ ⁺	149.132	Aromatic	0.2	0.05	0.03	0.02	0.01
C ₁₁ H ₁₅ ⁺	147.117	Aromatic	0.2	0.04	0.02	0.01	0.01
(C ₁₂ H ₁₈)H ⁺	163.148	Aromatic	0.2	0.03	0.02	0.01	0.01
(C ₉ H ₁₄)H ⁺	123.117	Aromatic	0.2	0.03	0.02	0.01	0.01
(C ₁₂ H ₁₆)H ⁺	161.132	Aromatic	0.2	0.02	0.01	0.01	0.01
(C ₉ H ₈)H ⁺	117.070	Aromatic	0.2	0.02	0.01	0.00	0.00
Other	-	Aromatic	0.15	0.06	0.05	0.00	0.00
C ₆ H ₇ O ⁺	95.049	Oxy-arom	0.44	0.13	0.07	0.05	0.03
(C ₆ H ₈ O)H ⁺	97.065	Oxy-arom	0.32	0.07	0.03	0.02	0.01
(C ₇ H ₆ O)H ⁺	107.049	Oxy-arom	0.32	0.05	0.02	0.02	0.01
C ₆ H ₇ O ₂ ⁺	111.044	Oxy-arom	0.39	0.03	0.01	0.01	0.00
(C ₁₀ H ₁₂ O ₂)H ⁺	165.091	Oxy-arom	0.2	0.00	0.00	0.00	0.00
C ₁₀ H ₁₅ O ₂ ⁺	167.107	Oxy-arom	0.2	0.00	0.00	0.00	0.00
Other NMOGs	> 79.054	Other NMOG	0.15	1.15	0.74	0.20	0.02

*SOA yields from literature (Alvarez et al., 2009; Chan et al., 2010; Chan et al., 2009; Chhabra et al., 2011; Hildebrandt et al., 2009; Nakao et al., 2011; Ng et al., 2007; Shakya & Griffin, 2010; Yee et al., 2013).

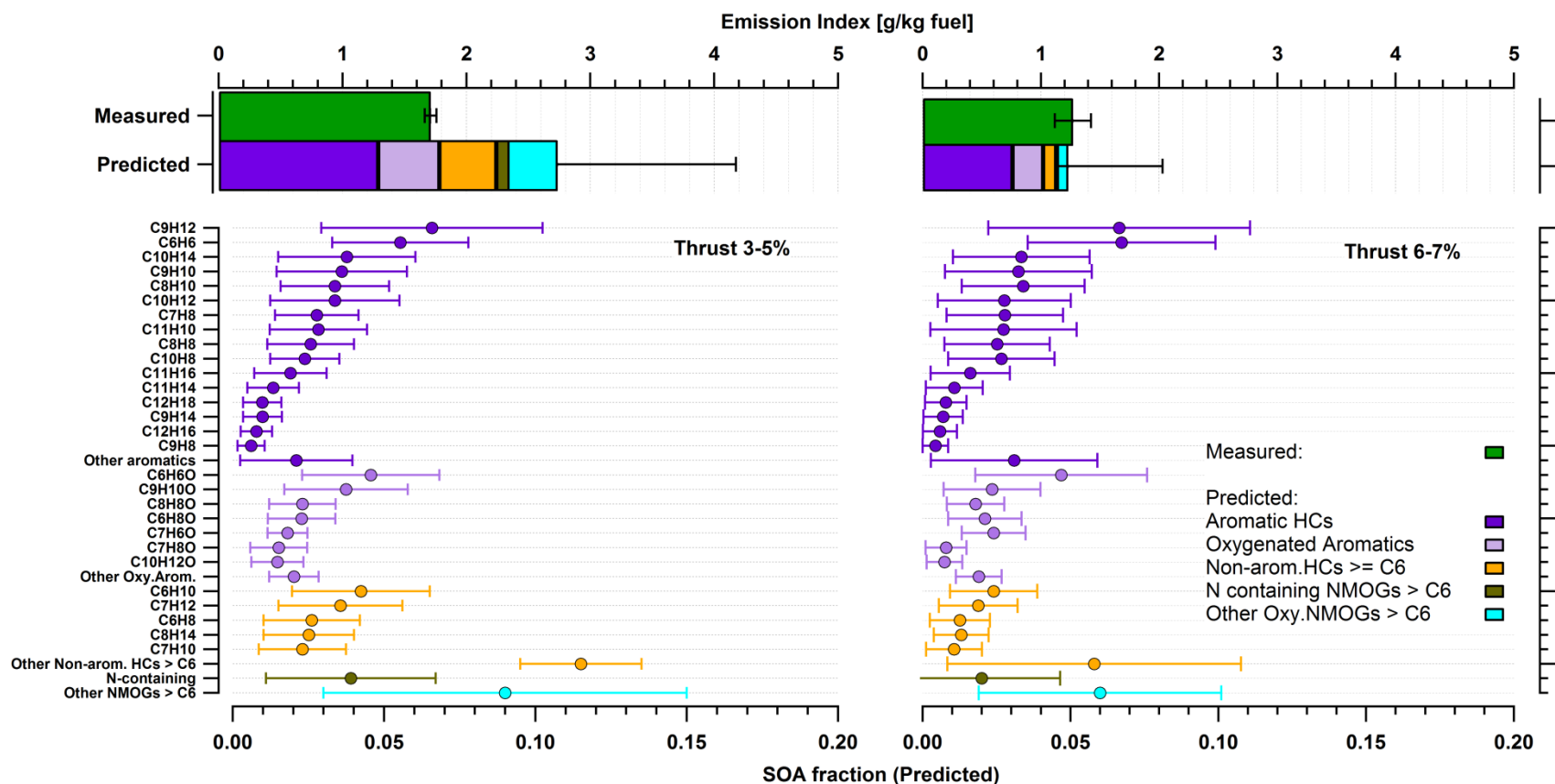


Figure 5-5: Comparison of the SOA measured by the AMS and the SOA predicted by the oxidation of NMOGs (top panel). The statistics are presented for low load idling (thrust 3-5%) on the left half and for idling 6-7% on the right. Aromatic hydrocarbons (purple) were the most abundant precursors of SOA at idle (thrust 3-7%) explaining all SOA formed (green, top panel) at thrust 3-5% and most (~90%) at thrust 6-7%. Aromatic SOA comprised the largest fraction followed by oxygenated aromatics (light purple - e.g. phenol, benzaldehydes), non-aromatic hydrocarbons (orange) with more than 6 carbon atoms in their molecular structure (non-arom. HCs \geq C6), nitrogen containing compounds (brown), other oxygenated-NMOGs $>$ C6 (cyan). Average fractions of individual NMOGs (bottom panel) were calculated by using SOA yields from literature (see Table 5-2) and the amount of NMOG reacted. Error bars show standard deviations of the means (CI: 95%).

Figure 5-5 indicates that the most important SOA precursors emitted by turbine engines at idle are aromatic hydrocarbons such as benzene derivatives but also oxygenated aromatics such as phenol. The predicted SOA formed by aromatics alone, both by aromatic hydrocarbons (60-70%) and oxygenated-aromatics (15-25%), explained all AMS-determined SOA at low loads (thrust 3-5%) and most of the SOA formed (by 80%) at thrust 6-7% (Figure 5-5). Predicted aromatic SOA from benzene (C_6H_6), C2-benzenes (C_8H_{10}), C3-benzenes (C_9H_{12}), C4-benzenes ($C_{10}H_{14}$), dimethylstyrenes ($C_{10}H_{12}$), toluene (C_7H_8), methylbenzaldehydes (C_8H_8O) and phenol (C_6H_6O) accounted for 60% of the AMS-determined SOA at 3-5% thrust (Figure 5-5). These results are consistent with those previously obtained using a smog chamber, confirming that aromatic compounds are indeed important SOA precursors in jet-engine emissions (Miracolo et al., 2011). Only a small fraction of these compounds was determined in previous experiments using GC/MS measurements and therefore traditionally considered as SOA precursors in models. Here, compared to previous experiments we show that non-traditional aromatic and oxy-aromatic compounds, including naphthalene and its alkyl derivatives, C>3 alkyl derivatives of single ring aromatics, and phenols, can explain the gap between measured SOA and SOA predicted based on traditional precursors.

Exhaust-aging experiments were repeated 6 times at thrust 3-5% and the oxidation of NMOGs varied during each of these aging experiments. Error bars shown in Figure 5-5 denote this variability in NMOG oxidation (in the PAM) during aging experiments of the same thrust level. Indeed, errors related to yield values used may significantly influence the results. These errors may be systematic and are complex to assess. They can be affected by potential differences between the oxidation conditions in chambers and in the PAM (e.g. NO_x, RH, particle mass). Yields obtained with the PAM are consistent with those obtained from chambers (Bruns et al., 2015), therefore we do not expect large systematic errors in the SOA predicted. However, based on the variability of yields in previous chamber experiments we estimate the accuracy of our prediction to be within a factor of 2, indicating that within our uncertainties a significant fraction of the precursors was identified.

NMOGs, including aromatic gases, were reduced with increasing thrust (from thrust 3-5% to thrust 6-7%) due to more efficient operation of the turbine engine. This decrease amounted to 40% for the sum of aromatic HCs and corresponded to a 30% decrease in SOA EI. Therefore, a more efficient engine operation implies less NMOG emissions and reduced SOA formation potential at idle.

5.3.4 SOA formation at cruise load

A comparison of the predicted SOA with the SOA determined by the AMS is presented in Figure 5-6 at cruise loads (top panel). Figure 5-6 also shows the SOA contribution predicted by the oxidation of NMOGs in the PAM (bottom panel) under the same engine conditions.

The SOA EI was 0.07 g/kg fuel for cruise load. The predicted SOA fraction accounted for only 30% of the AMS-determined SOA (green bar, Figure 5-6) during cruise load experiments. Aromatic SOA (predicted) accounted for only 4% of the AMS-determined SOA during these experiments. The major fraction of the remaining SOA mass that was assigned to the identified precursors was predicted to be from oxygenated NMOG molecules (Figure 5-6). Another 6% of the determined SOA may originate from non-aromatic HCs (aliphatics and HC fragments > C6).

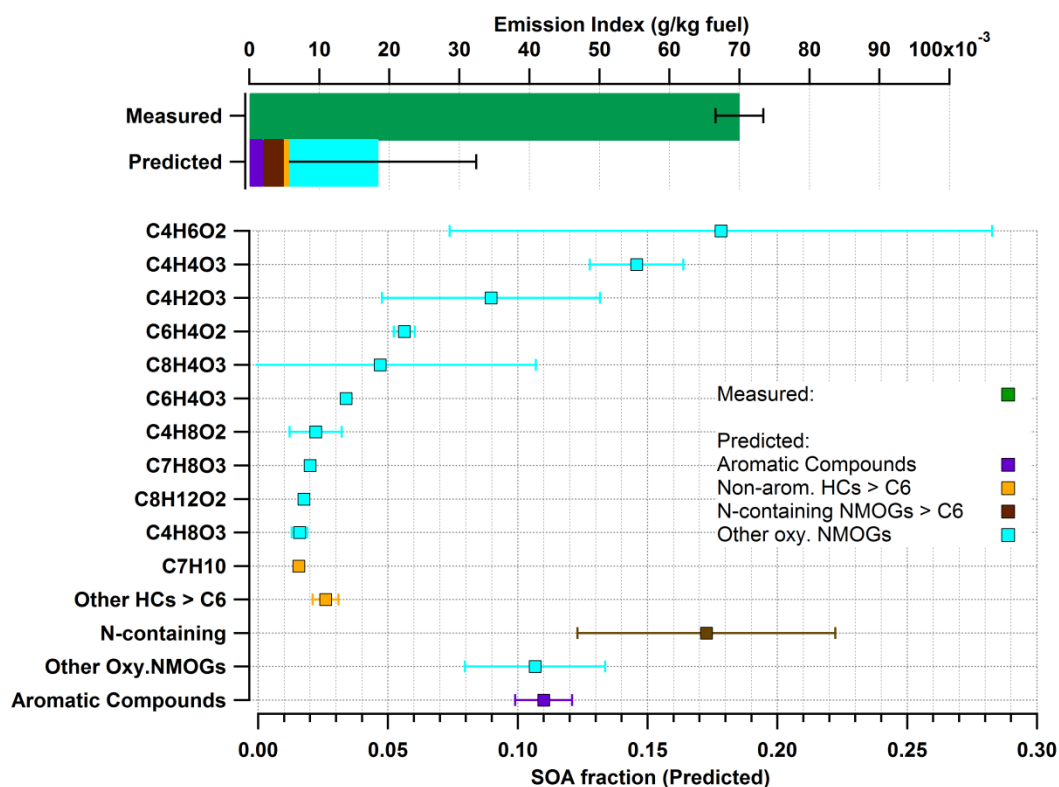


Figure 5-6: Measured and predicted SOA comparison at cruise load, using the same approach as in Figure 5-5. In contrast to idle conditions, total NMOGs detected do not explain SOA formed.

Predicted SOA was significantly lower compared to the measured SOA. While SOA precursors remain unidentified under these conditions, several hypotheses might explain the observation. First, we could not determine the contribution of alkanes smaller than 9 carbon atoms to the formed SOA, because these compounds are not directly detected by the PTR-ToF-MS. Depending on the number of carbon atoms in their molecular structure, the SOA potential of many alkanes may be comparable to that of single-ring aromatic hydrocarbons (Tkacik et al., 2012) and therefore may play a role in the formation of the observed SOA. However, our data do not suggest that a great part of the observed SOA is from non-measured alkanes, as we do not observe any increase in the contribution of hydrocarbon fragments in the PTR-MS compared to idling emissions. Second, the oxidation of primary semi-volatile compounds may yield significant SOA, because of their elevated

yields of near unity (Robinson et al., 2007). However, we note that these semi-volatile precursors would play an important role at low aerosol concentrations, when most of these precursors reside in the gas-phase where they can be oxidized. Under our conditions, concentrations range between 10 and 50 $\mu\text{g m}^{-3}$ and a substantial fraction of these products resides already in the particle phase. Therefore the oxidation of these products in the gas-phase by OH is unlikely to explain the observed entire 10-fold increase in the OA mass upon oxidation, but only part of the mass. Finally, the PTR-MS data suggest that a great part of the precursors measured are highly oxygenated gases, with O:C ratios ranging from 0.2 to 0.7, including, among others, anhydrides (e.g. phthalic, succinic and maleic) and quinone derivatives. Unlike aromatic compounds and alkanes present in the fuel, these compounds are likely formed at high temperature during combustion. The SOA yields of these compounds remain unknown and it is likely that the yield value of 0.15 used here is a lower estimate, which would result in an underestimation of the contribution of these compounds to the observed SOA. We also note that unlike precursors detected under idle conditions, the ionization efficiency and the fragmentation pattern of these compounds in the PTR-MS are highly uncertain, resulting in large uncertainties in our predicted SOA. Therefore, results in Figure 6 should be considered with care. Notwithstanding these uncertainties, we note that at cruise conditions the SOA contribution to the total secondary PM is minor compared to sulfate and therefore these uncertainties have little impact on the implications of our results.

5.4 Conclusions and implications for ambient air quality

Gas-phase primary emissions and SA formation from an in-production turbofan were investigated in a test cell. The engine loads (thrusts) during experiments were selected to simulate different aircraft operations. These operations are summarized as landing take-off (LTO) cycle under four modes taxi/idle, approach, climb and take-off with corresponding engine loads of 3-7%, 30%, 85% and 100%, respectively. In addition an approximated cruising load (60%) was selected.

At idle conditions, SOA formation was mostly attributed to the oxidative processing of aromatic gases. Benzene derivatives together with phenol were predicted as the major SOA precursors for an idling aircraft. Meanwhile, during cruise load the emission of aromatic compounds was much lower and only explained a minor fraction of SOA (4%). During these conditions, however, sulfate was found to dominate SA, contributing ~85% of the total mass of aged aerosols and therefore its fraction is more relevant aloft.

The oxidation of NMOGs in the PAM yielded an SOA EI 100 times greater than POA under idling conditions and 10 times greater at cruise load. According to our calculated production rates SOA from airport emissions (idling jet engines) exceeds POA by a factor of 10 after only 3 hours of atmospheric aging and therefore considerably impacts urban areas downwind of airport emissions. Compared to idling aircraft emissions, aging of vehicle exhaust emissions

results in much lower enhancements, ranging between factors of 5-10 and 1.5-3, for gasoline and diesel vehicles, respectively (Gordon et al., 2014a; 2014b).

The NMOG emission factors and SOA potential can be used in conjunction with emission inventories and fuel use data to assess the impact of aircraft emissions on air quality in comparison with other mobile sources. Here, we have considered the Zurich international airport as an example (Switzerland, 23 million passengers in 2010). Combining the recorded aircraft fuel use with the standard LTO cycle and the NMOG EIs measured, we estimate aircraft NMOG emissions in Zurich for 2010 to be in the range of 90–190 tons/year (Kilic et al., 2017). Based on the average SOA bulk yields (SOA/total NMOG) obtained herein (~5-8%), we estimate a total SOA production potential from airport emissions for the area of Zurich to range from 5.4 to 13.2 tons/year. These SOA production potential values can be directly compared to emissions from on-road vehicles derived from the EDGARv4.2 emission inventory, which provides worldwide temporally and spatially resolved NMOG emissions from road vehicles with a grid size of ~200 km². For the grid cell containing Zurich (47.25° North, 8.75° East) the NMOG emissions from on-road vehicles is estimated to be 631 tons/year. While SOA yields from diesel vehicle emissions are expected to be more elevated than those from gasoline car emissions, due to the presence of intermediate volatility species, recent reports suggest these yields to be comparably high, ~15% (Gentner et al., 2017). Using this yield value for emissions from both types of vehicles (Platt et al., 2017), we estimate the total SOA production potential from on road vehicles for the area of Zurich to be ~94 tons/year, 10 fold higher than SOA from aircraft emissions. However, the airport is a point source within this region and thus the relative contribution of the airport emissions to a specific location downwind of this source is significantly higher than implied by this calculation. Although this estimate applies to a specific airport, it does indicate that aircraft NMOG emissions may constitute significant SOA precursors downwind of airports, while other fossil fuel combustion sources dominate urban areas in general.

Acknowledgements

Funding was provided by the Swiss Federal Office of Civil Aviation (FOCA). This project would not have been possible without the support of Rene Richter (PSI) and SR Technics personnel. Many individuals from SR Technics contributed to the project but we owe special thanks to those from the Maintenance and Test Cell Group. JGS acknowledges support from the Swiss National Science Foundation starting grant BSSGI0_155846.

6 Vehicle dependent characterization of the organic gases from mobile sources: aircraft, ships and motor vehicles

D. Kilic¹, J. G. Slowik¹, I. El Haddad¹, S. Hellebust³, R. Huang¹, F. Klein¹, N. Kumar¹, S. M. Pieber¹, S. M. Platt^{1,*}, B. Temime-Roussel³, J. Wang², R. Zimmermann^{4,5}, A. A. Zardini⁶, M. Clairotte⁶, R. Suarez-Bertoa⁶, C. Astorga⁶, N. Marchand³, U. Baltensperger¹ and A. S. H. Prevot¹

¹Paul Scherrer Institute, Laboratory of Atmospheric Chemistry, CH-5232 Villigen, Switzerland,

²Laboratory for Advanced Analytical Technologies, Empa, 8600 Dübendorf, Switzerland,

³Aix Marseille Université, CNRS, LCE FRE 3416, 13331 Marseille, France,

⁴Helmholtzzentrum Munich, Ingolstädter Landstrasse 1, 85764 Oberschleissheim, Germany,

⁵Institute of Piston Machines and Internal Combustion Engines, University of Rostock, 18059 Rostock, Germany,

* Now at: Department of Atmosphere and Climate, Norwegian Institute for Air Research, Kjeller, Norway,

⁶European Commission Joint Research Centre, Institute for Energy and Transport, 21027 Ispra, Italy

In preparation for Atmospheric Chemistry and Physics

Abstract

The emission factors and chemical composition of the organic gases (OGs) emitted by aircraft turbine engines, a diesel ship engine and motor vehicles were studied using a proton-transfer-reaction mass spectrometer (PTR-ToF-MS). To simplify conceptual and modelling analyses of ambient sources, we investigated not only individual OGs but also in terms of functionality-based OG groups. OG group classifications included acids, alcohols, aromatics, carbonyls, aliphatics, Nitrogen and Sulfur-containing OGs. In addition to the measurement of individual compounds, organic gases were also grouped according to their functionality *e.g.* aromatics, acids, carbonyls. 2S-Scooters and the ship fueled by heavy fuel oil (HFO) emitted the highest total NMOG per kg fuel. 2S-Scooters also have the highest aromatic gases emission factor (EF). However the fraction of polycyclic-aromatic hydrocarbons (PAHs) was highest for the ship fueled by HFO with a total EF of 1.6 g/kg fuel. An idling turbine engine of an aircraft also emits 20-30 times more NMOGs than light duty vehicles under similar ambient conditions. This work also provides relative gaseous trace composition of each source that can be used for source apportionment studies of OGs in ambient air.

6.1 Introduction

Approximately 90 million barrels of crude oil were burned daily in 2015. More than half of this was used as distillate/diesel, gasoline and jet fuel (28.4%, 23.8% and 6%, respectively) and consumed mostly by mobile sources *e.g.* motor vehicles, ships and aircraft (EIA, 2016). Significant amounts of gaseous and particulate pollutants including organic gases (OGs) are emitted due to the combustion of these different fuel types.

Substantial amounts of OGs, *e.g.* hydrocarbons, acids, carbonyls, are emitted by aircraft during a flight. Both the amount of pollutants and exhaust chemical composition depend on (i) fuel content (Brem et al., 2015) and (ii) engine load (Kilic et al., 2017). These emissions potentially affect local air quality (Hudda et al., 2014; Unal et al., 2005), public health (Lin et al., 2008) and global climate (Lee et al., 2009; Sausen et al., 2005) either by primary (directly emitted) emissions or secondary formation (as a result of transformation in the atmosphere) (Miracolo et al., 2011; Presto et al., 2011).

Similar to other combustion systems, the emissions from ships also depend on engine load and fuel type (Lack & Corbett, 2012; Sippula et al., 2014). The particles emitted by ships as part of these emissions lead to enhanced cloud formation on shipping routes as previously reported both via direct and satellite observations (Radke et al., 1989). Further the pollutants emitted by ships could increase pollutant concentrations both at coastal regions and near ports (De Meyer et al., 2008; Viana et al., 2014).

Traffic emissions due to on-road vehicles is a major source of air pollution worldwide (Fischer et al., 2000; Nielsen, 1996). Vehicles powered by the engines using gasoline and diesel fuel also emit organic gases amount and composition of which depends on the combustion conditions *e.g.* engine load, ambient temperature (Kean et al., 2003; Platt et al., 2013; Zardini et al., 2014). These vehicular emissions were reported as the source of the air pollution near roads and highways (Karner et al., 2010; Zhu et al., 2002) leading to adverse public-health effects (Lewis et al., 2005; Pope et al., 2004; Waldron et al., 1995).

In order to better monitor potential effects of the OG emissions from mobile sources, the quantification of the contribution from each source in a complex emissions microenvironment and the monitoring of the exhaust chemical composition for each source are required. This study provides an OG emission comparison of different vehicles for (i) the OG emissions per fuel consumed and (ii) the chemical composition of the OG exhaust. The exhausts from the engines of commercial aircraft, ship and on-road motor vehicles include some variation of ambient temperature, fuel type and engine load.

6.2 Instrumentation and methods

A proton-transfer-reaction time-of-flight mass spectrometer (PTR-ToF-MS 8000, Ionicon G.m.b.H., Innsbruck Austria) was used for the detection of organic gases. The PTR-ToF-MS enables the detection of organic gases that have a higher proton affinity than that of water. The air samples containing OGs were protonated by the H_3O^+ ion. The resulting positively charged ions were detected using a time-of-flight mass spectrometer (Graus et al., 2010; Hansel et al., 1995). The PTR-ToF-MS was operated at a drift voltage (U_{drift}) of 550 V, a drift chamber temperature (T_{drift}) of 60 °C, and a drift pressure (p_{drift}) of 2.2 mbar, maintaining a reduced electric field (E/N) of ~ 120 Townsends (Td). Data was collected with one second time resolution. Due to the exothermic nature of the protonation reaction, some ions fragment in the drift tube. The ion-transmission function was quantified using a gas standard containing a mixture of 12 compounds spanning mass-to-charge ratios (m/z) from m/z 33 to 181 (Carbagas AG., Zurich, Switzerland). Volume mixing ratios (ppbv) were calculated according to De Gouw and Warneke (2007), by using $\text{H}_3\text{O}^+/\text{NMOG}$ reaction rate constants (k) estimated by Cappelin et al. (2012), and assuming $k = 2 \times 10^{-9} \text{ cm}^3 \text{ s}^{-1}$ otherwise.

Fragments of organic gases, e.g. aldehydes, are attributed to their parent ion depending on the experiment (when the total mass fraction of the fragments was higher than 5%) according to Klein et al. (2016). The PTR-ToF-MS cannot detect, by H_3O^+ ionization, most alkanes with a carbon number below 12 due to their low proton affinity.

The Tofware version 2.4.5 (TOFWERK AG, Thun, Switzerland; PTR module as distributed by Ionicon Analytik GmbH, Innsbruck, Austria) running in the Igor Pro 6.3 environment (Wavemetrics Inc., Lake Oswego, OR, USA), was used to convert extracted ion intensities to volume mixing ratios (ppbv). The compounds were then grouped according to their functionality as acids, alcohols, aliphatic hydrocarbons (HCs), aromatic HCs, carbonyls (including e.g. aldehydes, ketones), nitrogen containing compounds, unclassified HC fragments, other oxygen containing compounds, sulfur containing compounds and unidentified compounds (species without an assigned molecular formula) same as Kilic et al. (2016). An exemplary figure for aircraft and ship, showing OG mass fractions on mass spectra and functional group fraction in a pie chart, can be found in the supplementary Figure S 6-1.

Picarro G2401 Cavity Ring-Down Spectroscopy (CRDS) was also used in parallel to the PTR-ToF-MS to quantify CO_2 , CO and H_2O volume mixing ratios. The carbon mass balance was used to calculate emission indices (EF , g/kg fuel) reported as shown in Eqn 6-1:

$$EF = [OG] \times \left[\frac{MW_{\text{CO}_2}}{MW_C \times \Delta \text{CO}_2} + \frac{MW_{\text{CO}}}{MW_C \times \Delta \text{CO}} \right] \times C_f \quad \text{Eqn 6-1}$$

where OG denotes the organic gas concentration, MW_x (g/mole) is the molecular weight of the compounds denoted by X . ΔCO and ΔCO_2 denotes background-subtracted CO and CO_2 concentrations, respectively. C_f is the carbon fraction of the fuel used during the campaigns.

6.3 Results and discussion

Total non-methane organic gases (NMOG) emission factors (EF, mg/kg fuel) for all sources studied are given in Figure 6-1. Among the vehicles tested, top two mobile sources were measured to be ship fueled by heavy fuel oil (HFO) and 2S-scooters (M2S) with the EFs of 32.6×10^3 and 27.8×10^3 mg/kg fuel, respectively. From highest to lowest, these two followed by idling aircraft and light duty gasoline vehicle during cold weather ($-7^\circ C$) with the EFs spanning from 10^3 to 10^4 mg/kg fuel. Although the heavy duty vehicles (HDD) were tested twice at low temperatures ($-7^\circ C$) and with an liquid petroleum gas (LPG) fueled engine at an ambient temperature of $+22^\circ C$, these tests imply that their NMOG EFs can be as high as both an idling aircraft or a LDG and even higher depending on the combustion conditions. EFs from the rest of the HDD tests and the LDD EFs measured under ambient temperatures of $-7^\circ C$ and $+22^\circ C$ were either equal to 10^3 mg/kg fuel or lower. Aircraft turbine engine operating at engine loads above 30% corresponding to approach, cruise and take-off operations emit lowest NMOG for the same amount of fuel burned compared to other vehicles tested.

Figure 6-2 presents the functional group mass fractions for the vehicles tested. Aircraft exhaust contained in relative terms most carbonyls with a fraction range of 40-45% at all engine loads tested. After carbonyls, aromatics were measured to be the second highest with a fraction of $\sim 18\%$ during idle (load 2.5-7%). At in-the-air engine loads ($\geq 30\%$), however, the exhaust contained more oxygenated OGs and acids were the second most abundant species group after carbonyls with a fraction spanning in the range of 20-30%.

Similar to aircraft, ships (engine load 50%) emit carbonyls the most ($\sim 50\%$) among all NMOGs when marine gas oil (MGO) used. This carbonyl fraction is lower (27%) while using heavy fuel oil (HFO) at the same engine load. Using HFO, the HC fraction of exhaust (sum of aromatics, aliphatics and HC fragments) increased to 50% from 21% (HC fraction of MGO exhaust).

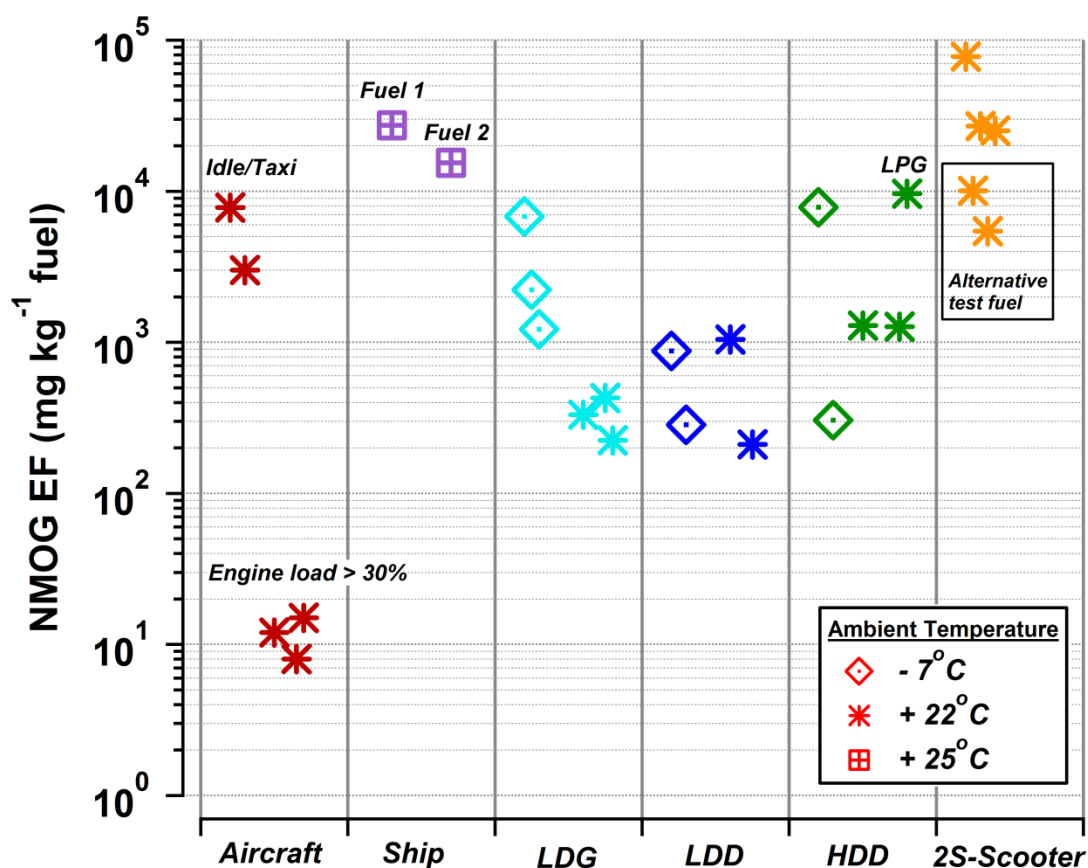


Figure 6-1: Total NMOG emission per fuel burned for mobile sources. Average EFs measured for seven aircraft turbine engines (red markers) presented for different engine loads. EFs of a diesel-engine ship for one engine load (cruise load 50%) is given for two fuel types; heavy fuel oil (Fuel 1, HFO) and marine gas oil (Fuel 2, MGO) in purple. The average (over the driving cycle) EFs of the on-road motor vehicles, three light duty gasoline vehicle (LDG), two light duty diesel vehicle (LDD), two heavy duty diesel vehicles –one powered by liquid petroleum gas (LPG)-, and two 2-stroke scooters can be found next to the ship and aircraft. The ambient temperatures during measurements are separated by the marker type.

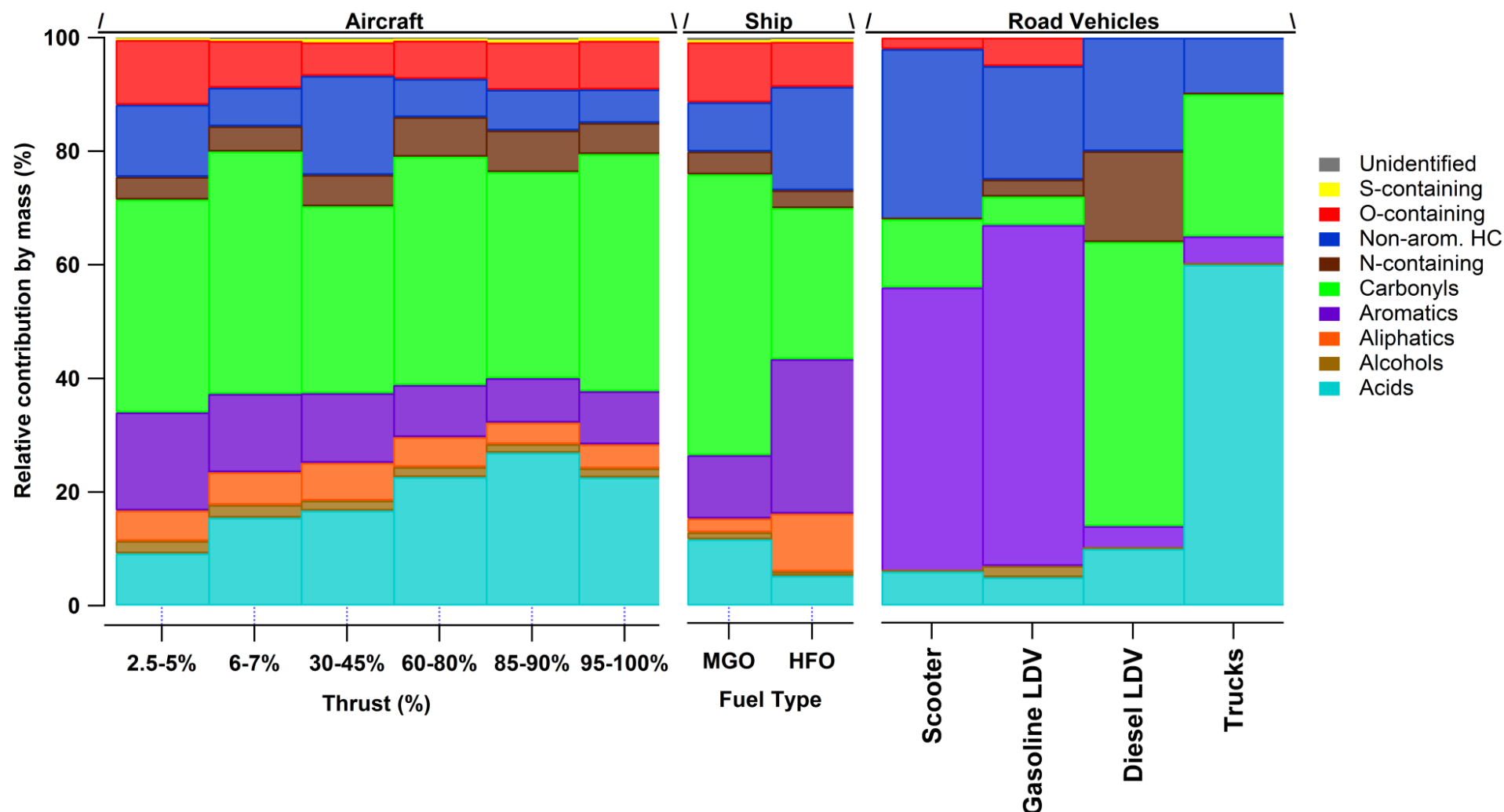


Figure 6-2: Average functional-group fractions of the vehicle exhausts: Aircraft at different engine load, Cruise load (50%) ship engine with different fuel type, and the motor vehicles for New European Driving Cycle (NEDC).

Among the motor vehicles, light duty diesel (LDD) vehicles have the highest carbonyl fraction with ~40% while the exhaust of the 2S-scooters and light duty gasoline vehicles dominated by aromatic compounds (Figure 6-2) with fractions of 50% and 65%, respectively. Besides, heavy duty diesel (HDD, trucks) vehicles contained mostly acids in their exhaust with a fraction of ~60%. The HC content of the HDDs were the lowest among all the vehicles tested with a fraction of ~15%.

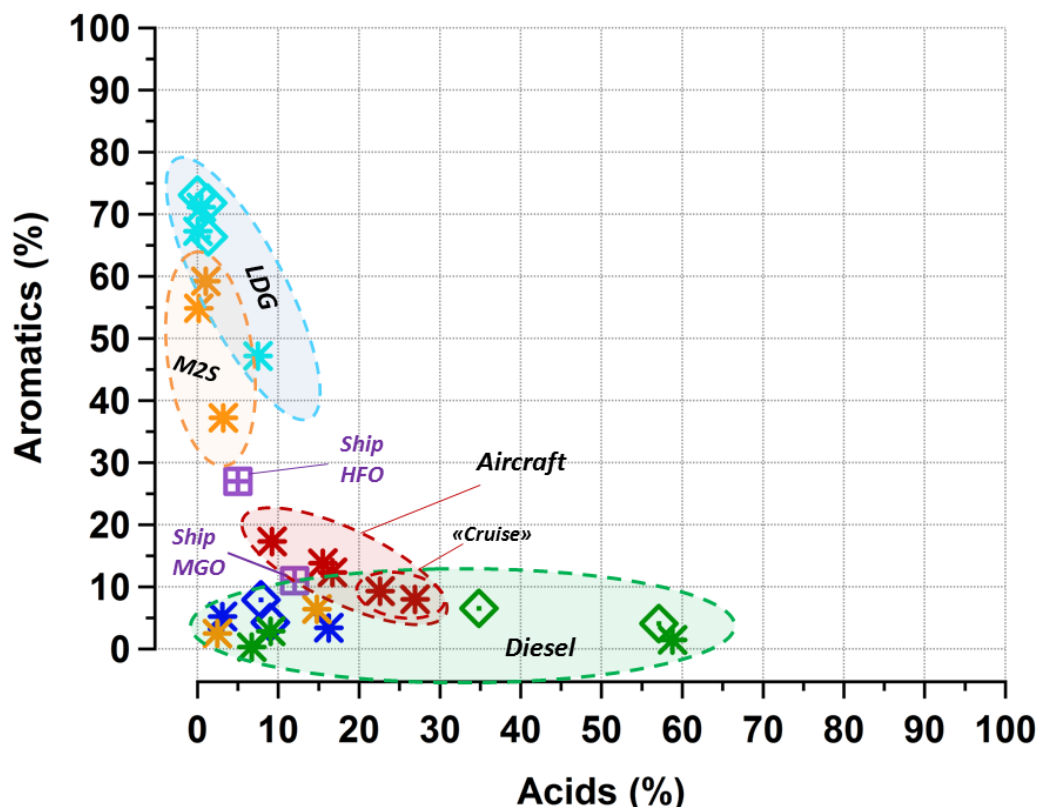


Figure 6-3: Scatter plot showing aromatic and acidic fractions for the exhaust experiments.

Figure 6-3 compares the acid and aromatic fractions of all vehicles. Diesel-fueled motor vehicles tend to have a higher acid fraction compared to aromatic HCs while the LDGs and 2S-scooters tend to have higher aromatic fraction. The exhaust of the ship fueled with MGO and aircraft turbine engine during cruise load have a more similar acid to aromatic ratio to LDGs and 2S-Scooters while the respective ratio for HFO-fueled ship is similar to 2S-scooters. However, the aromatic gases contributing to the total aromatic mass, are different between 2S-scooters and HFO-fueled ship. 2S-scooters emitted mostly single-ring aromatics (95% of the total aromatic gases) e.g. benzene, toluene, xylenes and methylbenzenes and a minor fraction of PAHs (<1%) while HFO-fueled ship contained 22% PAHs. Further HDDs have the largest variability in acids compared to other vehicles (green markers). This variability however does not correlate with the total NMOG EF of HDDs, ambient temperature or fuel type.

Further, two of the tests, when investigating 2S-scooters, were performed with an alternative fuel (reduced aromatic content). These two tests are shown in Figure 6-3 with orange markers. According to these 2S-scooters with the alternative fuel, aromatic OGs, in the exhaust, was decreased, and resulted in acid to aromatic ratios similar to LDDs.

Figure 6-4 compares the fraction of carbonyls and aromatics same as Figure 6-3. Diesel-fueled motor vehicles have higher carbonyl fraction in the exhaust compared to aromatic abundant LDGs and 2S-Scooters. Aircraft and MGO-fueled ship have a carbonyl to aromatic ratio more similar to diesel vehicles than LDGs. In contrast, the HFO-fueled ship emissions have a higher similarity to 2S-Scooters and LDGs in carbonyl and aromatic abundance.

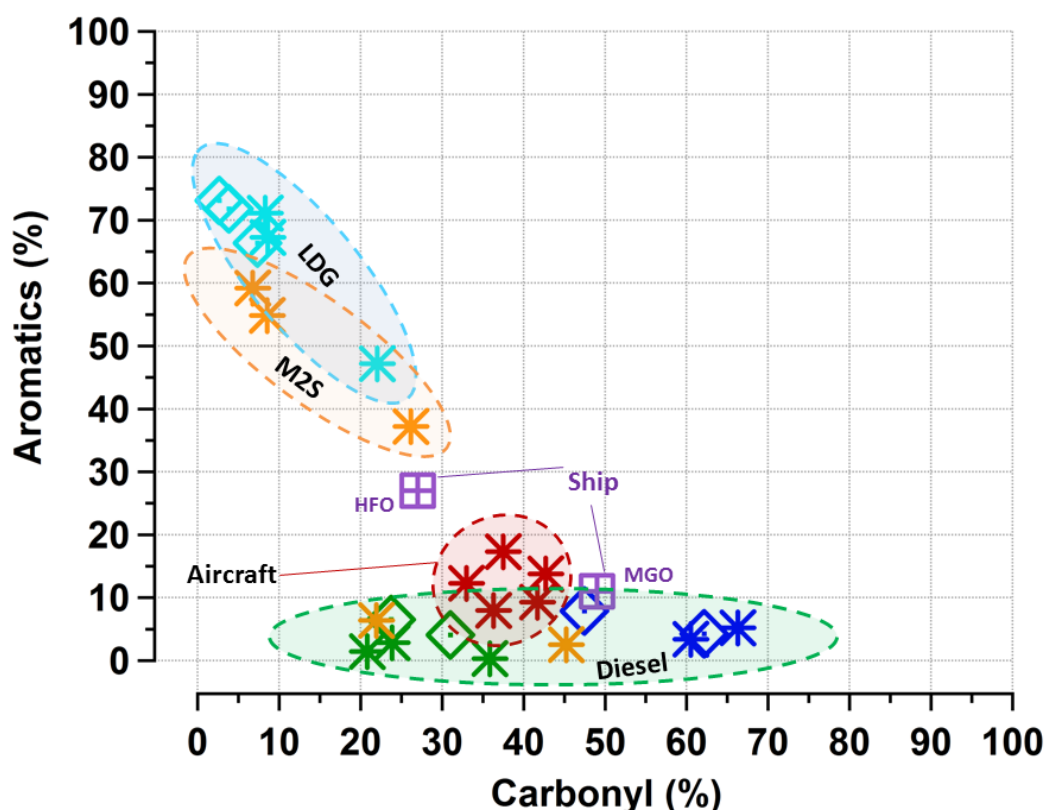


Figure 6-4: Scatter plot showing aromatic and carbonyl fractions for the exhaust experiments.

Emission factors for total NMOG, aromatic hydrocarbons and polycyclic aromatic hydrocarbons (PAHs) are given in Table 6-1. 2S-scooters were by far (about 2 times higher than the second highest HFO-fueled ship) the highest mobile source emitter of aromatics with an EF of 16.4×10^3 mg/kg fuel. However only a small fraction of the gaseous aromatics emitted by 2S-scooters (M2S) were PAHs (PAH EF is 43.7 mg/kg fuel). Compared to a 2S-scooter, MGO-fueled and HFO-fueled ships emitted about 20 and 40 times higher PAHs, respectively at cruise load (Table 6-1).

Table 6-1: Emission factors of mobile sources for total NMOG, aromatic HCs and PAHs.

Vehicle	Emission factor (mg kg ⁻¹ fuel)		
	Total NMOG	Aromatics	PAH
Light Duty Gasoline (-7°C)	3432	2417	38.1
Light Duty Gasoline (+22°C)	329	204	2.11
Light Duty Diesel (-7°C)	584	35.4	0.00
Light Duty Diesel (+22°C)	631	27.2	0.01
Heavy Duty Diesel (-7°C)	4086	217	0.07
Heavy Duty Diesel (+22°C)	1285	27.6	0.00
Heavy Duty Diesel (+22°C, LPG)	9676	31.9	0.00
2S-Scooter (+22°C)	32568	16426	43.7
2S-Scooter (+22°C, Fuel aromatics removed)	15290	681	0.39
Aircraft Idle (3-5% thrust)	7800	1357	81.4
Aircraft Idle (6-7% thrust)	3000	444	26.6
Ship (Cruise 50%, HFO)	27300	7371	1621.6
Ship (Cruise 50%, MGO)	15400	1694	745.4

6.4 Atmospheric implications

Scooters and HFO-fueled ship are the two top mobile sources with the highest NMOG EFs. For the same amount of fuel consumed, each of these sources emits 80-100 times more NMOG than an LDG under similar ambient temperature (20-25°C). In addition ships fueled by MGO also emit much more (50 times) than an LDG. The scooter and ship engine experiments (tested two different fuels) imply that a busy port or high 2S-scooter use relative to the other motor vehicles or both could be a major NMOG source in a city. These mobile sources individually or together potentially impact public health the areas nearby either directly or by forming aerosols (Platt et al., 2014).

Figure 6-5 shows the equivalent on-road distance to average aircraft taxi/idle for aromatics. The amount of aromatics emitted by a single turbine engine during taxiing/idling is calculated as 140 g for 26 minutes idling/taxiing (ICAO average duration). To match 140 g aromatics emitted by one turbine engine (See supplementary section 6.5.1 for the calculation details), an LDG needs to be driven for 1000 km during cold weather (-7°C) as shown in Figure 6-5. This distance is much longer for HDDs and LDDs under same weather conditions, with 11200 km and 68200 km, respectively.

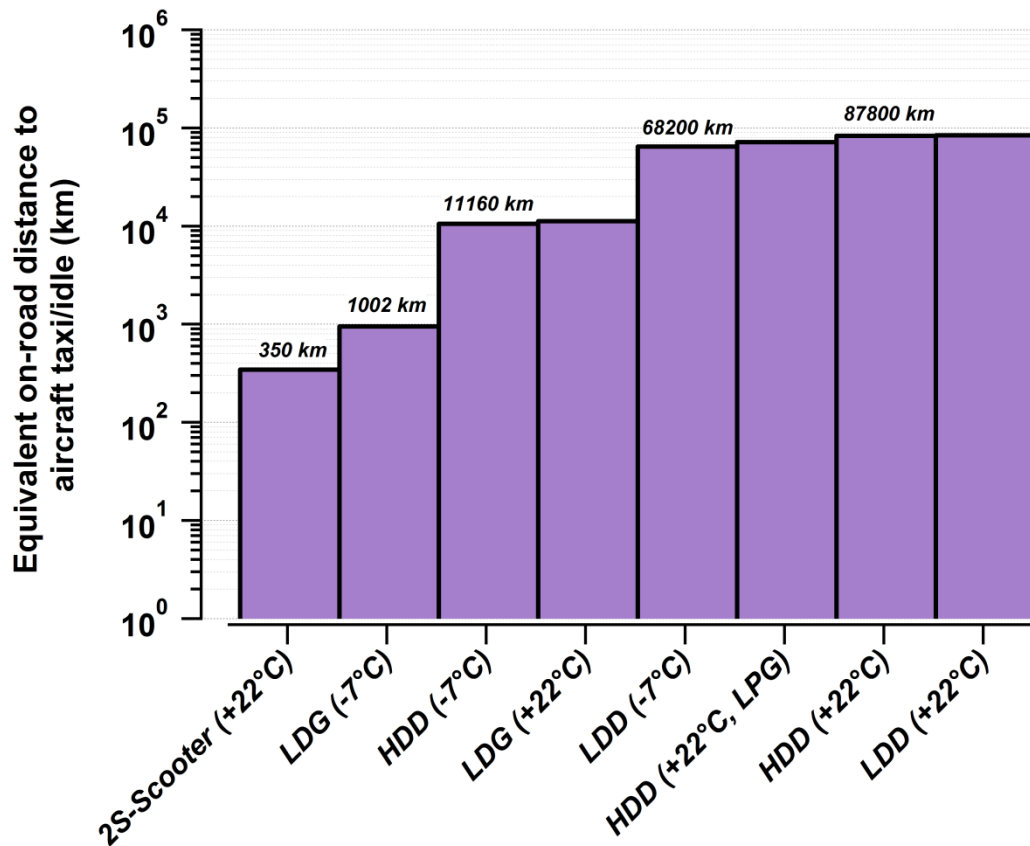


Figure 6-5: The distance (km) required to match an average idle/taxi operation of a turbine engine for motor vehicles.

The reduction of the NMOG emissions from ships such as containers, bulk carriers and tankers has both regional and global implications since ships do not only harbor at or near the ports but also travel over oceans. Heavy fuel oil accounts to ~80% of the ship fuel consumed globally (LR & UCL, 2014). Using MGO instead of HFO as fuel, reduces ship NMOG emissions by 50% and aromatics by ~80 times. Therefore switching to MGO could partially eliminate both direct (e.g. 50% lower PAH emissions which are hazardous to health) and indirect (e.g. secondary aerosol formation) effects of ship NMOG emissions.

A single idling turbine engine of an aircraft at the airport emits approximately as much as 100 people driving LDGs to their work in 10 km distance from home in cold weather (-7°C). The idling emissions are required to be decreased by reducing taxi-idle durations since the NMOG emissions from airports are dominated by idling aircraft (Kilic et al., 2017; Kim, 2009). Alternatively using electric tows to bring aircraft to the runway or single-engine taxi/idle at the airport could significantly reduce airport NMOG emissions.

6.5 Supplementary information

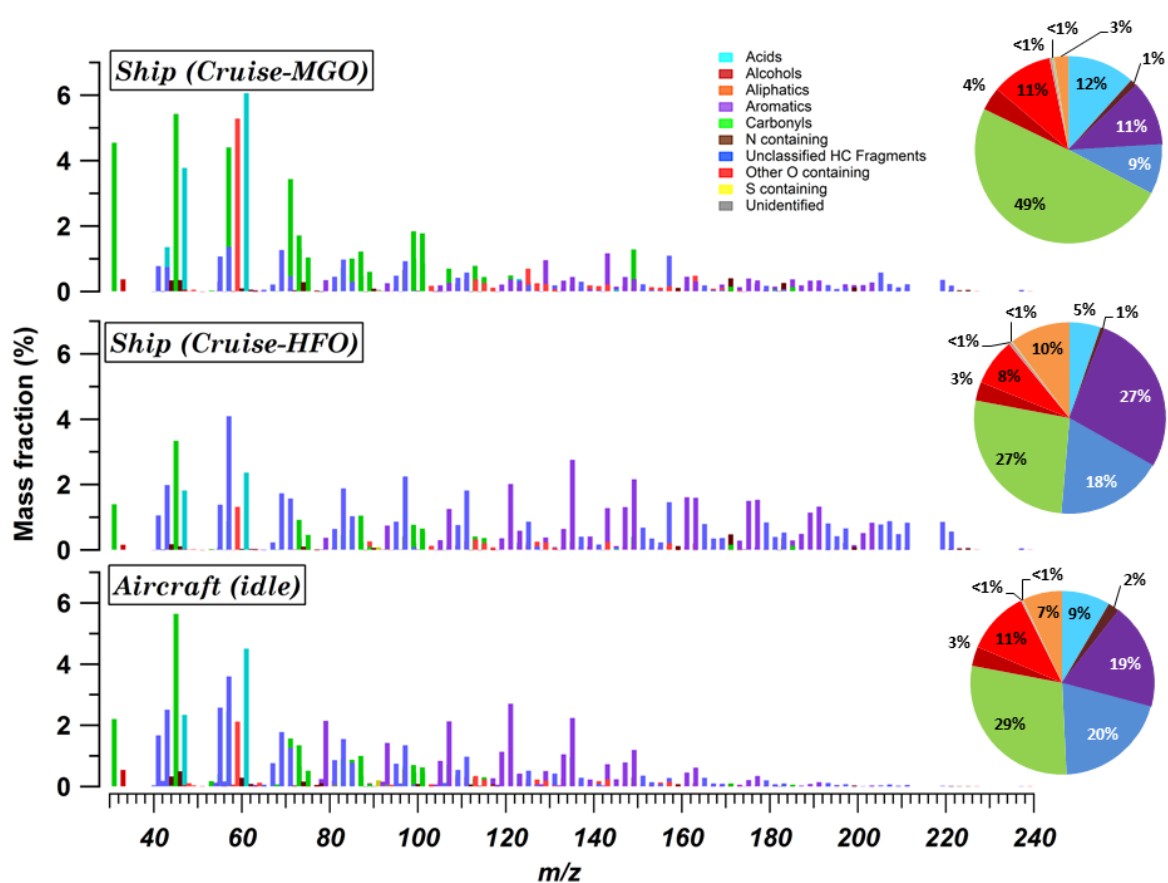


Figure S 6-1: Mass fraction of OGs (left) and functional group fractions (right, pie-charts) for cruising ship (two fuel types) and idling aircraft.

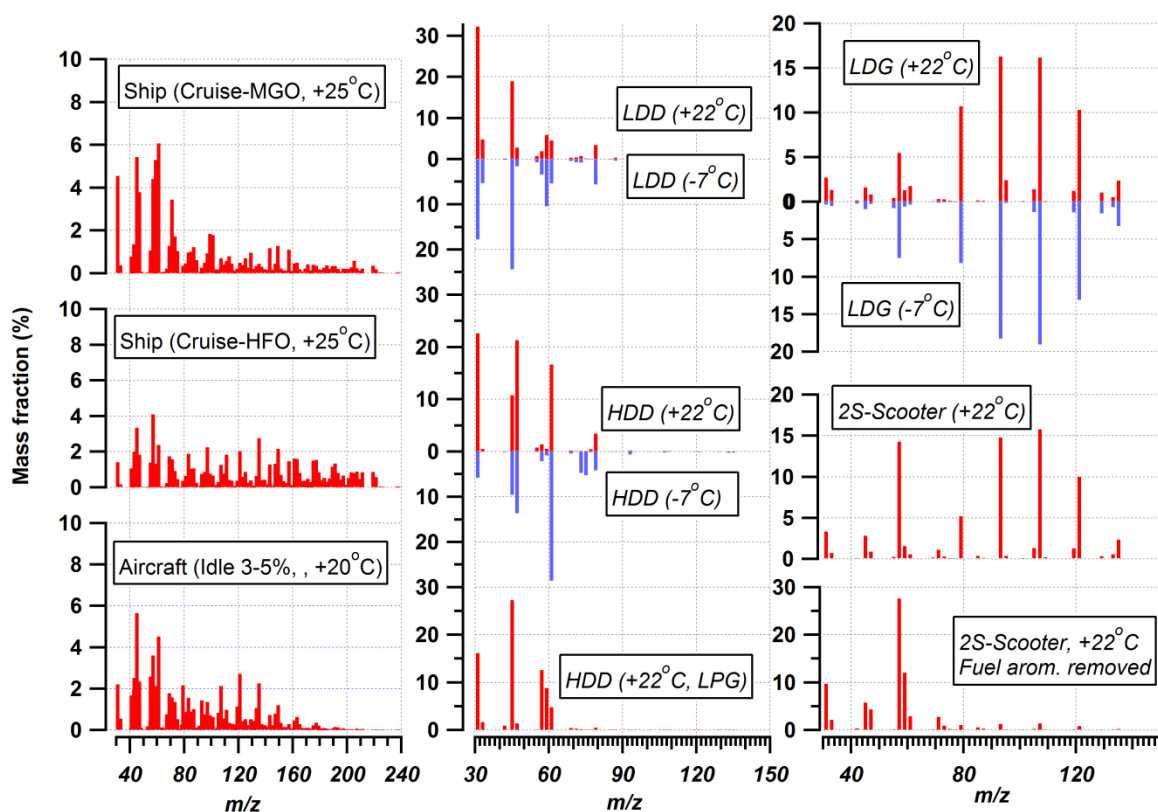


Figure S 6-2: OG fingerprints for all mobile sources tested.

6.5.1 Calculation of aircraft taxi-idle aromatic emission and equivalent distances for on-road vehicles

$$\text{Idling Aromatic OGs (g)} = EF(g \text{ kg}^{-1} \text{ fuel})_{\text{taxi-idle}} \times FC (kg \text{ sec}^{-1}) \times FD(\text{sec})$$

EF: Average taxi-idle aromatic emission factor = $0.9 \text{ g kg}^{-1} \text{ fuel}$

FC: Taxi/idle fuel consumption of 0.1 kg sec^{-1}

FD: ICAO-average taxi/idle duration = 26 minutes = 1560 seconds

Idling-aircraft aromatic OGs $\approx 140 \text{ g}$

For example, a 2S-Scooter emitting $0.4 \text{ g aromatics km}^{-1}$ (See Table S 7-1):

$$\text{Distance (km)} = 140 \text{ g} / 0.4 \text{ g km}^{-1} = \underline{350 \text{ km}}$$

Table S 6-1: Total NMOG, gaseous aromatic and PAH (gases) emission factors (per km) of on-road vehicles.

Vehicle	Emission Factor (mg km ⁻¹)		
	Total NMOG	Aromatic	PAH
Light Duty Gasoline (-7°C)	199.05	140.18	2.21
Light Duty Gasoline (+22°C)	19.10	11.82	0.12
Light Duty Diesel (-7°C)	33.85	2.06	0.00
Light Duty Diesel (+22°C)	36.62	1.58	0.00
Heavy Duty Diesel (-7°C)	237.01	12.58	0.00
Heavy Duty Diesel (+22°C)	74.51	1.60	0.00
Heavy Duty Diesel (+22°C, LPG)	561.22	1.85	0.00
2S-Scooter (+22°C)	766.97	386.83	1.03
2S-Scooter (+22°C, Fuel aromatics removed)	305.81	13.63	0.01

7 Conclusions

Primary gaseous and particulate emissions from in-service aircraft turbine engines were investigated using an experimental setup capable of measuring organic gases, CO, CO₂ and NR-PM₁. Exhausts from these engines were also aged using a flow tube (PAM) to simulate atmospheric oxidation. Measurements were conducted for different engine loads corresponding to LTO cycle flight modes of approach (thrust 30%), taxi-idle (thrust 2.5-7%), take-off (thrust 100%) and climb (thrust 85%). The aircraft NMOG emissions of different engine loads were also compared to the other mobile sources *i.e.* ship, 2S-scooter, LDGs, LDDs and HDDs.

Emission indices (EIs) of more than 200 NMOGs were quantified, and grouped according to their functionality (including acids, carbonyls, aromatics, and aliphatics). Total NMOG emissions were highest at idling with an average EI of 7.8 g/kg fuel and decreased with increasing thrust (being a factor of ~40 lower at take-off thrust compared to idling). The pure hydrocarbon fraction (particularly aromatics and aliphatics) of the engine exhaust decreased with increasing thrust, while the fraction of oxidized compounds, *e.g.* acids and carbonyls increased. Older engines emitted a higher fraction of non-oxidized NMOGs compared to newer ones showing that the exhaust chemical composition at idle was also affected by engine technology.

NMOG emissions during taxi and idle operations account for more than 90% of the NMOG emission mass during an LTO cycle. Emissions from these conditions dominate due to both the high idling EIs and the large fraction of time spent by an aircraft during idling (26 minutes). LTO emissions for idling aircraft, utilizing several engine operation protocols, were measured to have wide variability. The average total NMOG emissions from all the tested engines was 1.26 kg/LTO at idling <6%, and only 0.56 kg NMOG/LTO at 6-7%. This study showed that although all engine operation at ≤7% thrust is nominally classified as taxi/idle, the precise thrust used has a major effect on the total NMOG emissions.

The oxidation of NMOGs using the PAM yielded a SOA EI of 10 and 100 times more than POA during cruise and idling conditions, respectively. This high SOA/POA ratio implies that the major NRPM₁ contribution from turbine engines is due to unregulated secondary particles formed in the atmosphere due to the aging of primary emissions.

Further, SOA formation was attributed mostly to the oxidation of aromatic gases at idle. By considering published SOA yields, we achieved closure between measured SOA precursors and formed SOA mass, measured by the AMS. The most important SOA precursors were aromatic gases. In contrast to emissions at low thrust level conditions, aging of emissions generated at high thrust yielded mainly sulfate.

NMOG emissions from airports are dominated by idling aircraft making airports an important source of both gaseous and particulate pollutants. Due to the dominant contribution of idling emissions to total ground-level aircraft NMOG emissions, shut-down of half the aircraft engines at idle is suggested as a potentially beneficial emission reduction strategy. This shut-down does not only eliminate emissions from the deactivated engine, but increases the power load of the engines remaining in operation, leading them to a more efficient operation and lower emissions per fuel consumed. The effects of this shut-down on a twinjet aircraft from a single engine can be roughly estimated as a change from the thrust 2.5-5% to 6-7% decreasing the NMOG EI from 2.23 kg/LTO to 0.56 kg/LTO (approximately a factor of 4). Therefore, engine shut-down at idling could improve air quality in the airport micro-environment, by reducing NMOG emissions from aircrafts and SOA upon their aging. The use of electric tow tractors to reduce the idling duration could be another alternative to reduce gaseous pollutant concentrations from aircraft.

We also compared the airplane engine emissions to other fossil fuel combustion emissions from mobile sources. Scooters and HFO-fueled ship are the two mobile sources with the highest NMOG EFs. For the same amount of fuel consumed, each of these sources emits 80-100 times more NMOG than a light duty gasoline car under similar ambient temperatures (20-25°C). Although the aircraft EI were not the highest among the vehicles tested, the amount of aromatics emitted by a single turbine engine during taxiing/idling is calculated as 140 g for 26 minutes idling/taxiing (ICAO average duration). To match 140 g of aromatics emitted by one turbine engine, a gasoline car needs to be driven for 11200 km during low temperature (-7°C) or even 68200 km at 20-25°C. In other words a single idling turbine engine of an aircraft at the airport emits approximately as much as 1000 people driving LDVs to their work in 10 km distance from home.

8 Outlook

Many scientific goals were achieved by the successful A-PRIDE campaigns as discussed above including (i) characterization of the gaseous and particulate emissions from aircraft turbine engines for different engine operation modes, (ii) aging of the aircraft exhaust emissions and (iii) comparison of aircraft NMOG emissions to other mobile sources.

While a PTR-ToF-MS is capable of the quantification of a wide variety of organic gaseous, species with a proton affinity lower than water, *e.g.* alkanes, are not accessible. The PTR-ToF-MS measurements do not allow for a separation between isomeric compounds, with the same chemical formula. Therefore, coupling our measurements with online or offline gas-chromatography techniques would significantly extend our knowledge of the exhaust chemical composition.

SOA yields used here are for a limited number of compounds with uncertainties due to the different aging conditions *e.g.* NO_x level. The SOA potential of many other OGs needs to be verified as well under different aging conditions, preferentially using the PAM, with the same settings as in this thesis.

The quality of the fuel could also influence aircraft emissions. Previously Brem et al. (2015) reported that the fuel aromatic content influences aircraft particle emissions. Due to technical reasons, the influence of fuel doping with aromatics on SOA formation could not be assessed during our measurements. Similar to affecting the particle emissions, the fuel content may also influence the emissions of the organic gases during idling, which warrants further experiments.

Further, two of the older engines tested led to higher OG emission factors. This implies a likely engine age or manufacture year impact. Extending exhaust measurement for more engine types and ages could answer some open questions regarding the dependence of OG emissions on engine parameters.

Aging experiments were performed under ground level atmospheric conditions also for cruise loads. However, the atmospheric conditions at cruise altitudes are largely different from ground level. Specifically, pressure and temperature are much lower (100 mbar, -50 °C) compared to ground level (1000 mbar, +20 °C). The investigation of SOA under these cruise altitude conditions should be performed for a better representativeness of the emissions at high altitude.

Secondary aerosols (SA) from mobile sources are not directly regulated by any authority although being 10-100 times higher than POA for an aircraft for example. As shown in this study oxidizing flow tubes (*e.g.*, PAM) providing fast and atmospherically relevant aging simulations could be used to estimate the total SA formation potential of mobile sources.

Results here provided fingerprints of organic gases of an idling aircraft and also other vehicles. These fingerprints could help the apportionment of sources at receptor sites affected by these emissions. Such measurements using a stationary or mobile platform can be very valuable for the estimation of the effect of different mobile sources on ambient air quality.

List of Tables

Table 1-1: PM regulation standards from selected countries and institutions.	6
Table 3-1: Calibration gases and their abundance in the gas bottle.	18
Table 5-1: Volume mixing ratios of gaseous emissions, engine parameters and emission indices (EIs) for primary (directly emitted) and secondary (after aging) for all experiments.	52
Table 5-2: Precursor OGs, their corresponding functional group and protonated m/z, SOA yield coefficients* from literature, and average SOA EI estimated for different thrusts.	54
Table 6-1: Emission factors of mobile sources for total NMOG, aromatic HCs and PAHs.	69

Table of Figures

Figure 1-1: Artwork by Randy Russell showing the troposphere and stratosphere. The temperature in the troposphere decreases with the increasing altitude.....	1
Figure 1-2: Schematic showing the atmospheric aerosol size distribution for four modes (Finlayson-Pitts & Pitts Jr., 2000).	3
Figure 1-3: Radiative forcing estimates in 2011 relative to 1750 for the selected precursors of climate change. Global values are best estimates with the level of confidence (L: Low, M: Medium, H: High). Adapted from (IPCC, 2013).	5
Figure 1-4: Deposition of different sized particles in different segments of the respiratory system: N=Nasal, TB= Tracheobronchial, A=Alveolar (adapted from ATSDR, 1994).....	6
Figure 2-1: Historical inventories and future projections of civil-aviation CO ₂ emissions (based on civil and military aviation fuel sale statistics (IEA, 2007)) from a variety of sources. From Lee et al., (2009).	7
Figure 2-2: Near-ground flight operations of an aircraft: Landing take-off (LTO) cycle. Source http://www.icao.int/environmental-protection/Pages/local-air-quality.aspx	8
Figure 2-3: Aircraft emissions and their atmospheric implications. Figure by Lee et al., 2009) (adapted from Prather et al., 1999) and Wuebbles et al., 2007)).	9
Figure 2-4: The radiative forcing due to aviation emissions with components from Lee et al. (2009).	10
Figure 2-5: A sample spatial pattern of particle number concentrations from Los Angeles International Airport. (From Hudda et al. (2014).	11
Figure 3-1: A simplified scheme of the PTR-TOF instrument (Graus et al., 2010).	15
Figure 3-2: Separation of two OGs at the same integer m/z: Measured-ion signal of a gas sample containing acrylic acid (blue line) and butanone (green line) and modified-Gaussian fitted peaks (black line).....	16
Figure 3-3: Transmission coefficient (TR_{OG^+}) of the reference compounds (red) and the fitted transmission function (blue line).	17
Figure 3-4: Schematic showing the main component of the AMS (DeCarlo et al., 2006).	19
Figure 3-5: Simplified scheme of the experimental setup used for aging experiments.	21
Figure 4-1: Simplified sketch of the experimental setup.	26
Figure 4-2: Mean total NMOG emission index (g/kg fuel) and standard deviation (CI: 95%) as a function of thrust for engines operated in the SR Technics test cell. “e” is the number of engines tested and “n” is the total number of tests at the designated thrust. Inset: NMOG EIs for individual measurements as a function of thrust, separated by engine model (numbers) and thrust rating (pink=engines of the higher thrust rating with a range of 244.6 – 311.4 kN, green= engines of the lower thrust rating with a range of 111.2 – 155.7 kN).	30

- Figure 4-3: Mass fractions (%) of different compound classes presented as horizontal bars for the thrust bins (top panel). The emission indices of functional groups (in log scale) are shown in the bottom panel.33
- Figure 4-4: NMOG composition at idle for the different engines tested (top). The engines are sorted according to their thrust rating from lowest (top) to highest (bottom). Average idling (thrust $\leq 7\%$) EI of the different compound classes with the confidence interval (CI: 95%) are shown in the bottom panel. Blue markers denote engines within the thrust rating range of 111.2-155.7 kN, green markers those within the range of 244.6-311.4 kN.34
- Figure 5-1: Simplified scheme of the experimental setup.45
- Figure 5-2: Sample experiment showing mean NMOG emissions (top) and representative time series for particle and NMOG components (bottom) for varying OH exposures. Hydrocarbon concentrations (non-aromatic HCs (dark blue), aromatic HCs (purple) and carbonyls (green) decrease in the PAM while the concentrations of acids (mostly formic and acetic $\sim 90\%$ of the total acids) increase. The bottom panel shows the aerosol (Organic, SO_4 , NO_3 , NH_4) formed and gaseous aromatics ($\text{C}_{10}\text{H}_{14}$, $\text{C}_{11}\text{H}_{16}$) for the different OH exposures in the PAM given in the top panel.50
- Figure 5-3: Average emission indices (left) and EIs from individual test points (right) for primary non-methane organic gases (NMOGs), aromatic gases, primary organic aerosol (POA), equivalent black carbon (BC), secondary organic aerosol (SOA), nitrate (NO_3) and sulfate (SO_4). Error bars (+/-) are the standard deviations of the means with a confidence interval of 95%. The OH exposure was in the range of $91\text{--}113 \times 10^6 \text{ molecule cm}^{-1} \text{ h}$ for the secondary aerosol cases.51
- Figure 5-4: Fractions of aromatic compounds for primary emissions (directly emitted) at idle (thrust 3-7%). Benzene derivatives, xylenes, tri-, tetra-, pentamethylbenzene, benzene and toluene account for $\sim 60\%$ of all aromatics.53
- Figure 5-5: Comparison of the SOA measured by the AMS and the SOA predicted by the oxidation of NMOGs (top panel). The statistics are presented for low load idling (thrust 3-5%) on the left half and for idling 6-7% on the right. Aromatic hydrocarbons (purple) were the most abundant precursors of SOA at idle (thrust 3-7%) explaining all SOA formed (green, top panel) at thrust 3-5% and most ($\sim 90\%$) at thrust 6-7%. Aromatic SOA comprised the largest fraction followed by oxygenated aromatics (light purple - e.g. phenol, benzaldehydes), non-aromatic hydrocarbons (orange) with more than 6 carbon atoms in their molecular structure (non-arom. HCs $\geq \text{C}_6$), nitrogen containing compounds (brown), other oxygenated-NMOGs $> \text{C}_6$ (cyan). Average fractions of individual NMOGs (bottom panel) were calculated by using SOA yields from literature (see Table 2) and the amount of NMOG reacted. Error bars show standard deviations of the means (CI: 95%).55
- Figure 5-6: Measured and predicted SOA comparison at cruise load, using the same approach as in Figure 5-5. In contrast to idle conditions, total NMOGs detected do not explain SOA formed.57
- Figure 6-1: Total NMOG emission per fuel burned for mobile sources. Average EFs measured for seven aircraft turbine engines (red markers) presented for different engine loads. EFs of a diesel-engine ship for one engine load (cruise load 50%) is given for two fuel types; heavy fuel oil (Fuel 1, HFO) and marine gas oil (Fuel 2, MGO) in purple. The average (over the driving cycle) EFs of the on-road motor vehicles, three light duty gasoline vehicle (LDG), two light duty diesel vehicle (LDD), two heavy duty diesel vehicles –one powered by liquid petroleum gas (LPG)-, and two 2-stroke scooters can be found next to the ship and aircraft. The ambient temperatures during measurements are separated by the marker type.65
- Figure 6-2: Average functional-group fractions of the vehicle exhausts: Aircraft at different engine load, Cruise load (50%) ship engine with different fuel type, and the motor vehicles for New European Driving Cycle (NEDC).66
- Figure 6-3: Scatter plot showing aromatic and acidic fractions for the exhaust experiments.67

Figure 6-4: Scatter plot showing aromatic and carbonyl fractions for the exhaust experiments.....68

Figure 6-5: The distance (km) required to match an average idle/taxi operation of a turbine engine for motor vehicles.....70

Bibliography

Airbus - *Future Journeys 2013-2032, Global Market Forecast*. Technical report, Page 8, URL <http://www.airbus.com/company/market/forecast/>, 2013.

Alvarez, E. G., Borrás, E., Viidanoja, J., & Hjorth, J.: Unsaturated dicarbonyl products from the OH-initiated photo-oxidation of furan, 2-methylfuran and 3-methylfuran. *Atmospheric Environment*, 43(9), 1603–1612, 2009.

Anderson, B. E., Chen, G., & Blake, D. R.: Hydrocarbon emissions from a modern commercial airliner. *Atmospheric Environment*, 40(19), 3601–3612, 2006.

Andersson, S., Martinsson, B., Friberg, J., Brenninkmeijer, C., Rauthe-Schöch, A., Hermann, M., van Velthoven, P., & Zahn, A.: Composition and evolution of volcanic aerosol from eruptions of Kasatochi, Sarychev and Eyjafjallajökull in 2008–2010 based on Caribic observations. *Atmospheric Chemistry and Physics*, 13(4), 1781–1796, 2013.

Armstrong, B., Hutchinson, E., Unwin, J., & Fletcher, T.: Lung cancer risk after exposure to polycyclic aromatic hydrocarbons: a review and meta-analysis. *Environmental Health Perspectives*, 112(9), 970–978, 2004.

ASTM, D.5291: standard test methods for instrumental determination of carbon, hydrogen, and nitrogen in petroleum products and lubricants. *ASTM, West Conshohocken*, 1996.

Agency for Toxic Substances and Disease Registry (ATSDR): *Asbestos Expert Panel Report Appendix E*. Url: <https://www.atsdr.cdc.gov/hac/asbestospanel/finalpart4.pdf>, 1994

Barmet, P., Dommen, J., DeCarlo, P., Tritscher, T., Praplan, A., Platt, S., Prévôt, A., Donahue, N., & Baltensperger, U.: OH clock determination by proton transfer reaction mass spectrometry at an environmental chamber. *Atmospheric Measurement Techniques*, 5(3), 647–656, 2012.

Beyersdorf, A. J., Thornhill, K. L., Winstead, E. L., Ziemba, L. D., Blake, D. R., Timko, M. T., & Anderson, B. E.: Power-dependent speciation of volatile organic compounds in aircraft exhaust. *Atmospheric Environment*, 61, 275–282, 2012.

Brem, B. T., Durdina, L., Siegerist, F., Beyerle, P., Bruderer, K., Rindlisbacher, T., Rocci-Denis, S., Andac, M. G., Zelina, J., Penanhoat, O., & Wang J.: Effects of fuel aromatic content on nonvolatile particulate emissions of an in-production aircraft gas turbine. *Environmental Science & Technology*, 49(22), 13149–13157, 2015.

Brook, R. D., Rajagopalan, S., Pope, C. A., Brook, J. R., Bhatnagar, A., Diez-Roux, A. V., Holguin, F., Hong, Y., Luepker, R. V., Mittleman, M. A., Peters, A., Smith, S. C. Jr., Whitsel L., Kaufman J.D.: American Heart Association Council on Epidemiology and Prevention, Council on the Kidney in Cardiovascular Disease, and Council on Nutrition, Physical Activity and Metabolism. Particulate matter air pollution and cardiovascular disease an update to the scientific statement from the American Heart Association. *Circulation*, 121(21), 2331–2378, 2010.

Brown, P., Watts, P., Märk, T., & Mayhew, C.: Proton transfer reaction mass spectrometry investigations on the effects of reduced electric field and reagent ion internal energy on product ion branching ratios for a series of saturated alcohols. *International Journal of Mass Spectrometry*, 294(2), 103–111, 2010.

Brunekreef, B., Beelen, R., Hoek, G., Schouten, L., Bausch-Goldbohm, S., Fischer, P., Armstrong, B., Hughes, E., Jerrett, M. & van den Brandt, P.: Effects of long-term exposure to traffic-related air pollution on respiratory and cardiovascular mortality in the Netherlands: the NLCS-AIR study. *Res. Rep. Health Eff. Inst.* (139), 5–71, 2009.

Bruns, E., El Haddad, I., Keller, A., Klein, F., Kumar, N., Pieber, S., Corbin, J., Slowik, J., Brune, W., Baltensperger, U., & Prévôt, A., S., H.: Inter-comparison of laboratory smog chamber and flow reactor systems on organic aerosol yield and composition. *Atmospheric Measurement Techniques*, 8(6), 2315–2332, 2015.

Bruns, E. A., El Haddad, I., Slowik, J. G., Kilic, D., Klein, F., Baltensperger, U., & Prévôt, A., S., H.: Identification of significant precursor gases of secondary organic aerosols from residential wood combustion. *Scientific Reports*, 6:27881, 1-9, 2016.

Buhr, K., van Ruth, S., & Delahunty, C.: Analysis of volatile flavour compounds by proton transfer reaction-mass spectrometry: fragmentation patterns and discrimination between isobaric and isomeric compounds. *International Journal of Mass Spectrometry*, 221(1), 1–7, 2002.

Cappellin, L., Karl, T., Probst, M., Ismailova, O., Winkler, P. M., Soukoulis, C., Aprea, E., Märk, T. D., Gasperi, F., & Biasioli, F.: On quantitative determination of volatile organic compound concentrations using proton transfer reaction time-of-flight mass spectrometry. *Environmental Science & Technology*, 46(4), 2283–2290, 2012.

Chan, A., Chan, M., Surratt, J. D., Chhabra, P., Loza, C., Crounse, J., Yee, L., Flagan, R., Wennberg, P., & Seinfeld, J.: Role of aldehyde chemistry and NO_x concentrations in secondary organic aerosol formation. *Atmospheric Chemistry and Physics*, 10(15), 7169–7188, 2010.

Chan, A. W. H., Kautzman, K. E., Chhabra, P. S., Surratt, J. D., Chan, M. N., Crounse, J. D., Kürten, A., Wennberg, P. O., Flagan, R. C., & Seinfeld, J. H.: Secondary organic aerosol formation from photooxidation of naphthalene and alkylnaphthalenes: implications for oxidation of intermediate volatility organic compounds (IVOCs). *Atmospheric Chemistry and Physics*, 9(9), 3049–3060, 2009.

Chhabra, P., Ng, N., Canagaratna, M., Corrigan, A., Russell, L., Worsnop, D., Flagan, R., & Seinfeld, J.: Elemental composition and oxidation of chamber organic aerosol. *Atmospheric Chemistry and Physics*, 11(17), 8827–8845, 2011.

de Gouw, J. & Warneke, C.: Measurements of volatile organic compounds in the earth's atmosphere using proton-transfer-reaction mass spectrometry. *Mass Spectrometry Reviews*, 26(2), 223–257, 2007.

De Meyer, P., Maes, F., & Volckaert, A.: Emissions from international shipping in the Belgian part of the North Sea and the Belgian seaports. *Atmospheric Environment*, 42(1), 196–206, 2008.

DeCarlo, P. F., Kimmel, J. R., Trimborn, A., Northway, M. J., Jayne, J. T., Aiken, A. C., Gonin, M., Fuhrer, K., Horvath, T., Docherty, K. S., Worsnop D., R., Jimenez, J., L.: Field-deployable, high-resolution, time-of-flight aerosol mass spectrometer. *Analytical Chemistry*, 78(24), 8281–8289, 2006.

Drinovec, L., Močnik, G., Zotter, P., Prévôt, A. S. H., Ruckstuhl, C., Coz, E., Rupakheti, M., Sciare, J., Müller, T., Wiedensohler, A., & Hansen, A., D., A.: The "dual-spot" Aethalometer: an improved measurement of aerosol black carbon with real-time loading compensation. *Atmos. Meas. Tech.*, 8(5), 1965–1979, 2015.

Energy Information Administration (EIA): International Energy Outlook 2016. Chapter 8. Transportation sector energy consumption. DOE/EIA-0484 (2016), 127-137, 2016.

Erickson, M., Gueneron, M., & Jobson, B.: Measuring long chain alkanes in diesel engine exhaust by thermal desorption PTR-MS. *Atmospheric Measurement Techniques*, 7(1), 225–239, 2014.

Ferry, D., Rolland, C., Delhay, D., Barlesi, F., Robert, P., Bongrand, P., & Vitte, J.: Jet exhaust particles alter human dendritic cell maturation. *Inflam. Res.*, 60(3), 255–263, 2011.

Finlayson-Pitts, B. & Pitts Jr., J., N.: *Chapter 9 - Particles in the Troposphere, in: Chemistry of the Upper and Lower Atmosphere, edited by Finlayson-Pitts, B.J. and Pitts Jr., J. N, pp. 349 - 435. Academic Press, San Diego, 2000.*

Fischer, P. H., Hoek, G., van Reeuwijk, H., Briggs, D. J., Lebret, E., van Wijnen, J. H., Kingham, S., & Elliott, P. E.: Traffic-related differences in outdoor and indoor concentrations of particles and volatile organic compounds in Amsterdam. *Atmospheric Environment*, 34(22), 3713–3722, 2000.

Gerencher, C.: Survey of Operational Practices that Result in Improved Fuel Efficiency and Potential Emissions Reduction Benefits—"Overview of Survey Results. *Technical Report International Civil Aviation Organization (ICAO) Committee on Aviation Environmental Protection (CAEP) WG2-TG4-IP.* url: http://www.theicct.org/sites/default/files/publications/ICCT_HDVreplacement_bestprac_20150302.pdf, 2005

Gentner D. R., Shantanu H. Jathar H. S., Gordon D. T., Bahreini R., Day D. A., Imad El Haddad, Hayes P. L., Pieber S. M., Platt S. M., de Gouw J., Goldstein H. A., Harley R. A., Jimenez L. J., Prévôt A. S. H., and Robinson L. A.: Review of urban secondary organic aerosol formation from gasoline and diesel motor vehicle emissions, *Environ. Sci. Technol.*, 51 (3), 1074–1093. doi: 10.1021/acs.est.6b04509, 2017

Gordon, T., Presto, A., Nguyen, N., Robertson, W., Na, K., Sahay, K., Zhang, M., Maddox, C., Rieger, P., Chattopadhyay, S., Maldonado, H., Maricq, M. M., and Robinson, A. L.: Secondary

organic aerosol production from diesel vehicle exhaust: impact of aftertreatment, fuel chemistry and driving cycle. *Atmos. Chem. Phys.*, 14(9), 4643–4659, 2014a.

Gordon, T. D., Presto, A. A., May, A. A., Nguyen, N. T., Lipsky, E. M., Donahue, N. M., Gutierrez, A., Zhang, M., Maddox, C., Rieger, P., Chattopadhyay, S., Maldonado, H., Maricq, M. M., & Robinson, A. L.: Secondary organic aerosol formation exceeds primary particulate matter emissions for light-duty gasoline vehicles. *Atmos. Chem. Phys.*, 14(9), 4661–4678, 2014b.

Graus, M., Müller, M., & Hansel, A.: High Resolution PTR-TOF: Quantification and Formula Confirmation of VOC in Real Time. *Journal of the American Society for Mass Spectrometry*, 21(6), 1037–1044, 2010.

Gueneron, M., Erickson, M. H., VanderSchelden, G. S., & Jobson, B. T.: PTR-MS fragmentation patterns of gasoline hydrocarbons. *International Journal of Mass Spectrometry*, 379, 97–109, 2015.

Hallquist, M., Wenger, J., Baltensperger, U., Rudich, Y., Simpson, D., Claeys, M., Dommen, J., Donahue, N., George, C., Goldstein, A., Hamilton, J. F., Herrmann, H., Hoffmann, T., Linuma, Y., Jang, M., Jenkin, M. E., Jimenez, J. L., Kiendler-Scharr, A., Maenhaut, W., McFiggans, G., Mentel, Th. F., Monod, A., Prévôt, A. S. H., Seinfeld, J. H., Surratt, J. D., Szmigielski, R., & Wildt, J.: The formation, properties and impact of secondary organic aerosol: current and emerging issues. *Atmospheric Chemistry and Physics*, 9(14), 5155–5236, 2009.

Hansel, A., Jordan, A., Holzinger, R., Prazeller, P., Vogel, W., & Lindinger, W.: Proton transfer reaction mass spectrometry: on-line trace gas analysis at the ppb level. *International Journal of Mass Spectrometry and Ion Processes*, 149, 609–619, 1995.

Herndon, S. C., Rogers, T., Dunlea, E. J., Jayne, J. T., Miake-Lye, R., & Knighton, B. (2006): Hydrocarbon emissions from in-use commercial aircraft during airport operations. *Environmental Science & Technology*, 40(14), 4406–4413, 2006.

Hildebrandt, L., Donahue, N. M., & Pandis, S. N.: High formation of secondary organic aerosol from the photo-oxidation of toluene. *Atmospheric Chemistry and Physics*, 9(9), 2973–2986, 2009.

Hudda, N. & Fruin, S.: International airport impacts to air quality: Size and related properties of large increases in ultrafine particle number concentrations. *Environmental Science & Technology*, 50(7), 3362–3370, 2016.

Hudda, N., Gould, T., Hartin, K., Larson, T. V., & Fruin, S. A.: Emissions from an international airport increase particle number concentrations 4-fold at 10 km downwind. *Environmental Science & Technology*, 48(12), 6628–6635, 2014.

Hudda, N., Simon, M., Zamore, W., Brugge, D., & Durant, J.: Aviation emissions impact ambient ultrafine particle concentrations in the greater Boston area. *Environmental Science & Technology*, 50(16), 8514–8521, 2016.

International Agency for Research on Cancer (IARC): Formaldehyde, 2-Butoxyethanol and 1-tert-Butoxypropan-2-ol, *IARC Monographs on the Evaluation of Carcinogenic Risks to Humans*, Volume 88, Url: <http://monographs.iarc.fr/ENG/Monographs/vol88/mono88.pdf>, 2006.

International Air Transport Association (IATA): *Annual Review 2016*, Dublin. Url: <https://www.iata.org/publications/Documents/iata-annual-review-2016.pdf>, 2016.

Iavicoli, I., Chiarotti, M., Bergamaschi, A., Marsili, R., & Carelli, G.: Determination of airborne polycyclic aromatic hydrocarbons at an airport by gas chromatography-mass spectrometry and evaluation of occupational exposure. *Journal of Chromatography. A*, 1150(1-2), 226–235, 2007.

International Civil Aviation Organization (ICAO): Annex 16—Environmental Protection Volume II—Aircraft Engine Emissions. *Technical report*, ISBN 978-92-9231-123-0, 2008.

International Civil Aviation Organization (ICAO): Airport Air Quality Manual, 1st Edition. *Technical report*, Doc 9889, ISBN 978-92-9231-862-8, 2011.

Intergovernmental Panel on Climate Change (IPCC): Climate change 2001: the scientific basis. Contribution of working group I to the third assessment report of the Intergovernmental Panel on Climate Change. *Weather*, 57(8), 267–269, 2002.

Intergovernmental Panel on Climate Change (IPCC): Climate Change 2013: The Physical Science Basis. Contribution of Working Group I to the Fifth Assessment Report of the Intergovernmental Panel on Climate Change [Stocker, T.F., D. Qin, G.-K. Plattner, M. Tignor, S. K. Allen, J. Boschung, A. Nauels, Y. Xia, V. Bex and P.M. Midgley (eds.)] Summary for Policymakers, 2013.

Jordan, A., Haidacher, S., Hanel, G., Hartungen, E., Märk, L., Seehauser, H., Schotchkowsky, R., Sulzer, P., & Märk, T.: A high resolution and high sensitivity proton-transfer-reaction time-of-flight mass spectrometer (PTR-TOF-MS). *International Journal of Mass Spectrometry*, 286(2), 122–128, 2009.

Kang, E., Root, M., Toohey, D., & Brune, W.: Introducing the concept of potential aerosol mass (PAM). *Atmospheric Chemistry and Physics*, 7(22), 5727–5744, 2007.

Karner, A. A., Eisinger, D. S., & Niemeier, D. A.: Near-Roadway Air Quality: Synthesizing the Findings from Real-World Data. *Environmental Science & Technology*, 44(14), 5334–5344, 2010.

Kean, A. J., Harley, R. A., & Kendall, G. R.: Effects of Vehicle Speed and Engine Load on Motor Vehicle Emissions. *Environmental Science & Technology*, 37(17), 3739–3746, 2003.

Kebabian, P. L., Robinson, W. A., & Freedman, A.: Optical extinction monitor using cw cavity enhanced detection. *Review of Scientific Instruments*, 78, 063102, doi:10.1063/1.2744223, 2007.

- Kilic, D., Brem, B. T., Klein, F., El-Haddad, I., Durdina, L., Rindlisbacher, T., Setyan, A., Huang, R., Wang, J., Slowik, J. G., Baltensperger, U., & Prevot, A. S. H.: Characterization of gas-phase organics using proton transfer reaction time-of-flight mass spectrometry: Aircraft turbine engines. *Environ. Sci. Technol.*, 2017, 51 (7), 3621–3629. doi: 10.1021/acs.est.6b04077, 2017.
- Kim, B. & Rachami, J.: Aircraft emissions modeling under low power conditions. In *Proceedings of the A&WMA's 101st Annual Conference and Exhibition, Portland, OR, USA*, 2008.
- Kim, B. Y.: *Guidebook on Preparing Airport Greenhouse Gas Emissions Inventories, Airport Cooperative Research Program Report*, Volume 11, pp. 1-64, 2009.
- Kim, S., Karl, T., Helmig, D., Daly, R., Rasmussen, R., & Guenther, A.: Measurement of atmospheric sesquiterpenes by proton transfer reaction-mass spectrometry (PTR-MS). *Atmospheric Measurement Techniques*, 2(1), 99-112, 2009.
- Kinsey, J. S., Dong, Y., Williams, D. C., & Logan, R.: Physical characterization of the fine particle emissions from commercial aircraft engines during the aircraft particle emissions experiment (Apex) 1–3. *Atmospheric Environment*, 44(17), 2147–2156, 2010.
- Klein, F., Platt, S. M., Farren, N. J., Detournay, A., Bruns, E. A., Bozzetti, C., Daellenbach, K. R., Kilic, D., Kumar, N. K., Pieber, S. M., Slowik, J. G., Temime-Roussel, B., Marchand, N., Hamilton, J. F., Baltensperger, U., Prévôt, A. S. H., El Haddad, I.: Characterization of gas-phase organics using proton transfer reaction time-of-flight mass spectrometry: Cooking emissions. *Environmental Science & Technology*, 50(3), 1243–1250, 2016.
- Knighton, W. B., Rogers, T. M., Anderson, B. E., Herndon, S. C., Yelvington, P. E., & Miake-Lye, R. C.: Quantification of aircraft engine hydrocarbon emissions using proton transfer reaction mass spectrometry. *Journal of Propulsion and Power*, 23(5), 949–958, 2007.
- Kosmulski, M.: *Chemical properties of material surfaces*, volume 102. Surfactant Science Series. Volume 102. Edited by Arthur T. Hubbard (Santa Barbara Science Project, Santa Barbara, CA). Marcel Dekker, Inc.: New York, Basel. 2001.
- Kuenen, J. J. P., Visschedijk, A. J. H., Jozwicka, M., & Denier van der Gon, H. A. C.: TNO-MACC_II emission inventory; a multi-year (2003-2009) consistent high-resolution European emission inventory for air quality modelling. *Atmos. Chem. Phys.*, 14(20), 10963–10976, 2014.
- Lack, D. A. & Corbett, J. J.: Black carbon from ships: a review of the effects of ship speed, fuel quality and exhaust gas scrubbing. *Atmos. Chem. Phys.*, 12(9), 3985–4000, 2012.
- Lai, C.-H., Chuang, K.-Y., & Chang, J.-W.: Characteristics of nano-/ultrafine particle-bound PAHs in ambient air at an international airport. *Environmental Science and Pollution Research*, 20(3), 1772–1780, 2012.

- Lall, R., Kendall, M., Ito, K., & Thurston, G. D.: Estimation of historical annual pm 2.5 exposures for health effects assessment. *Atmospheric Environment*, 38(31), 5217–5226, 2004.
- Lambe, A., Chhabra, P., Onasch, T., Brune, W., Hunter, J., Kroll, J., Cummings, M., Brogan, J., Parmar, Y., Worsnop, D., Kolb, C. E., Davidovits, P.: Effect of oxidant concentration, exposure time, and seed particles on secondary organic aerosol chemical composition and yield. *Atmospheric Chemistry and Physics*, 15(6), 3063–3075, 2015.
- Lee, D. S., Fahey, D. W., Forster, P. M., Newton, P. J., Wit, R. C., Lim, L. L., Owen, B., & Sausen, R.: Aviation and global climate change in the 21st century. *Atmospheric Environment*, 43(22), 3520–3537, 2009.
- Lewis, E. R. & Schwartz, S. E.: Chapter 2: Fundamentals, Sea Salt Aerosol Production: Mechanisms, Methods, Measurements and Models-A Critical Review, *Geophysical Monograph Series*, American Geophysical Union, (pp. 9–99), ISBN: 9781118666050, 2004.
- Lewis, S. A., Antoniak, M., Venn, A. J., Davies, L., Goodwin, A., Salfield, N., Britton, J., & Fogarty, A. W.: Secondhand smoke, dietary fruit intake, road traffic exposures, and the prevalence of asthma: a cross-sectional study in young children. *American Journal of Epidemiology*, 161(5), 406–411, 2005.
- Liat, A., Brem, B. T., Durdina, L., Vögtli, M., Dasilva, Y. A. R., Eggenschwiler, P. D., & Wang, J.: Electron microscopic study of soot particulate matter emissions from aircraft turbine engines. *Environmental Science & Technology*, 48(18), 10975–10983, 2014.
- Lin, S., Munsie, J., Herdt-Losavio, M., Hwang, S., Civerolo, K., McGarry, K., & Gentile, T.: Residential proximity to large airports and potential health impacts in New York State. *International Archives of Occupational and Environmental Health*, 81(7), 797–804, 2008.
- Lloyds Register Marine & University College London Energy Institute: *Global marine fuel trends 2030*. Technical report. Url: https://www.bartlett.ucl.ac.uk/energy/news/documents/Global_Marine_Fuel_Trends_2030_single_page_v2_tcm155-249392.pdf, 2014.
- Mao, J., Ren, X., Brune, W., Olson, J., Crawford, J., Fried, A., Huey, L., Cohen, R., Heikes, B., Singh, H., et al.: Airborne measurement of oh reactivity during intex-b. *Atmospheric Chemistry and Physics*, 9(1), 163–173, 2009.
- Masiol, M. & Harrison, R. M.: Aircraft engine exhaust emissions and other airport-related contributions to ambient air pollution: a review. *Atmospheric Environment*, 95, 409–455, 2014.
- Miracolo, M., Hennigan, C., Ranjan, M., Nguyen, N., Gordon, T., Lipsky, E., Presto, A., Donahue, N., & Robinson, A.: Secondary aerosol formation from photochemical aging of aircraft exhaust in a smog chamber. *Atmospheric Chemistry and Physics*, 11(9), 4135–4147, 2011.

Miracolo, M. A., Drozd, G. T., Jathar, S. H., Presto, A. A., Lipsky, E. M., Corporan, E., & Robinson, A. L.: Fuel composition and secondary organic aerosol formation: Gas-turbine exhaust and alternative aviation fuels. *Environmental Science & Technology*, 46(15), 8493–8501, 2012.

Morris, K. M.: *Results from a number of surveys of power settings used during taxi operations; British Airways Technical Documents Relating to the Aircraft Operations Supporting the Project for the Sustainable Development of Heathrow, Document*. Technical report, [url: https://www.britishairways.com/cms/global/pdfs/csr/PSDH_Technical_Reports.pdf](https://www.britishairways.com/cms/global/pdfs/csr/PSDH_Technical_Reports.pdf), 2005.

Nakagawa, M. & Ohba, T.: Minerals in volcanic ash 1: Primary minerals and volcanic glass. *Global Environmental Research-English Edition*, 6(2), 41–52, 2002.

Nakao, S., Clark, C., Tang, P., Sato, K., & Cocker III, D.: Secondary organic aerosol formation from phenolic compounds in the absence of NO_x. *Atmospheric Chemistry and Physics*, 11(20), 10649–10660, 2011.

Negri, E. & La Vecchia, C.: Epidemiology and prevention of bladder cancer. *European Journal of Cancer Prevention*, 10(1), 7–14, 2001.

Negri, E. & Vecchia, C. L.: Epidemiology and prevention of bladder cancer. In P. B. MD & F. P. MD (Eds.), *Invasive Bladder Cancer* (pp. 1–14). Springer London. DOI: 10.1007/978-1-84628-377-2_1, 2007.

Nel, A.: Air pollution-related illness: effects of particles. *Science*, 308(5723), 804–806, 2005.

Ng, N., Kroll, J., Chan, A., Chhabra, P., Flagan, R., & Seinfeld, J.: Secondary organic aerosol formation from m-xylene, toluene, and benzene. *Atmospheric Chemistry and Physics*, 7(14), 3909–3922, 2007.

Nielsen, T. (1996). Traffic contribution of polycyclic aromatic hydrocarbons in the center of a large city. *Atmospheric Environment*, 30(20), 3481–3490, 1996.

Odum, J. R., Jungkamp, T. P. W., Griffin, R. J., Forstner, H. J. L., Flagan, R. C., & Seinfeld, J. H.: Aromatics, Reformulated Gasoline, and Atmospheric Organic Aerosol Formation. *Environmental Science & Technology*, 31(7), 1890–1897, 1997.

Peng, Z., Day, D. A., Ortega, A. M., Palm, B. B., Hu, W., Stark, H., Li, R., Tsigaridis, K., Brune, W. H., & Jimenez, J. L.: Non-OH chemistry in oxidation flow reactors for the study of atmospheric chemistry systematically examined by modeling. *Atmos. Chem. Phys.*, 16(7), 4283–4305, 2016.

Peng, Z., Day, D. A., Stark, H., Li, R., Lee-Taylor, J., Palm, B. B., Brune, W. H., & Jimenez, J. L.: HO_x radical chemistry in oxidation flow reactors with low-pressure mercury lamps systematically examined by modeling. *Atmos. Meas. Tech.*, 8(11), 4863–4890, 2015.

Pieber S. M., Kumar N. K., Klein F., Comte P., Bhattu D., Dommen J., Bruns E. A., Kilic D., Keller A., Baltensperger U., Czerwinski J., Heeb N., Slowik J. G. and Prévôt A. S. H.: Gas phase

composition and secondary organic aerosol formation from gasoline direct injection vehicles investigated in a batch and flow reactor: effects of prototype gasoline particle filters. *Atmospheric Chemistry and Physics*, <https://doi.org/10.5194/acp-2017-942>, 2017.

Platt, S. M. , El Haddad, I., Pieber, S. M., Zardini, A., Clairotte, M., Suarez-Bertoa R., Daellenbach, K.R., Huang, R.-J., Slowik, J. G., Hellebust S., Temime-Roussel B., Marchand N., de Gouw J., Jimenez J.L., Hayes P. L., Robinson A. L., Baltensperger U., Astorga C. Prévôt, A. S. H.: Gasoline cars produce more carbonaceous particulate matter than modern filter-equipped diesel cars, *Sci. Rep.*, 7, 4926, 2017.

Platt, S., El Haddad, I., Pieber, S., Huang, R., Zardini, A., Clairotte, M., Suarez-Bertoa, R., Barmet, P., Pfaffenberger, L., Wolf, R., Slowik, J.G., Fuller, S.J., Kalberer, M., Chirico, R., Dommen, J., Astorga, C., Zimmermann, R., Marchand, N., Hellebust, S., Temime-Roussel, B., Baltensperger U. & A.S.H. Prévôt: Two-stroke scooters are a dominant source of air pollution in many cities, *Nat. Communications*, 5, 3749. doi:10.1038/ncomms4749, 2014.

Platt, S. M., El Haddad, I., Zardini, A. A., Clairotte, M., Astorga, C., Wolf, R., Slowik, J. G., Temime-Roussel, B., Marchand, N., Ježek, I., Drinovec, L., Močnik, G., Möhler, O., Richter, R., Barmet, P., Bianchi, F., Baltensperger, U., & Prévôt, A. S. H.: Secondary organic aerosol formation from gasoline vehicle emissions in a new mobile environmental reaction chamber. *Atmos. Chem. Phys.*, 13(18), 9141–9158, 2013.

Pope, C. A., Burnett, R. T., Thurston, G. D., Thun, M. J., Calle, E. E., Krewski, D., & Godleski, J. J.: Cardiovascular mortality and long-term exposure to particulate air pollution: epidemiological evidence of general pathophysiological pathways of disease. *Circulation*, 109(1), 71–77, 2004.

Prather, M., Sausen, R., Grossman, A., Haywood, J., Rind, D., & Subbaraya, B.: Potential climate change from aviation. *Aviation and the Global Atmosphere. A Special Report of IPCC Working Groups I and III*. Cambridge University Press, Cambridge, UK, (pp. 185–215), 1999.

Presto, A. A., Nguyen, N. T., Ranjan, M., Reeder, A. J., Lipsky, E. M., Hennigan, C. J., Miracolo, M. A., Riemer, D. D., & Robinson, A. L.: Fine particle and organic vapor emissions from staged tests of an in-use aircraft engine. *Atmospheric Environment*, 45(21), 3603–3612, 2011.

Presto, A. A., Miracolo, M. A., Donahue, N. M., & Robinson, A. L.: Secondary organic aerosol formation from high-NO_x photo-oxidation of low volatility precursors: n-alkanes. *Environ. Sci. Technol.*, 44(6), 2029–2034, 2010.

Radke, L. F., Coakley, J. A., & King, M. D.: Direct and Remote Sensing Observations of the Effects of Ships on Clouds. *Science*, 246(4934), 1146–1149, 1989.

Robinson, A. L., Donahue, N. M., Shrivastava, M. K., Weitkamp, E. A., Sage, A. M., Grieshop, A. P., Lane, T. E., Pierce, J. R., & Pandis, S. N.: Rethinking organic aerosols: Semivolatile emissions and photochemical aging. *Science*, 315(5816), 1259–1262, 2007.

Rundle, A., Hoepner, L., Hassoun, A., Oberfield, S., Freyer, G., Holmes, D., Reyes, M., Quinn, J., Camann, D., Perera, F., & Whyatt, R.: Association of childhood obesity with maternal

exposure to ambient air polycyclic aromatic hydrocarbons during pregnancy. *American Journal of Epidemiology*, 175(11), 1163–1172, 2012.

Sausen, R., Isaksen, I., Grewe, V., Hauglustaine, D., Lee, D. S., Myhre, G., Köhler, M. O., Pitari, G., Schumann, U., Stordal, F. & Zerefos C.: Aviation radiative forcing in 2000: An update on IPCC (1999). *Meteorologische Zeitschrift*, 14(4), 555–561, 2005.

Self, S., Zhao, J.-X., Holasek, R. E., Torres, R. C., & King, A. J.: The atmospheric impact of the 1991 Mount Pinatubo eruption. *Url: <http://pubs.usgs.gov/pinatubo/self/>, 1993.*

Shakya, K. M. & Griffin, R. J.: Secondary organic aerosol from photooxidation of polycyclic aromatic hydrocarbons. *Environmental Science & Technology*, 44(21), 8134–8139, 2010.

Sippula, O., Stengel, B., Sklorz, M., Streibel, T., Rabe, R., Orasche, J., Lintelmann, J., Michalke, B., Abbaszade, G., Radischat, C., Gröger, T., Schnelle-Kreis, J., Harndorf, H., & Zimmermann, R.: Particle Emissions from a Marine Engine: Chemical Composition and Aromatic Emission Profiles under Various Operating Conditions. *Environmental Science & Technology*, 48(19), 11721–11729, 2014.

Slemr, F., Giehl, H., Habram, M., Slemr, J., Schlager, H., Schulte, P., Haschberger, P., Lindermeir, E., Döpelheuer, A., & Plohr, M.: In-flight measurement of aircraft CO and nonmethane hydrocarbon emission indices. *Journal of Geophysical Research: Atmospheres*, 106(D7), 7485–7494, 2001.

Spicer, C., Holdren, M., Riggan, R., & Lyon, T.: Chemical composition and photochemical reactivity of exhaust from aircraft turbine engines. In *Annales Geophysicae*, Volume 12 , pp. 944–955), 1994.

Timko, M. T., Herndon, S. C., Wood, E. C., Onasch, T. B., Northway, M. J., Jayne, J. T., Canagaratna, M. R., Miake-Lye, R. C., & Knighton, W. B.: Gas Turbine Engine Emissions—Part I: Volatile Organic Compounds and Nitrogen Oxides. *Journal of Engineering for Gas Turbines and Power*, 132(6), 061504–061504, 2010.

Tkacik, D. S., Presto, A. A., Donahue, N. M., & Robinson, A. L.: Secondary organic aerosol formation from intermediate-volatility organic compounds: cyclic, linear, and branched alkanes. *Environmental Science & Technology*, 46(16), 8773–8781, 2012.

Tunnicliffe, W. S., O’Hickey, S. P., Fletcher, T. J., Miles, J. F., Burge, P. S., & Ayres, J. G.: Pulmonary function and respiratory symptoms in a population of airport workers. *Occupational and Environmental Medicine*, 56(2), 118–123, 1999.

Unal, A., Hu, Y., Chang, M. E., Odman, M. T., & Russell, A. G.: Airport related emissions and impacts on air quality: Application to the Atlanta International Airport. *Atmospheric Environment*, 39(32), 5787 – 5798, 2005.

Viana, M., Hammingh, P., Colette, A., Querol, X., Degraeuwe, B., Vlieger, I. d., & van Aardenne, J.: Impact of maritime transport emissions on coastal air quality in Europe. *Atmospheric Environment*, 90, 96–105, 2014.

- Waldron, G., Pottle, B., & Dod, J.: Asthma and the motorways—one District's experience. *Journal of Public Health Medicine*, 17(1), 85–89, 1995.
- Wang, J, Flagan, R.C & Seinfeld, J. H.: Diffusional losses in particle sampling systems containing bends and elbows. *Journal of Aerosol Science*, 33: 843-857, 2002.
- Westerdahl, D., Fruin, S. A., Fine, P. L., & Sioutas, C.: The Los Angeles International Airport as a source of ultrafine particles and other pollutants to nearby communities. *Atmospheric Environment*, 42(13), 3143–3155, 2008.
- Whelan, E. A., Lawson, C. C., Grajewski, B., Petersen, M. R., Pinkerton, L. E., Ward, E. M., & Schnorr, T. M.: Prevalence of respiratory symptoms among female flight attendants and teachers. *Occupational and Environmental Medicine*, 60(12), 929–934, 2003.
- World Health Organization: Burden of disease from household air pollution for 2012. *World Health Organization: Geneva, Switzerland*, 2014.
- Wuebbles, D., Gupta, M., & Ko, M.: Evaluating the impacts of aviation on climate change. *Eos*, 88(14), 157–160, 2007.
- Yee, L., Kautzman, K., Loza, C., Schilling, K., Coggon, M., Chhabra, P., Chan, M., Chan, A., Hersey, S., Crounse, J., Wennberg, P. O., Flagan, R. C., Seinfeld & J. H.: Secondary organic aerosol formation from biomass burning intermediates: phenol and methoxyphenols. *Atmospheric Chemistry and Physics*, 13(16), 8019–8043, 2013.
- Yelvington, P. E., Herndon, S. C., Wormhoudt, J. C., Jayne, J. T., Miake-Lye, R. C., Knighton, W. B., & Wey, C.: Chemical speciation of hydrocarbon emissions from a commercial aircraft engine. *Journal of Propulsion and Power*, 23(5), 912–918, 2007.
- Zardini, A. A., Platt, S. M., Clairotte, M., El Haddad, I., Temime-Roussel, B., Marchand, N., Ježek, I., Drinovec, L., Močnik, G., Slowik, J. G., Manfredi, U., Prévôt, A. S. H., Baltensperger, U., & Astorga, C.: Effects of alkylate fuel on exhaust emissions and secondary aerosol formation of a 2-stroke and a 4-stroke scooter. *Atmospheric Environment*, 94, 307–315, 2014.
- Zhang, Q., Jimenez, J. L., Canagaratna, M. R., Ulbrich, I. M., Ng, N. L., Worsnop, D. R., & Sun, Y.: Understanding atmospheric organic aerosols via factor analysis of aerosol mass spectrometry: a review. *Analytical and Bioanalytical Chemistry*, 401(10), 3045–3067, 2011.
- Zhao, J. & Zhang, R.: Proton transfer reaction rate constants between hydronium ion (H_3O^+) and volatile organic compounds. *Atmospheric Environment*, 38(14), 2177–2185, 2004.
- Zhu, Y., Hinds, W. C., Kim, S., Shen, S., & Sioutas, C.: Study of ultrafine particles near a major highway with heavy-duty diesel traffic. *Atmospheric Environment*, 36(27), 4323–4335, 2002.

Acknowledgements

It was a great experience to be a PhD student at the Laboratory of Atmospheric Chemistry (LAC) at the Paul Scherrer Institute (PSI) and I feel lucky to meet and work with the people coming from all around the world. They are exciting, friendly and enjoyable people. It was a pleasure to work with you.

I want to express special thanks of gratitude to

...Prof. Ulrike Lohmann and Dr. Richard Miake-Lye for being my co-examiners and reviewing the thesis, and an additional thank you to Dr. Richard Miake-Lye for taking a long way to Zurich for my defense.

...my doctoral advisor Prof. Urs Baltensperger and my supervisor Dr. André Prévôt for creating the atmosphere at LAC, accepting me as a PhD student, for their support and their constructive inputs during my PhD.

...my direct supervisor Dr. André Prévôt for being such an approachable person and supporting me.

...Jay and Imad, great scientists, thank you for being there for me all the time. Thank you so much!

...best technician ever, René.

...Dr. Benjamin Brem, Theo Rindlisbacher and Lukas Durdina for helping me during measurement campaigns. It was a pleasure to meet you and to work with you. Thank you very much for your scientific inputs.

...Siegerist Frithjof and SR Technics test cell personnel for their help during the measurement campaigns.

...Dr. Michel Rossi for his support and answering all my questions concerning combustion chemistry. Thank you very much Michel...

...Prof. Stefan Brönnimann and Prof. Thomas Peter for being my supervisors for my master thesis, heartfelt thanks to Prof. Brönnimann for his support and encouragement to start a PhD.

...Prof. Mete Tayanc, Prof. Tayfun Kindap and Prof. Alper Unal for introducing me to academia as they did for many other young scientists.

...my former colleagues at AYBE: Emir, Esra, Fatma, Gönenc, Nalan, Pinar, Seden, Semih, Zeynep and all the others.

...Seyhan Güler and Havva Ergun for helping me and many others to do their work better, and for bringing many to an upper educational level.

...Remo, Andreas and Burak for making me feel at home in Switzerland by being three of my best friends. Thank you wolves...

...my officemates and communio-cl friends, Carlo, Felix, Manu, Roman, Peter.

...my travel companions and friends from LAC, Giulia, Jun, Kaspar, Manoulis, Marco, Miriam, Nassia, Nivedita, Robert.

...early birds of LAC, Carla, Claudia, Julia and Emily.

...my cirrus group, Emre, Ersan, Korkut, Kutlu, Murat, Seden.

...my friends Ihsan Dogan, Argun, Serdar.

...my uncle, for being a second father to me in Switzerland.

...my family who was supporting me my whole life.

...and last, the most precious person in my life, Sine, thank you for all your support. I wouldn't have made it without you!

Curriculum vitae

Dogushan Kilic

Born on September 9th, 1985

In Istanbul, Turkey

Education

09/2003 – 06/2008	Faculty of Engineering Istanbul, Turkey BSc. Environmental Engineering <i>Major: The designing of the water treatment plants and water supply systems</i>	<i>Marmara University</i>
09/2010 – 10/2012	Geographisches Institut Bern, Schweiz MSc. Climate Sciences <i>Major: Atmospheric Chemistry (Modelling)</i> <i>Supervised by Prof. Stefan Brönnimann and Prof. Thomas Peter</i>	<i>Universität Bern</i>
12/2012 – 11/2016	ETH Zurich Villigen, Schweiz PhD. Atmospheric Sciences (Defense date: November 9th, 2016)	<i>Paul Scherrer Institut</i>

Publications

Published

Dogushan Kilic, Benjamin T. Brem, Felix Klein, Imad El-Haddad, Lukas Durdina, Theo Rindlisbacher, Ari Setyan, Ru-Jin Huang, Jing Wang, Jay G. Slowik, Urs Baltensperger and Andre S. H. Prevot (2016). Characterization of gas-phase organics using proton transfer reaction time-of-flight mass spectrometry: Aircraft turbine engines. *Environmental Science & Technology*, 2017, 51 (7), pp 3621–3629

Emily A. Bruns, Imad El Haddad, Jay G. Slowik, **Dogushan Kilic**, Felix Klein, Urs Baltensperger & André S. H. Prévôt (2016). Identification of significant precursor gases of secondary organic aerosols from residential wood combustion. *Scientific Reports* 6, Article number: 27881, doi:10.1038/srep27881

Felix Klein, Stephen M. Platt, Naomi J. Farren, Anais Detournay, Emily A. Bruns, Carlo Bozzetti, Kaspar R. Daellenbach, **Dogushan Kilic**, Nivedita K. Kumar, Simone M. Pieber, Jay G. Slowik, Brice Temime-Roussel, Nicolas Marchand, Jacqueline F. Hamilton, Urs Baltensperger, André S. H. Prévôt, & Imad El Haddad (2016). Characterization of Gas-Phase Organics Using Proton Transfer Reaction Time-of-Flight Mass Spectrometry: Cooking Emissions. *Environmental Science & Technology*, 50(3), pp.1243-1250.

Emily A. Bruns, Jay G. Slowik, Imad El Haddad, **Dogushan Kilic**, Felix Klein, Josef Dommen, Brice Temime-Roussel, Nicolas Marchand, Urs Baltensperger and André S. H. Prévôt Characterization of gas-phase organics using proton transfer reaction time-of-flight mass spectrometry: fresh and aged residential wood combustion emissions. *Atmospheric Chemistry and Physics*, 17, 705-720, 2017

Felix Klein, Naomi Farren, Carlo Bozzetti, Kaspar Dällenbach, **Dogushan Kilic**, Nivedita Kumar, Simone Pieber, Jay Slowik, Rosemary Tuthill, Jacqueline Hamilton, Urs Baltensperger, André Prévôt, and Imad El Haddad (2016). Indoor terpene emissions from cooking with herbs and pepper and their secondary organic aerosol production potential. *Scientific Reports*, 6, Article number: 36623 (2016)

Submitted

Dogushan Kilic, Ru-Jin Huang, Benjamin Brem, Imad El Haddad, Emily Bruns, Felix Klein, Avi Lavi, Simone M. Pieber, Theo Rindlisbacher, Yinon Rudich, Jing Wang, Jay G. Slowik, Urs Baltensperger, and Andre S. H. (2016). Identification of the precursor gases of secondary organic aerosols from aircraft turbine engine. *Atmospheric Chemistry and Physics*

ETH

Eidgenössische Technische Hochschule Zürich
Swiss Federal Institute of Technology Zurich

PAUL SCHERRER INSTITUT

PSI